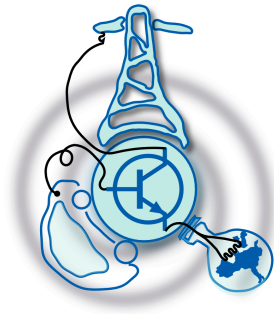


Design of a Three-port Solid State Transformer for High Power applications

by

Guirguis Zaki Guirguis Abdelmessih



Submitted to the Department of Electrical Engineering, Electronics,
Computers and Systems
in partial fulfillment of the requirements for the degree of
Master Course in Electrical Energy Conversion and Power Systems
at the
UNIVERSIDAD DE OVIEDO

June 2015

© Universidad de Oviedo 2015. All rights reserved.

Author

Certified by

Pablo García Fernández
Associate Professor
Thesis Supervisor

Design of a Three-port Solid State Transformer for High Power applications

by

Guirguis Zaki Guirguis Abdelmessih

Submitted to the Department of Electrical Engineering, Electronics, Computers and
Systems

on July xx, 2015, in partial fulfillment of the
requirements for the degree of

Master Course in Electrical Energy Conversion and Power Systems

Abstract

In this thesis, a Three-Port Active Bridge converter for high power high voltage application is designed. The design includes the Solid state high frequency transformer, and the required reactive elements the series inductors, and the DC-link capacitors. Also the choice of the switches, and the heat sink is defended, and a design of a stack for them is made, this stack will include also the driver boards of the switches and the capacitors with the bus-bars for the DC-link. The thesis also presents a simulation for each part, and a final simulation for the real model containing almost all the losses and parasitics elements. Using simulation based tools, the design for each of the parts and the full converter assembly is achieved. The simulation includes losses calculation and considers the effects of parasitic elements. The selected design is compared versus a Half-Bridge Triple Active Port topology, in order to analyze the differences in the performance and reliability. Finally a simulation is presented to illustrated the behavior of the full model under the closed loop condition.

Thesis Supervisor: Pablo García Fernández

Title: Associate Professor

Acknowledgments

First I would like to thank my Professor, advisor, and supervisor, Professor Pablo Garcia. For me, he is not just a Professor who teach some material you can find anywhere, but he is rather a professor who teach his student how to think, how find the problem, and how to create your own way for solving it, as he is the cleaverest man I have ever worked with. Without him, I wouldn't reach this point now, finishing my Master Degree, of course for his technical support, but also for finding me the opportunity that helped me a lot till finish all this.

I am concerned to give a great thanks to the Master " Electric Energy Conversion and Power System " as due to this program my knowledge was exponentially increasing during these two years, mentality changed, and also my life is changed.

I shouldn't finish this part without saying three sentences to three Professors;

Professor Jorge Garica, you are the man I would like to be, for your working perfection, your great ability to give support to others and to care.

Professor Pablo Arboleya, I what to tell you that whenever I saw you I felt happy, you are a very hard worker person, thanks for what your are doing for our Master, and for solving our problems.

Professor Fernando Briz, I would like to really thank, you was like the wise reference to me, every time I had an issue I was trying to look at you to find out the perfect way to handle it.

My father, a thank you word will not be enough to say, for your love, care, support and many other values ... I know that finalizing this my Master thesis with the level that I have means something to you, so I am presenting it to you as a gift, not comparable with what you are giving to me.

My great mother I am sorry for being all this time away from you, but trust me it is more hard for me to be away from you, than it is for you. Thank you very much my mother your phone calls and prayers is the reason I am alive.

My sister and my brother, the two precious persons in my life, I want to apologize to you for being away all this period, but I really believe that what I am doing is a

great thing that you will pass by it one day.

I would like to thank a person who I considered a best friend who I shared struggling moments with, Eng. Sara Saeed

Thanks to all my Master colleagues Engs. ” Sandra, Adrain, Emilio, Mohamed, Sujay, Elli, Manish, Evode, and Pablo” . Also I want to thank some friends who helped me in hard times Eng. Ramy, Eng. Angel, Eng. Bassam, and Dr. Islam.

Finally, and most importantly, I would like to thank my future life partner Eng. Mariam Saeed. Her support, encouragement, quiet patience and unwavering love were undeniably the rock upon which the past two years of my life have been built. Your presence in my life, give it a meaning, and a value, so thanks for being there.

Contents

1	Introduction	21
1.1	Introduction	21
1.2	Objectives	24
1.3	Motivation	25
1.4	Document flow	26
2	State of the art	29
2.1	Solid State Transformer	30
2.1.1	Solid State Transformer basic concept	30
2.1.2	Solid State Transformer configurations	30
2.1.3	Open issues	33
2.2	Dual Active Bridge (DAB)	36
2.2.1	Structure and Main topology	36
2.2.2	The power flow control algorithm	38
2.2.3	Upgrading to the DAB from the point of view of the energy conversion	39
2.3	Triple Port Active Bridge (TAB)	42
2.3.1	Simplified explanation for the working concept of this converter	43
2.3.2	Research topics of the triple-port Active Bridge	45
3	Project Description	49
3.1	A glance at the full project	49
3.2	The triple port Active Bridge structure and specification	50

4	High frequency transformer	53
4.1	Proposed Design	53
4.2	Transformer operation and performance	60
4.2.1	Transformer losses and non-ideality	60
4.2.2	TAB operation and performance	64
4.3	Alternative design: Magnetically coupled core	66
4.3.1	Effects of primary windings resistance asymmetries	67
4.3.2	Effects of parameters mismatch between the two cores	68
4.3.3	Effects of leakage flux asymmetries	69
5	Reactive Elements Design	73
5.1	Inductor Design	73
5.1.1	Role of inductor in TAB operation	73
5.1.2	Design of the inductor	74
5.1.3	Comparing the Symmetrical Design inductors at all the ports with the Single side inductors at the Secondary	79
5.1.4	Manufacturing and Analysis	81
5.2	DC-Link Capacitors Design	82
6	IGBT, Heat sink, and stack and Cabinet design	89
6.1	IGBT choice and specification	89
6.1.1	Why Insulated-Gate Bipolar Transistor	89
6.1.2	2MBI200HH-120-50 HIGH SPEED IGBT MODULE 1200V / 200A / 2 in one package	90
6.2	Heat sink choice	91
6.3	Stack design	92
6.4	Cabinet design for fitting all the project components	94
7	Simulation	97
7.1	Full model real simulation	97
7.2	Comparison with the Half-Bridge TAB	103

7.3	Control simulation	104
8	Conclusion and Future Work	109
8.1	Conclusion	109
8.2	Future Work	110
A	Data sheets	113
B	Stack Design	121

List of Figures

1-1	A figure showing an example for a centralized power network [1].	21
1-2	A figure showing an example for a centralized power network [2].	22
1-3	Layout of Combined Wind/PV Generating System with Double-Input, Single-Output DC/DC Converter [3].	23
1-4	Two PV stand-alone structures, (a) conventional independent converter structure; (b) new integrated structure [4].	23
2-1	Generalised solid-state transformer circuit [5].	30
2-2	SST configurations: a) single-stage, b) two-stage with LVDC link, c) two-stage with HVDC link, and d) three-stage [6].	31
2-3	Modular single-stage SST [6].	32
2-4	Modular two-stage SST [6].	33
2-5	Modular two-stage SST [6].	33
2-6	Two port bi-directional DC-DC converter (DAB) [7].	36
2-7	Comparative photo of 50-Hz LF and 20-kHz HF transformers [8].	37
2-8	The first wave form shows the voltage at AC the terminal of the primary converter, and the second one shows the voltage at the AC terminal of the secondary converter, and the third represents the voltage difference on the two terminals of the inductor and the fourth represents the current passing through the inductor [9].	38
2-9	Dual Half Bridge (DHB) schematic [10].	40

2-10	A modular converter with the DAB as main component, the input DC voltage is connected in parallel but the output in series to boost the DC output voltage [11].	40
2-11	Schematic of the TAB converter [12].	42
2-12	Fundamental system model: three square-wave voltage sources that exchange energy through a grid of inductors, as a consequence of the phase shift angle between the switching patterns. The network of inductors is derived from the transformer based on a π -model representation [13].	43
2-13	In the first plot the voltages on the output terminal of the three full bridges rectifier, and The second plot shows the current passing through the inductors, in blue the current of the first secondary port, in red the current of the second secondary port, then in black the current of the primary port [12].	44
2-14	Six different cases for the shift between the two secondary and the primary, each plot represents one case and have the three voltages wave forms and in red the current at the primary [12].	44
2-15	Configuration of phase modular three-port bidirectional DC-DC converter in wye wye-delta connection [14].	46
2-16	Conventionally wound three-port three-phase spatially symmetrical transformer [15].	46
2-17	Proposed three-port triple-half-bridge bi-directional dc-dc converter [16].	47
3-1	LEMUR Micro-Grid Project.	50
3-2	The triple-port active bridge Structure including some design specification and component naming.	51
4-1	The figure shows a structure for the proposed transformer design with its number of turns.	54

4-2	The modeling of the transformer using an ideal transformer, and the magnetizing inductance, and resistance, and the series leakage inductance and resistance [17].	55
4-3	The Figure in (a) shows the structure of a E-core transformer where the center winding fix the voltage, in (b) the electrical modeling of this transformer using coupling inductors, (c) shows the same transformer in (a) but the voltage is fixed by the first winding, in (d) its wrong modeling due to the lag in description [18].	56
4-4	The PLECS model for the transformer shown in Figure 4-2 [17].	58
4-5	The PLECS model of the proposed three port transformer composed of two separated cores, with the two primary windings are connected in parallel, and the two winding of each secondary port are connected in series.	58
4-6	fig(a) contain three plots each plot represents the voltage in blue and the current in red in one port, the first plot belongs to the primary port, the second plot belongs to the first secondary port (750 V) while the third plot belongs to the second secondary port (375 V). In fig(a) there in a dashed rectangle this is to indicate the part that fig (b) will show in a wide view, to will analyze it.	61
4-7	The first plot represents the Power losses, while the second one represents the voltage drop at the two secondary ports, both with respect the loading percentage.	63
4-8	The flux density at the core of the transformer.	64

4-9	Each plot shows in dashed black the voltage at the primary port, in red the voltage at the first secondary port, in magenta the voltage at the second secondary port, and in blue the current. The combinations mainly represents two case with the two shifts are positive, the first one the shift belongs to the lower voltage port is bigger (first plot), and the second the opposite (second plot). Two others with negative shifts, the first case where the shift belongs to the low voltage port is deeper in the negative (third plot), and the second is the opposite (fourth plot), then one with negative shift at the high voltage port, and positive shift at the low voltage port (fifth plot), and the opposite (sixth plot).	65
4-10	The magnetic circuit for the invented transformer that will have the same number of windings with the same connection between them, but placed on one core.	66
4-11	The difference in the current of the two windings of the primary port due to a change of 50 % of the series resistance of only one winding than the other winding.	68
4-12	The difference in the current of the two windings of the primary port due to a change of 10 % in the effective length of the parameter of one core than the other one.	69
4-13	The difference in the current of the two windings of the primary port due to a change 10 % in the permeance capacitance of one coupling inductor than the other one.	70
4-14	The assembly of the mechanical structure of the transformer.	71
4-15	This figure show the real transformer.	71
5-1	The inductor representation of the transformer [12].	74
5-2	The first plot shows in blue the primary voltage and in red the secondary voltage, the second plot shows the voltage at the inductor terminal, and in the third plot shows the current in the inductor.	75

5-3	The colored plane represents the maximum value of the primary current with respect to the value of the two secondary inductors, the surface indicate the 300 Amps. The intersection of those two surfaces create the blue contour (line) in the x-y plane, The red line in the x-y plane also represents the line for equal inductances at the two secondary sides.	77
5-4	The Power Output at different phase shift value, for two secondary inductances of $40\mu H$. In red the power at the second secondary port, in blue the power at the first secondary port, and in black the primary port power.	78
5-5	fig (a) shows the inductive model for the TAB with two inductors placed at the two secondary port, while fig (b) shows the model but for a symmetry design with inductors in all the ports.	80
5-6	The efficiency of the converter taking into account the estimated losses in the inductor and the losses of the transformer.	82
5-7	The Ripple voltage with respect to the DC-Link capacitance value, in blue the ripple at the first secondary port, and in red the ripple in the second secondary port.	84
5-8	The efficiency of the converter after adding the DC-Link losses with respect to the loading percentage.	87
6-1	The thermal resistance of the heat sink with respect to the power dissipated for all the all the four heat sink sub-model [19].	92
6-2	The Stack proposed design containing in the first layer the heat sink and its fan, and in the second layer the positive DC-Link layer, then the negative layer of the DC-Link, on top of it comes the DC-Link capacitors and the Bus-bar connected to the middle point of the first IGBT package, on top of it comes the Bus-bar connected to the middle point of the second IGBT package, finally comes the Bus-bar connected to the third one.	93

6-3	A 3D view for the cabinet drawn in red, which contain in the extreme bottom the transformer, next to it in the bottom also there is the four inductors, on top of them there is the three stacks.	95
6-4	A front view for the cabinet, where all the dimensions are placed, in blue the three stacks, in red the transformer, and in violet tow of the four inductors.	95
7-1	The schematic of the Full project, the top schematic shows the project overview, in the bottom there is two other schematic, the one on the left shows the schematic of the inverter, and on the right the schematic of the DC-Link.	98
7-2	The turn on losses got it from the generated report by PLECS software for the created model for the IGBT.	99
7-3	The forward voltage with respect to the current, the graph indicating the conduction losses got it from the generated report by PLECS software for the created model for the IGBT.	99
7-4	The Efficiency of the whole project with respect to the Loading percentage.	100
7-5	In blue the current at the primary port, in red the first secondary port current, and in green the current at the second secondary port.	101
7-6	In blue the current before the DC-Link, in red the current inside the DC-Link, and in green the current after.	101
7-7	The first plot the current ripple in the first secondary port, and in the second plot the ripple in the second secondary port.	102
7-8	The schematic of the Full project working in Half-Bridge mode, the top schematic shows the project overview, in the bottom there is the schematic of the inverter.	103
7-9	The Efficiency of the whole project using the half bridge topology with respect to the Loading percentage.	104

7-10	The Matlab representation of the control loops, the upper diagram represents the control of the first secondary port, while the lower one shows the control diagram for the second secondary port.	105
7-11	The Schematic of the main block used in the control simulation. . . .	106
7-12	The first plot shows the voltage at the first secondary port, in blue is the reference and in red is the actual, the second plot shows the current at the battery, in blue the reference current coming from the division of the reference power to the actual battery voltage, and in red the actual current, finally the last plot shows the power at each port, in blue the power of the primary port, in red the first secondary port, and in green the power at the battery.	107

List of Tables

3.1	The Project specification and limitation.	51
4.1	The parameter of the proposed Transformer.	54
4.2	The parameter of the Core used for the proposed transformer.	59
4.3	The flux density, and the leakage percentage of the proposed transformer.	59
4.4	The Transformer Dimensions.	70
5.1	The theoretical values for the maximum power and maximum peak current at all the ports of the transformer for the $40\mu H$ inductors	79
5.2	The proposed Inductor Specification.	81
5.3	The Inductor Dimensions.	81
5.4	The values of the peak, calculated RMS and simulated RMS of the currents at all the ports.	85
5.5	The chosen capacitor EGB-DCL-420-1100-1754 (HYDRA) Specification [20].	86
5.6	The chosen capacitor EGB-DCL-420-1100-1754 (HYDRA) Dimensions [20].	86
6.1	The Heat Sink Dimensions.	92
7.1	The values of currents at the two secondary ports.	102

Chapter 1

Introduction

1.1 Introduction

During all the twentieth century, the basic structure of the electrical power grid is fixed. this structure is based on the centralized concept or what is called also the hierarchical concept. Figure 1-1 shows what is meant by the centralized concept, as all the power is coming from only one huge power plant.

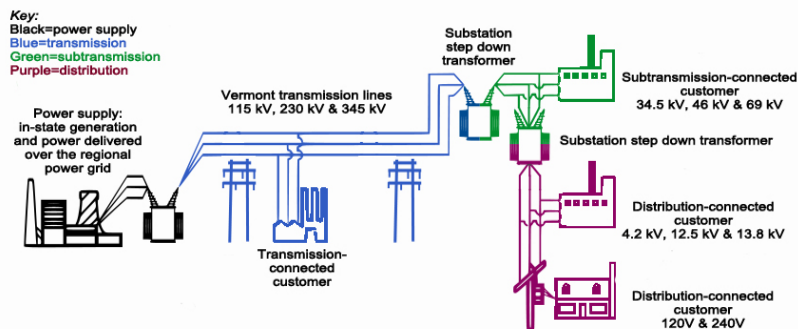


Figure 1-1: A figure showing an example for a centralized power network [1].

Nowadays this concepts are no more compatible with the twenty-one century needs. Due to that all the world wide great concern goes toward the Smart Grid or the Micro-Grid concepts. The Smart grid is a new convention in power distribution system infrastructure, done in order to upgrade the reliability and increase the efficiency. to achieve this goal an advancement should be done in a lot of fields like;

the automated control, the high-power converters, the modern communications infrastructure, sensing and smart meters technologies, and modern energy management techniques based on the optimization of demand, energy and network availability, and so on. [2]

Beyond this small goals the most important and environmental critical goal is to integrate more renewable energy plants or small sources to the grid. And that's what will configure the shape of the smart grid that is previously explained and shown in Figure 1-2.

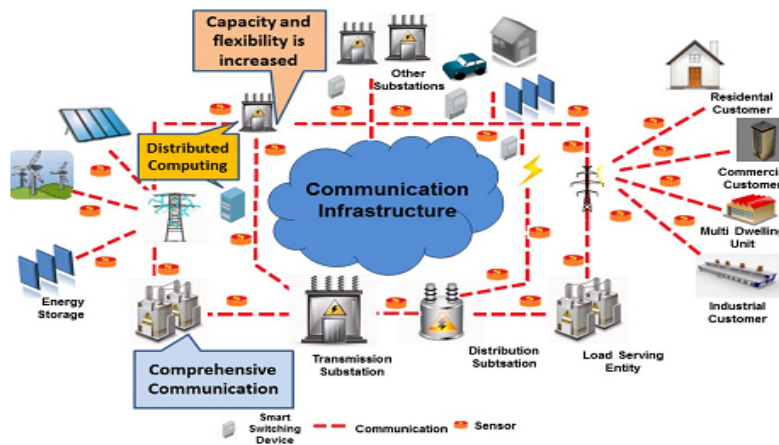


Figure 1-2: A figure showing an example for a centralized power network [2].

One of the most promising renewable energy sources is the solar energy through the photovoltaic (PV) panels, as it is a clean, quiet source of energy, and also suitable for grid and stand-alone applications. due to the physical constraints of the solar energy the stand-one application is quiet impossible without a feasible energy. the usage of this storage system is important as it get the excess energy during the day light and supply during the night or when the available energy is not sufficient to supply the actual load [2]. The literature provide another solution which is to integrate the solar energy with the wind energy [21].

For this reason the need of a three port device increases daily, as the use of multi-port converters allow for a compact integration of multiple energy sources/sinks in a single device. The thing that not only reduces the size a lot, but also has a side advantage which are, first the coordinated control within a single device, and also

the high performance. The need create a concern at the power electronics researchers to invent new topologies. The main application of such a devices could be like what is illustrated in Figure 1-3 this one shows a simple configuration for the multi-port topology. But also Figure 1-4 shows a complex configuration for the same topology, this one is for those how are concerned about the best control and the efficiency no matter how complex it is.

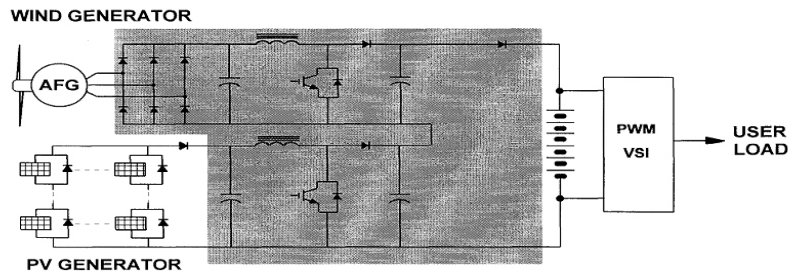


Figure 1-3: Layout of Combined Wind/PV Generating System with Double-Input, Single-Output DC/DC Converter [3].

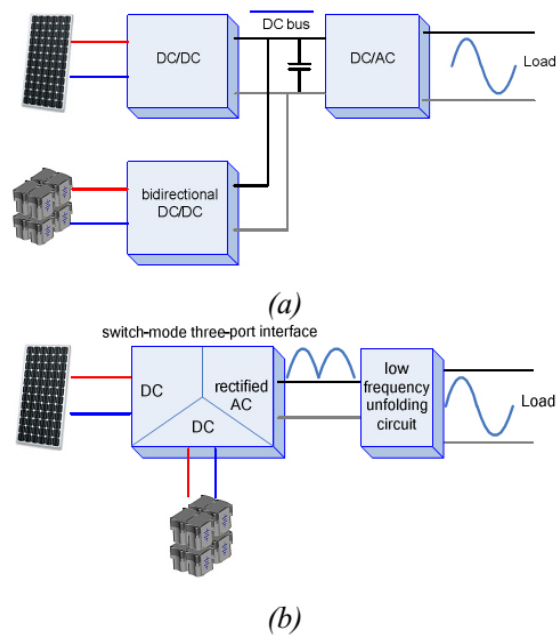


Figure 1-4: Two PV stand-alone structures, (a) conventional independent converter structure; (b) new integrated structure [4].

1.2 Objectives

The objective of this work is to design this triple port device, that is going to be used in an extremely big project belongs to LEMUR research group, this triple port device will connect the Main Grid with a storage system with a Micro Grid. The topology chosen for building this triple port device is the Triple port Active Bridge. The design is not for a prototype, it is going to be a part of the final application project, which mean that the design should be extremely precises, accurate and compatible with all the specification and limitation of the full project, like the handled power, the maximum currents. Another limitation is that one of the port is going to be connected to an energy storage system (Battery), which makes the ripple current also is important, thus the DC-Link design should be will done enough in order to handle this issue.

The design is divided into two main part;

- Operation design

The operation design should insure that the produced design is able to work as expected with the highest efficiency, and the best performance. The design work flow will be based on theoretical calculations of parameters, simulation and communications with the different manufacture companies. And for insuring the excellency of the performance, a wide study should be made in order to be able to modify the will known topology, by removing or adding any features to increase its performance level.

- Mechanical Structure design

The converter will be placed in a cabinet with fixed dimension, The length is 800 mm, the width is 400 mm, and the height is 1200 mm. Which means that the design should take into account all the required components not only the main ones, but also the auxiliary important components, like the measurements sensors, the driving boards, and the protection devices, in the placement and the fitting.

- Simulation

In this part to main simulations should be made, a simulation for the efficiency in all parts in the system, and a closed loop simulation controlling the voltage at one of the ports, and controlling the power in the other one.

1.3 Motivation

As previously mentioned in the introduction; the integration between the Grid, the storage systems or renewable energy sources, with the loads is a very important issue nowadays. That is what makes LEMUR research group takes the intention of thinking to implement a real model for this integration. This is done by designing a Micro-Grid, that is composed of a number of Nano-Grids, connected through DC-link connections in order to facilitate the future desire of varying the number of connected Nano-Grids.

Regarding, the presented work in this document, it is important because it is considered as the inner core of LEMUR Micro-Grid project, which is the design of a three port Active Bridge that handles a power of 150 KW. The complexity of the project design comes from its high voltage ports, as the high voltage ports will handle 750 Volts. Also the chosen topology have a drawback is that the current ripple is related to the amount of power delivered, so, for delivering the 150 Kw, the ripple of the current becomes huge (i.e 500 Amps Peak to Peak current ripple). Also by fixing the operating frequency of the produced AC waveforms to 20 KHz, which is an extremely high frequency, makes the designs of the Solid State Transformer and the series inductors become very complex. One of the big issues is the reliability, as this project is a final application, then the system should be stable and homogeneously integrated to the others project parts. Finally, taking into account the mechanical structure point of view in order not to have a placement problem, limits the overall design capability.

In my point of view the project requires an extremely wide knowledge in a significant number of fields. Magnetics for the transformer, power electronics for the

switches and the drivers, converters for taking care of the full topology and last DC-link design. Also it is required to be aware of all the new technologies in the market, and the problems that the system may have; for example using film capacitors otherwise the losses in the capacitors will kill it one hour after operating the setup; this is due to the huge ripple that the system is subjected to.

1.4 Document flow

The following part of the document is divided into seven main chapters that will try to cover all the work done as much as possible.

- Chapter 2

In this chapter the State of the art is presented, the State of the art will try to cover the new technology of the solid state transformer, then using this technology in the topology of the Dual Active Bridge, finally upgrading this topology to illustrate the Triple-port Active Bridge.

- Chapter 3

Chapter 3 will give a glance about the project of the Micro-Grid belongs to LEMUR research group, then goes into specification and explanation of the work presented in this document.

- Chapter 4

This chapter will illustrate the design of the high frequency Solid state transformer, a simulation to compare the behavior of a two separated cores transformer, with a single core transformer. Finally simulate the proposed design of the manufacture company, to test its operation, efficiency and its behavior in the TAB topology.

- Chapter 5

This is a very important chapter as it shows the design of the reactive elements. Which are mainly into two elements, the series inductor that is re-

sponsible for the current ripple and also for the power delivery technique. And the capacitors of the DC-link.

- Chapter 6

In this chapter the choice of the IGBT and the Heat sink will be defended, than a stack design will be made in order to compact the size as much as possible, and also for designing the DC-link bus bars.

- Chapter 7

Finally the Simulation chapter, that will illustrate some interesting results on the full model simulation taking into account almost all the losses and parasitic effects. Also another simulation will shows the new technology of the Half-Bridge Triple-Port Active Bridge in order to compare its efficiency with the normal TAB topology. Finally a controlled simulation will be made it shows the system working in closed loop.

- Chapter 8

Ending the document with a conclusion and a glance for the future work.

Chapter 2

State of the art

The normal low frequency power transformer are a widely used devices specially in the distributed systems. This is due to their low cost, high reliability, and high efficiency. But as always as there is advantages there is also some disadvantages the low frequency power transformer has few power quality issues like; the voltage drop in loading time, inability to mitigate “flicker”, sensitivity to harmonics, environmental concerns regarding mineral oil, limited performance under DC-offset load unbalances, and a need for protection of the primary system from problems arising inside or beyond the transformer. It is clear that the Power quality is an extremely important issue specially with utility end users, this is the fact that makes these problems more serious today than before [22, 23].

The solution was founded in 1980, when the concept of a solid-state transformer (SST) was mentioned as an alternative to the low frequency power transformer. At that time the successful demonstration of the concept wasn't so clear, however the advantages of this new concepts were clear. Nowadays with the recent advancements in the field of power electronics and semiconductors, and with the deep understanding of the multilevel converters, the concept became more viable [5].

This chapter will initially illustrate the concept of Solid State Transformer, configuration, applications and open issues. After that, different power topologies alternatives and challenges in the control implementation will be considered.

2.1 Solid State Transformer

2.1.1 Solid State Transformer basic concept

The basic solid-state transformer topology is mainly composed of three main sections, the first one is the converter or converters which is responsible to transform the line low frequency AC with required high frequency AC, the second section is the a high frequency transformer and finally a converter or converters to produce line frequency AC from the high frequency AC. The high frequency transformer provides an isolation between its terminals, which divides the transformer into two: the high and low voltage sides [5]. Figure 2-1 shows a basic structure diagram for a solid state transformer.

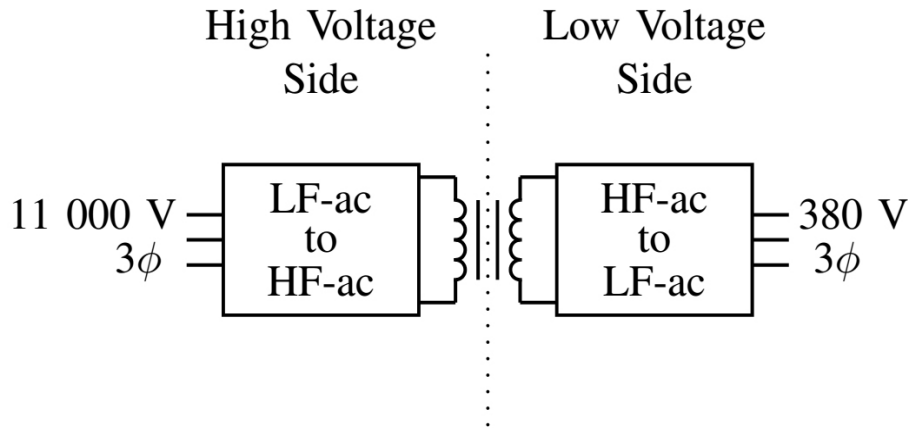


Figure 2-1: Generalised solid-state transformer circuit [5].

2.1.2 Solid State Transformer configurations

In the literature, many alternatives for the solid state transformer power topology can be found. In [23] they create an approach to classify the SST topologies and select the appropriate configuration according to the specific needs. However, it is good to discover that all those configurations could be covered by four main classification [6];

1. Single-stage with no DC link.
2. Two-stage with low voltage DC link (LVDC).

3. Two-stage with high voltage DC link (HVDC).
4. Three-stage with both high and low voltage DC links.

Figure 2-2 shows a graphical representation for all the previously stated classes to illustrate them.

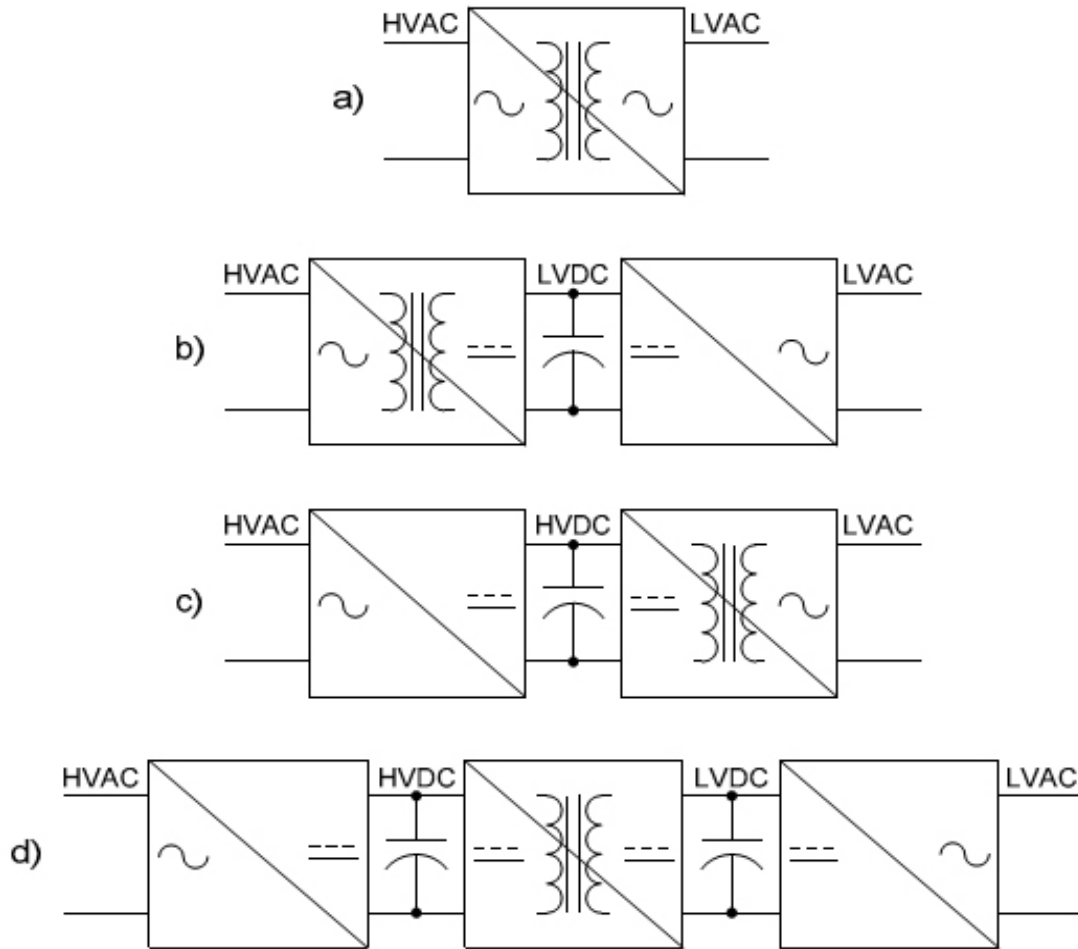


Figure 2-2: SST configurations: a) single-stage, b) two-stage with LVDC link, c) two-stage with HVDC link, and d) three-stage [6].

At the moment, Insulated Gate Bipolar Transistors (IGBT) and high frequency transformers with high voltage ratings like the one needed in the distribution system are not readily available. Which make one of the solution of this problem, could be a modular approach. Also using the interleaving approach, the ripple of the current

will decrease, which lead to the reduction of the size of the filter needed to smooth the current.

Figure2-3 shows the configuration of the modular single-stage solid state transformer. One of the great advantages of this topology is that the voltage and current sharing is intrinsic; which means that there is no need for a specific control to ensure that. However, this is not true for all of the AC-AC converters[6].

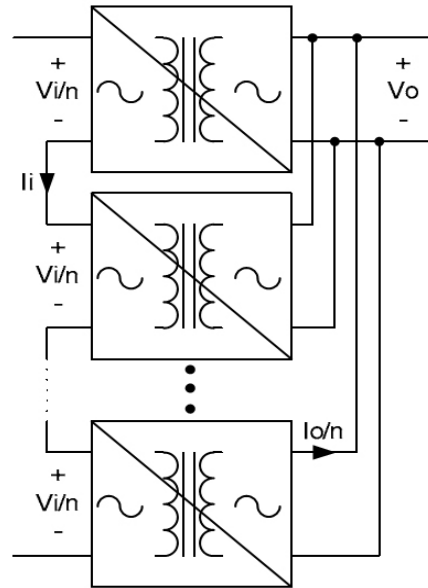


Figure 2-3: Modular single-stage SST [6].

Figure 2-4 shows a modular two-stage configuration where only the AC-DC stage requires a modular implementation as the DC side is at the low voltage side of the high frequency transformer. For this configuration the voltage and current sharing may not be intrinsic since it depends on the type of AC-DC converter [6].

Figure2-5 shows a modular three-stage configuration. In which the input stage is implemented by a multilevel converter; therefore, depending on its type, it may not require a modular implementation. However, the isolated DC-DC stage needs to be modular. In this configuration, current and/or voltage control is required to ensure voltage and current sharing depending on the selected topology [6].

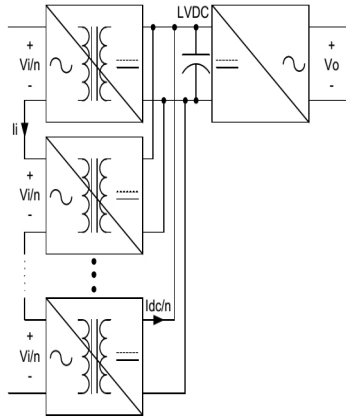


Figure 2-4: Modular two-stage SST [6].

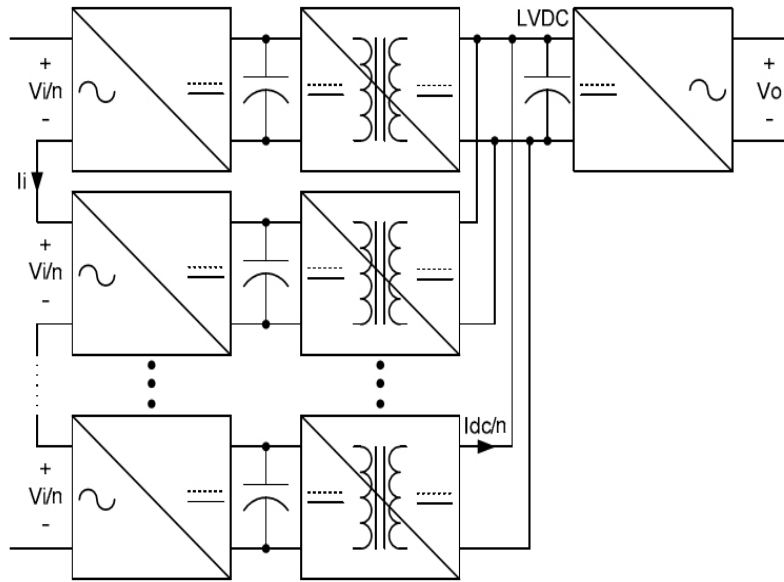


Figure 2-5: Modular two-stage SST [6].

2.1.3 Open issues

- Cost

The cost of the low frequency transformer is much less than the cost of the same rating solid state transformer. And this is due to the extremely much more number of devices used in the solid state transformer, so the cost of the SST is driven by the price of the special equipment, the high frequency transformer,

and also by the price of the semiconductors, and for the heat sinks required for this semiconductors and for the transformer itself, and also Control boards (The main brain Board, The driver circuits boards, and also the measurements boards), and passive components [5].

- Reliability

Generally speaking the low frequency transformer are very reliable, therefore the comparison between the reliability of the low frequency transformer and the SST will be against the SST. The lack of the reliability of the SST comes from its complexity, the more number of components increases the probability of the failure. A solution for this could be using the modular algorithm and make the system flexible and have the capability to work without one of the units, so if there is a failure in one unit the system will remain working. However the inclusion of redundant cells would allow for continued operation of the SST in the event of a cell failure, the system would still require maintenance in that the faulty cell would have to be replaced. Some measurements of the SST system could be used to estimate and predict component failures for preventative maintenance purposes, such as capacitor ripple current and heat sink temperature. This measurements also will aid in improving the design [5].

- Efficiency

The efficiency of a 80 KVA, 11KV / 400 V low frequency transformer could be in the range of 97%, but for a corresponding SST the efficiency will be lower. Found in literature that the efficiency of the SST varies from 90% to 98.1% and this is without taking into account the output inverter loss. Mainly the losses in the low frequency transformer is separated into two, first the Core losses and it is proportional to the applied voltage, and the winding losses and this one corresponds to the delivered power. And this is not the case for the SST because in addition to these losses, there is the conduction losses in all the converters. Which is considered in the high power application a of the big issues as it is the reason of decreasing the efficiency to much. This losses depend on the power

and also the used topology for the converter, as [24] propose some topologies to reduce this losses. But on the other hand it is well known also that the non-linear loads affect the efficiency of the low frequency transformer, which is not the case for the SST [5].

2.2 Dual Active Bridge (DAB)

The Dual active bridge (DAB) is one of the promising DC to DC converters nowadays as it is very suitable for the high power application [25]. This topology also is demonstrated to have very moderate component ratings and low switching loss, also working with high frequency reduces the size of the passive elements a lot, and the size of the transformer as well. Consequently, the DAB topology is considered to be more attractive, especially where power density is important [26]. Also it has a lot of great advantages like, its high performance, high efficiency, galvanic isolation, and inherent soft-switching property [7].

2.2.1 Structure and Main topology

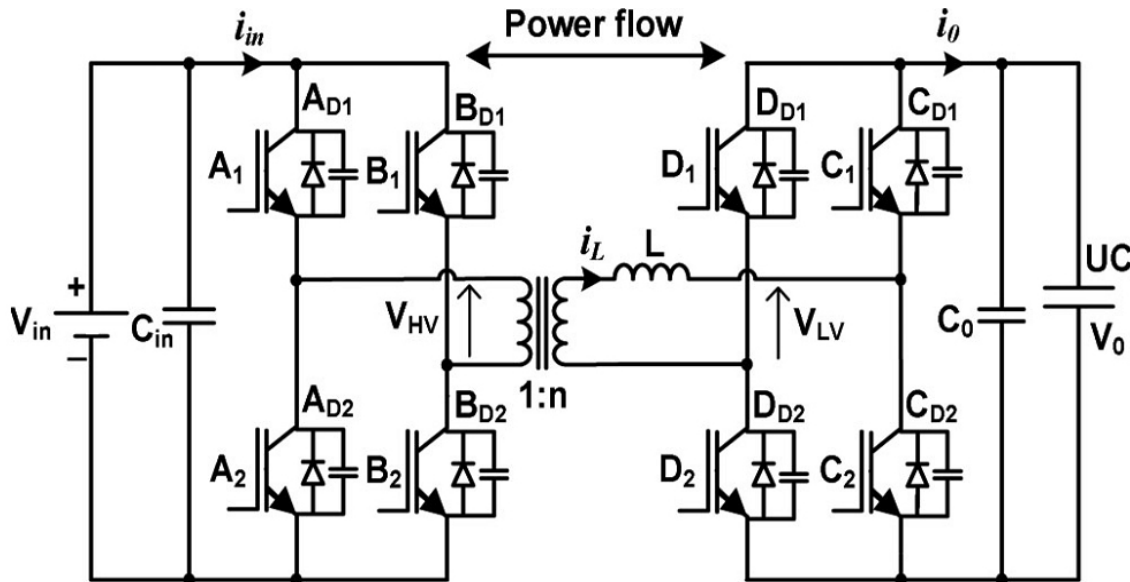


Figure 2-6: Two port bi-directional DC-DC converter (DAB) [7].

Figure 2-6 shows the main structure of the DAB. It is composed from four main parts:

- DC to High frequency converter ” Primary Converter ”

The first Stage in this topology is done by converting the DC input to a High frequency AC square wave signal that vary from positive the input voltage

to its negative value.

- High frequency Transformer

The High frequency Transformer as mentioned before have a great advantages which are; first its size related to the power that it can handle and this is due to the high frequency, Figure2-7 shows a practical comparison between the low and high frequency size, second that it uses its leakage inductance as the main energy transfer element [26].

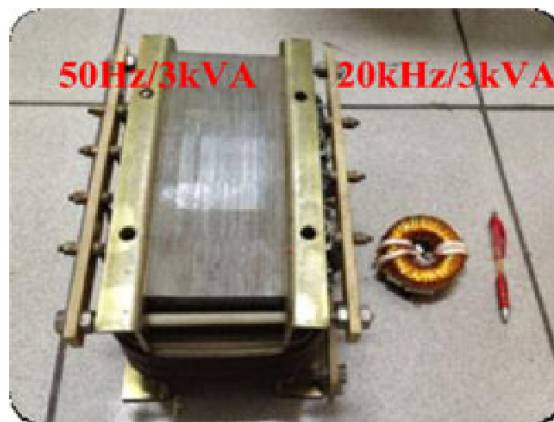


Figure 2-7: Comparative photo of 50-Hz LF and 20-kHz HF transformers [8].

- DC to High frequency Converter ” Secondary converter ”

The secondary converter do exactly the same job of the primary converter but for the output voltage. But it has a degree of freedom to shift the created wave form than the main one by a phase shift ϕ .

- Inductance

This is the key element of this topology, as it is the element that is responsible of the power sharing. As stated before normally the voltage AC signal created by the secondary has are phase shifted from the main one, therefor this will create a voltage difference on the inductor which will lead to a current flow.

2.2.2 The power flow control algorithm

The power flow theory is very simple and clear, as explained before the phase shift created by the secondary converter create a voltage difference on the inductor terminals which produces a current, and power flow. Figure2-8 represent some useful wave forms in the DAB main parts.

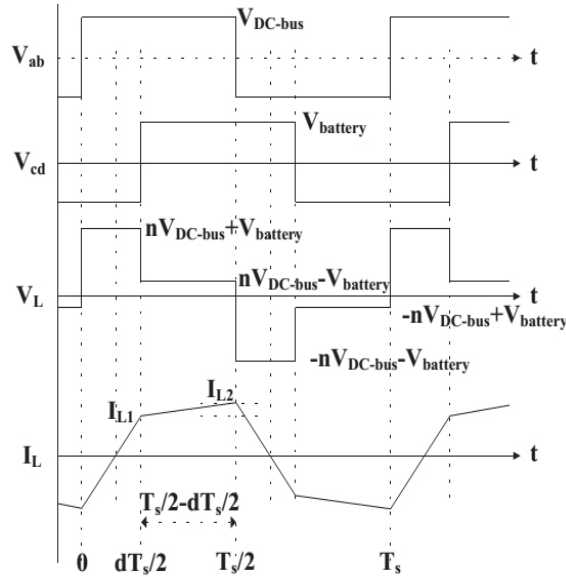


Figure 2-8: The first wave form shows the voltage at AC the terminal of the primary converter, and the second one shows the voltage at the AC terminal of the secondary converter, and the third represents the voltage difference on the two terminals of the inductor and the fourth represents the current passing through the inductor [9].

The following are the ideal equations used in the Power flow estimation and in the control. Equation 2.1 represents Ohm's law for the current in the inductor.

$$\frac{di}{dt} = \frac{V_1 - V_2}{L} \quad (2.1)$$

The voltage on the terminals of the inductor is a square wave voltage, but a reasonable simplification, is to consider only the first harmonic, therefore the voltages will be:

$$V_1 = |V_{max}| \sin(\omega t) \quad (2.2)$$

$$V_2 = |V_{max}| \sin(\omega t - \phi) \quad (2.3)$$

Substituting those two equations in the inductor equation and get the integration the current in the inductor will be represented by this equation:

$$I = \frac{2 \cdot |V_m| \sin\left(\frac{\phi}{2}\right) \sin\left(\omega t - \frac{\phi}{2}\right)}{\omega L} \quad (2.4)$$

Finally using the equations stated before get the power flow equation, this is going to be done by multiplying the rms value of the previous equation with the rms of the voltage at the converter terminal by the cosine of the angle between them, which is going to be equal to the half of the phase shift done by the secondary converter, all those equations are for assuming the system is ideal.

$$P = \frac{|V_{max}^2| \sin(\phi)}{2\omega L} \quad (2.5)$$

It is clear now from the power equation that the only variable is the phase shift ϕ . Which make it the obligatory option to control the power flow.

2.2.3 Upgrading to the DAB from the point of view of the energy conversion

- Dual Half Bridge (DHB) with Zero Voltage Switching (ZVS) modeling technique for losses reduction.

The Dual Half-Bridge (DHB) converter is a new proposed topology, and it is very promising as it considered as a hot research topic. This is due to its great additional advantages; decreased the number of devices which lead to a decreases in the conduction losses, and decreasing the cost. Talking about the soft-switching implementation this is for reducing the switching losses, that constitute a major concern due to the high frequency specified for this application [10].

Figure 2-9 shows the schematic of the DHB used in [10].

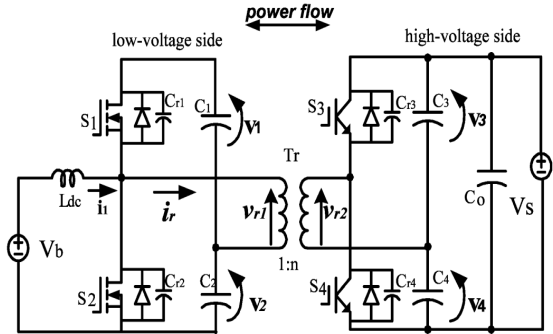


Figure 2-9: Dual Half Bridge (DHB) schematic [10].

- Modular Converter

In order to use this converter with a high voltage application, like in the distribution field, a lot of changes have to be done to make this converter fit to the application. Figure 2-5, shows the schematic of one of the modular topologies, which is used for the interface with a high voltage AC at the input. Also the same topology could be used for a high voltage AC at the output. Also Figure 2-10 shows another topology used for boosting the DC output voltage [11].

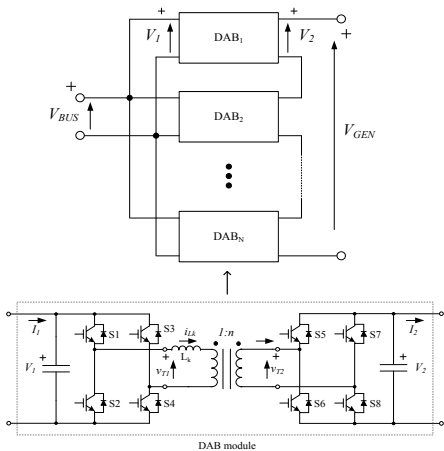


Figure 2-10: A modular converter with the DAB as main component, the input DC voltage is connected in parallel but the output in series to boost the DC output voltage [11].

- The Triple-Port Active Bridge (TAB)

One of the great advantage of the DAB topology is the possibility of adding new terminals, to create for instance the TAB or even the Multi-port concept. The TAB will be explained in the following subsection and all over the document.

2.3 Triple Port Active Bridge (TAB)

The Triple Port Active Bridge (TAB) is a derivative of the DAB converter, and is simply formed by adding an additional winding and full bridge to the transformer. It is much more suitable to the needs of the nowadays renewable and distributed generation. The feature that the TAB provide is the additional port, that connect another output to the same point, which create another degree of freedom for the power sharing and solve the problem of the inequality of the power in the input to the output.

Figure 2-10 shows the main structure of the TAB converter. As previously said the TAB will have an extra full bridge and an extra winding terminal at the transformer, which will gives the additional third DC terminal.

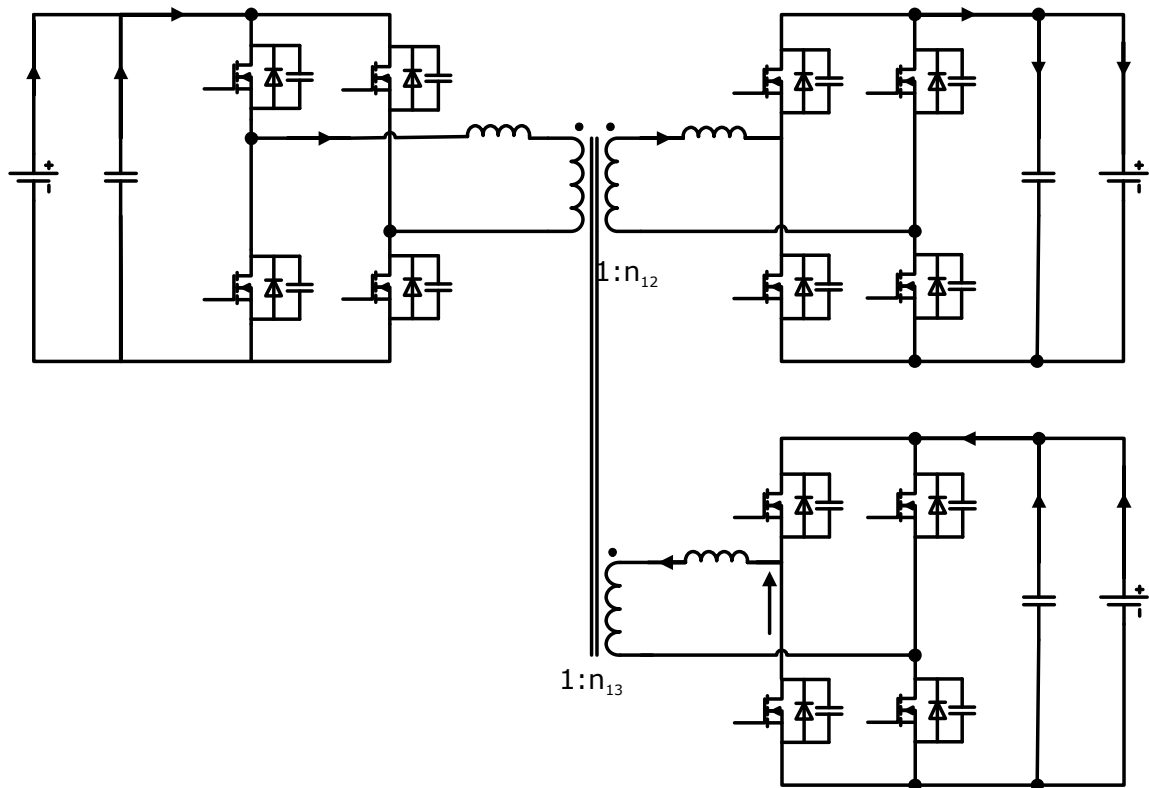


Figure 2-11: Schematic of the TAB converter [12].

2.3.1 Simplified explanation for the working concept of this converter

As stated in [13], the circuit in Figure 2-11 can be replaced by a simplified structure composed of square-wave voltage sources and a set of inductors (the transformer magnetizing inductor, leakages and external inductors). The voltage sources are phase shifted by a phase angle which identify the power flow as stated in the DAB converter.

Figure 2-12 shows the previously explained model based on the transformer π -equivalent representation illustrated in [13] with the magnetizing inductance and the leakages referred to the primary side.

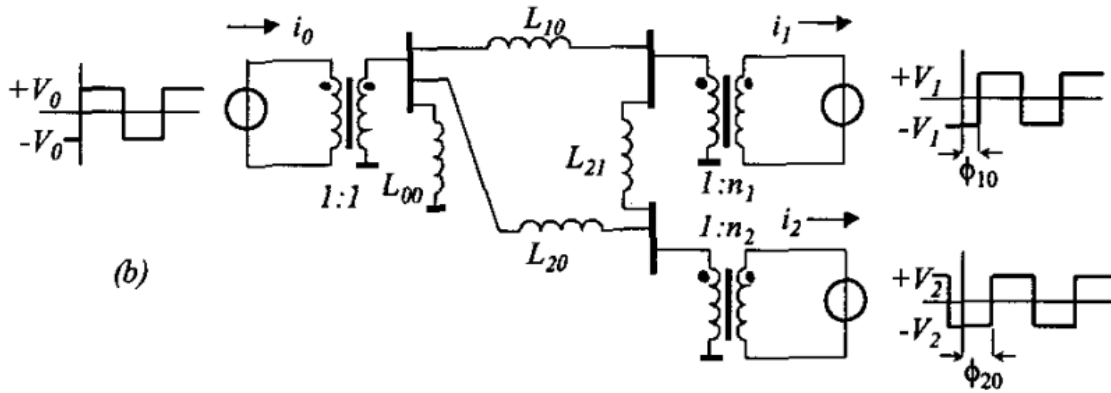


Figure 2-12: Fundamental system model: three square-wave voltage sources that exchange energy through a grid of inductors, as a consequence of the phase shift angle between the switching patterns. The network of inductors is derived from the transformer based on a π -model representation [13].

Figure 2-13 shows in the first plot the voltages on the output terminal of the three full bridges rectifier. The waveforms are shifted from each other, the first secondary port voltage is shifted by ψ_{12} , which is bigger than the shift that the second secondary port voltage had ψ_{13} . The second plot shows the current passing through the inductors, in blue the current of the first secondary port, in red the current of the second secondary port, then in black the current of the primary port, which is the addition of the two others ports. In this figure the slop of the two secondary sides are the same, which is not valid as the voltages level are different, except if the inductors are different and calculated to give the same current slop.

2.3.2 Research topics of the triple-port Active Bridge

- Control technique

The application used in [13] is a bidirectional TAB, that had at its terminal; 25–39 V, 500-W PEM fuel cell stack, 48-V lead acid batteries, and the third port has the load with a 400-V inverter output. For this reason they implement two types of control:

- Voltage control

The voltage control is used at the load terminal, this is to fix the voltage at the load no matter the value of the required power. However this done by making the phase shift of the load voltage waveform the output of a classic analog (PID) compensator, to keep the voltage constant. For instance if the voltage increases due to some load variation, the shift will be decreased accordingly such that less power will be delivered to the dc buffer capacitor at the load side, to make the voltage go back to its previous value [13].

- Power control

The power control is used at the fuel cell terminal, this is to make the fuel cell gives the value of the power that it wants, normally it will be the nominal power of the fuel cells. However this is done by calculating the right shift to put at the battery terminal to get the power mismatch, the calculation is made by a digital signal processor [13].

- Three phase

Another direction in the research was to create a model for the three port but also three phase converter. [14], [15] propose a three-Port three-Phase Dual Active Bridge DC-DC Converter.

State-of-the-art power conversion applications linking grid and distributed sources have low power rating compared to the conventional utilities connected to the grid in medium-voltage level. To solve this problem a large value of inductance is required, also making parallel connected bridges on low voltage side to

share the current for high efficiency. Or use the multi-port inductor integrated isolation transformer which is more compact and have high reliability [14].

Figure 2-15 shows the proposed configuration by [14], as Figure 2-16 shows the proposed winding convention by [15].

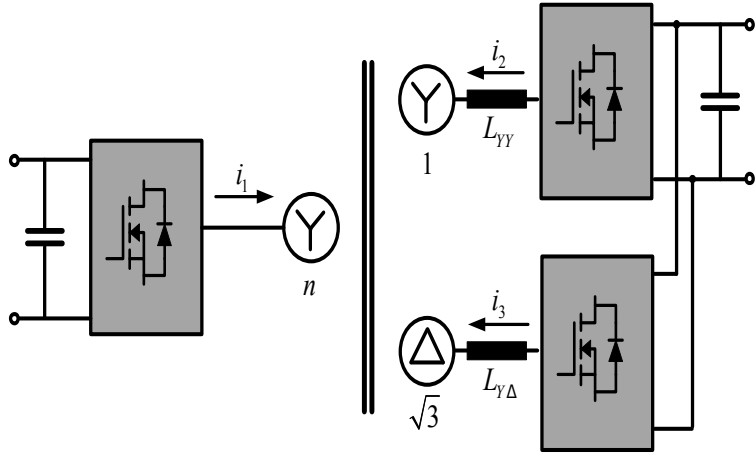


Figure 2-15: Configuration of phase modular three-port bidirectional DC-DC converter in wye wye-delta connection [14].

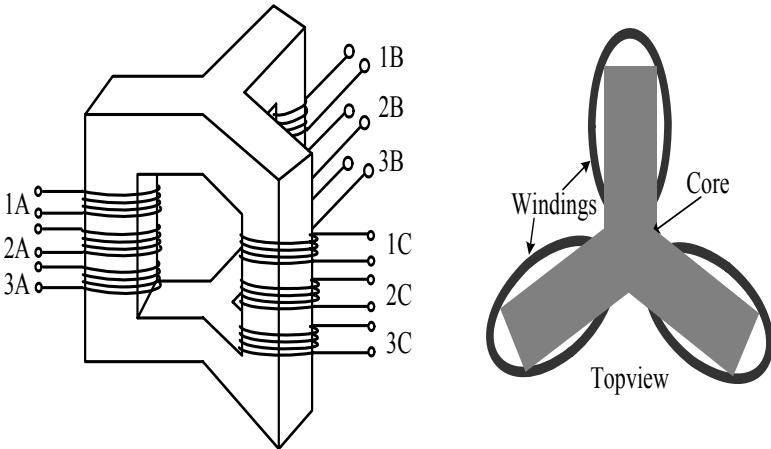


Figure 2-16: Conventionally wound three-port three-phase spatially symmetrical transformer [15].

- Three-port Triple Half Bridge converter

As proposed in [16, 27, 28, 29, 30], this time the topology is a bit different the inductors as shown in figure 2-17, they are placed next to the DC source, before the switches which makes the converter works as a Boost converter. The topology has a great advantages like, it has less component counts, higher power density, higher overall efficiency than two individual DC-DC converters, and low current ripple can be achieved for the capacitors port due to the current-fed structure of the Boost converter.

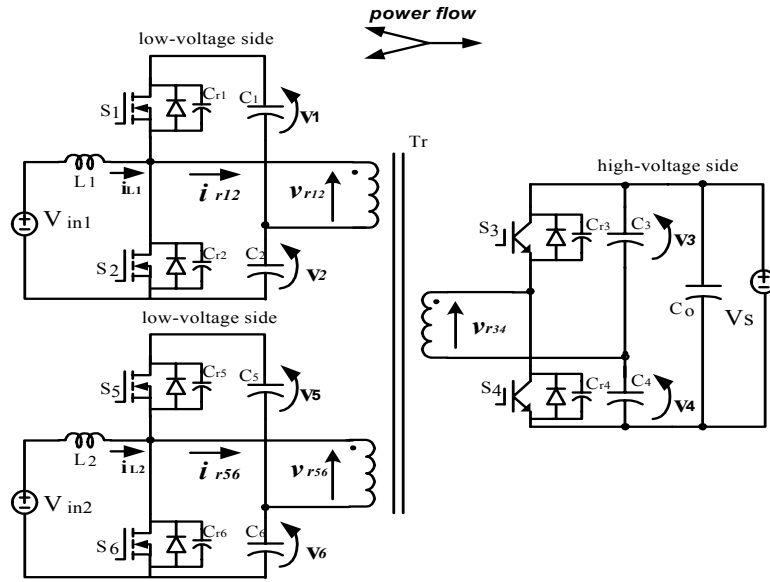


Figure 2-17: Proposed three-port triple-half-bridge bi-directional dc-dc converter [16].

The operation technique is exactly the same as the normal TAB, by making the shift between the port the power starts to flow from one port to the other, the only main difference is that the previously stated advantages and also that the voltage at the terminal of the transformer will not be as the DC value, it will flow the relation between input-output voltage of the Boost as in equation 2.6.

$$V_{out} = \frac{1}{1-D} V_{in} \quad (2.6)$$

Chapter 3

Project Description

3.1 A glance at the full project

The project belongs to LEMUR research group, the project is to build a Micro-Grid. Figure 3-1 shows the full structure of the projects, not with specific details but with blocks that create an idea about what is inside. The figure shows the AC Grid at the extreme left of it, coming out from it a Point of Common coupling (PCC), this PCC connect the Grid to the Standard distribution Grid and also to the project. From the PCC the project start by a filter then to AC-DC converter, the output of this converter is going be the first secondary port of a Three-Port Solid State. Its second secondary port is going to be connected to the storage system, and the main is going to be connect to the main DC-link. From this DC-link The Micro-Grid starts, as it is going to be composed of a number of Nano-Grids. Each Nano-Grid is started by a DC-AC converter, then a filter then the shunt elements. The shunt elements are classified as; Single phase loads, Three phase loads, Non linear loads, and distributed generation.

The research group tries to don't just build this project, but to specify some group members at each particular part in the project, to research and investigate to implement it on the head of the technology.

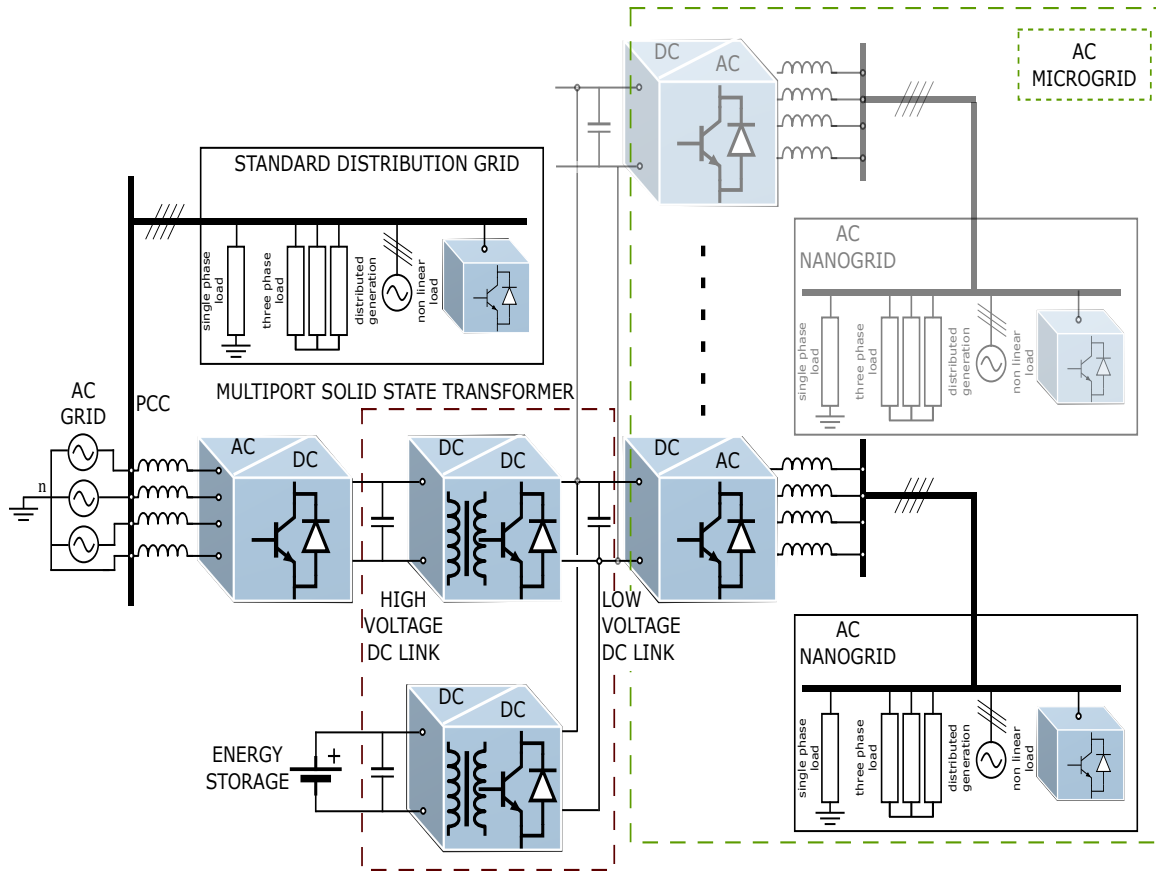


Figure 3-1: LEMUR Micro-Grid Project.

3.2 The triple port Active Bridge structure and specification

The work presented in this thesis is, the design of the triple port Active Bridge, required in the interface of LEMUR Micro-Grid project. Figure 3-2 shows the main structure of the power components of the TAB. The figure contain the naming of the important parts used in the rest of the document. The figure also highlight the main components; The triple port solid state transformer, The Series Inductors, The DC-Link capacitors, The IGBTs, and the Heat sink. The figure didn't illustrate the components parasitic elements, however they are presented in all the simulations.

The Table 3.1 represents almost all the specification and the limitation given by the full project. Any simulation will be presented will have the same parameters shown in this Table.

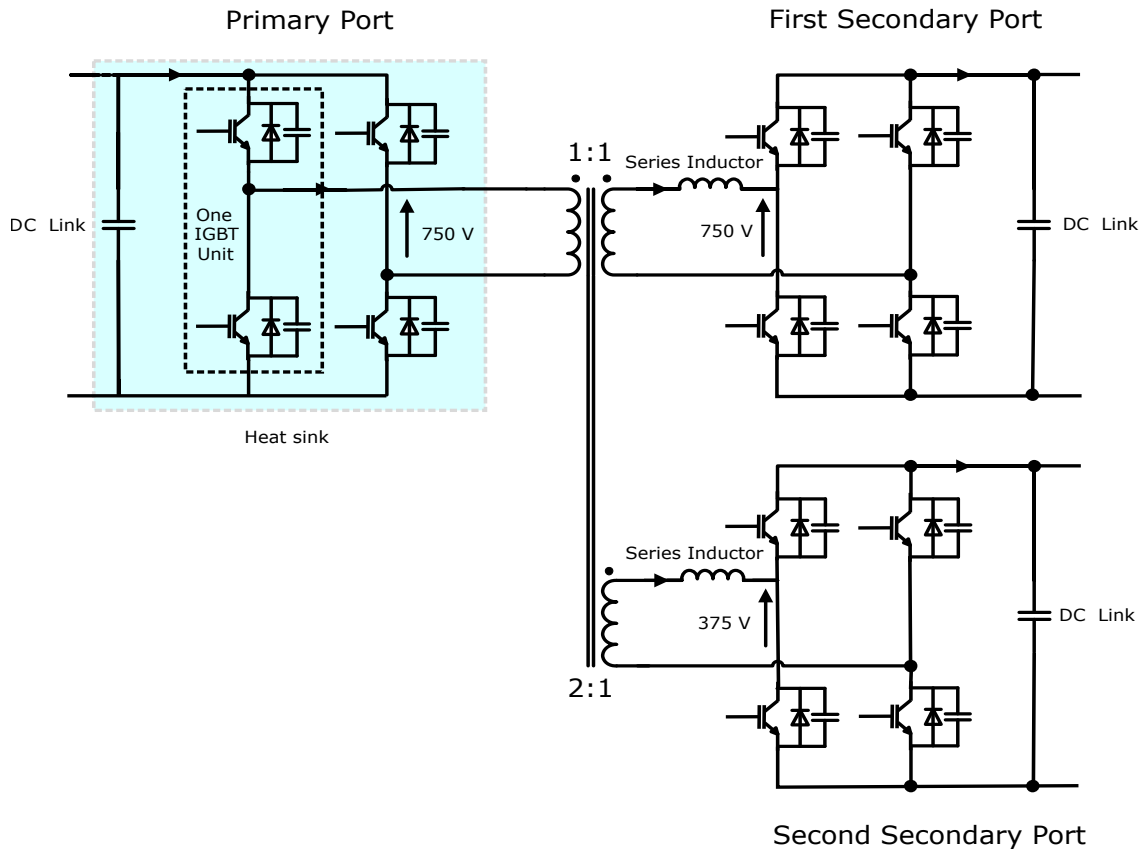


Figure 3-2: The triple-port active bridge Structure including some design specification and component naming.

Table 3.1: The Project specification and limitation.

The Maximum Power	150 (KW)	The Primary Port Voltage	750 (V)
The First Secondary Voltage	750 (V)	The Second Secondary Voltage	375 (V)
The Min. Battery Voltage	300 (V)	The Max. Battery Voltage	438 (V)
The Nominal Battery Voltage	396 (V)	The max. Charging current	100 (A)
The max. Discharging current	150 (A)	The Max. Peak-to-Peak Ripple	4 %
The switching Frequency	20 KHz		

Chapter 4

High frequency transformer

The design application required the voltages at the terminals of the transformers to be 750 Volts at the primary terminal, 750 Volts at the first secondary terminal, and 375 Volts at the second secondary terminal. The desired working frequency is set to be 20 KHz. And the power rating of the transformer was designed to be the maximum power of the micro-grid which is 150 KW.

4.1 Proposed Design

All this specification was sent to a company to manufacture the transformer with the requirements previously stated. It was a big issue to implement a transformer that could handle all this power with this extremely high frequency in just one core, that's what makes the company thinks to split the transformer into two separate cores. Of course the two separated cores will have two winding for each port, the design was made in order to make the two winding of the primary port should be connected in parallel, but the two winding of each port of the secondary ports should be connected in series.

Figure 4-1 shows the proposed structure of the transformer with it number of turns. Also Table 4.1 shows the parameter sent for the proposed transformer, the parameter includes the magnetizing inductance, the leakage inductance, and the series resistance of each port.

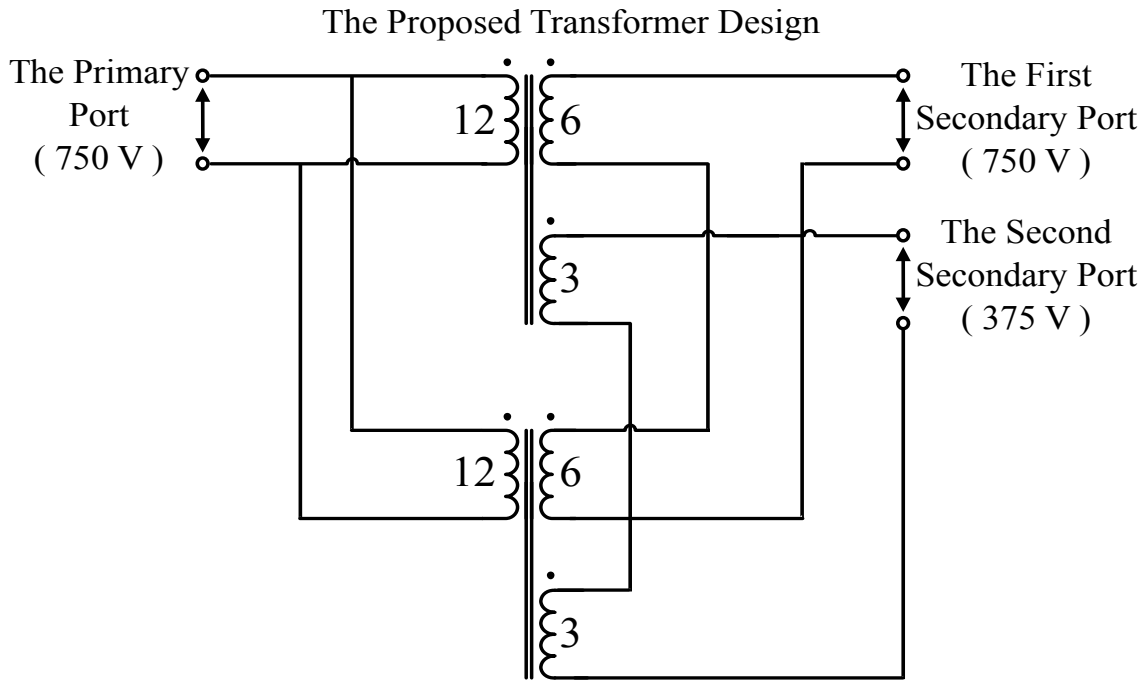


Figure 4-1: The figure shows a structure for the proposed transformer design with its number of turns.

Table 4.1: The parameter of the proposed Transformer.

	Primary (750 V)	First Secondary (750 V)	Second Secondary (375 V)
Magnetizing Inductance (mH)	2.3	2.3	0.48
Leakage Inductance (nH)	800	800	17.6
Series Resistance ($m\Omega$)	3.9	3.3	0.78

After having the proposed structure, and the parameters, a simulation had to be made in order to check if this matches the required performance or it will not fit the project requirements. For modeling the transformer there is a lot of ways to do it, found in literature three of them; The coupled inductor, Reluctance-resistance analogy, and Permanence-capacitance analogy [17]. The modeling of the transformer using the coupled inductor or the ideal transformer is the widely used and that's due to its simplicity as it replace all the magnetic elements and paths with electrical elements, inductors and resistances.

Figure 4-2 shows an example for a two-winding transformer, where $L_{\sigma 1}$ and $L_{\sigma 2}$ represent the leakage inductances, L_m the non-linear magnetization inductance and R_{fe} the iron losses. The copper resistances of the windings are modeled with R_1 and R_2 [17].

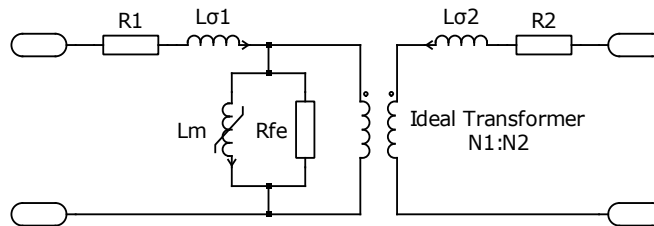


Figure 4-2: The modeling of the transformer using an ideal transformer, and the magnetizing inductance, and resistance, and the series leakage inductance and resistance [17].

However it has some drawbacks, it miss the physical structure beyond this components, as the parallel paths in the magnetic circuit is replaced with series inductors in the electrical equivalent circuit. Also for more complicated magnetic circuits like the multiple-winding transformers or integrated magnetic components, the equivalent circuit is going to be more complicated, difficult to drive and understand [17, 31]. And stated in [18] some cases in which the modeling using the coupling inductors fails, like the case of the E-core for three windings wanted to be modeled. If the voltage is fixed by the center winding as in the Figure 4-3 (a) the polarities on the winding will be as shown in 4-3 (b). The dots in 4-3 indicate the terminal of the positive polarity. Now if the voltage is fixed by the first winding as in 4-3 (c) the polarity

of the third winding is reversed, and did not reversed in its electrical model in 4-3 (d). Hence in this case, the modeling using the coupling inductors failed to describe the real polarity behavior of the windings, which is one of the main working concepts [18].

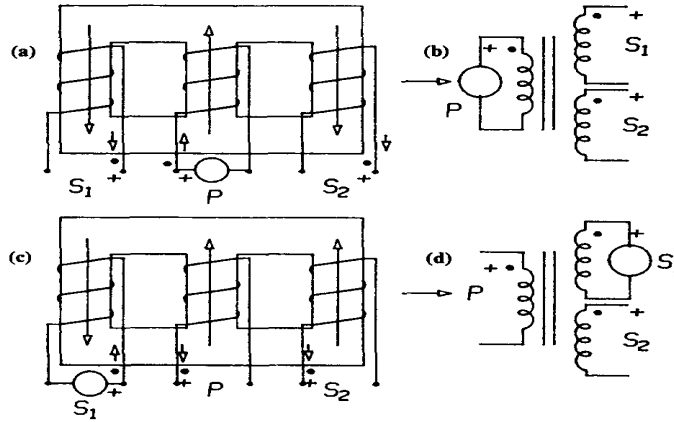


Figure 4-3: The Figure in (a) shows the structure of a E-core transformer where the center winding fix the voltage, in (b) the electrical modeling of this transformer using coupling inductors, (c) shows the same transformer in (a) but the voltage is fixed by the first winding, in (d) its wrong modeling due to the lag in description [18].

This modeling technique wasn't enough for the required simulation as the first issue, want to be tested is the effect of the decoupling of the two cores magnetically as it could affect the current sharing between the two ports.

For this reasons the chosen technique for the modeling will be the permeance-capacitance analogy. This technique represents the magnetic circuits, so it is a bit realistic and more accurate, as the effects of the magnetic elements could be simulated. The following equations will be needed in order to understand the modeling technique.

The Magneto-Motive Force (mmf) is the magnetic quantity that could be equivalent to the voltage in the electrical platform. While the Rate of change of the magnetic flux $\dot{\Phi}$ the magnetic one that represents the current. For this the first equation could be;

$$\dot{\Phi} = \frac{1}{\mathfrak{R}} \frac{dF}{dt} \quad (4.1)$$

The previous equation express the relation with the reluctance, which could be ex-

pressed with the permeances;

$$\dot{\Phi} = \mathcal{P} \frac{dF}{dt} \quad (4.2)$$

And in this case the permeance could represents the capacitance, and the permeance could be expressed as following

$$\mathcal{P} = \frac{1}{\mathfrak{R}} = \frac{\mu_0 \mu_M A}{L} \quad (4.3)$$

Those equation was for the magnetic equations also there is some equations that combine the magnetic with the electrical, the first on could be the equation of the flux produced by the voltage put on the windings;

$$V = N \dot{\Phi} \quad (4.4)$$

And the equation represents the current;

$$i = \frac{F}{N} \quad (4.5)$$

The simulation was made using PLECS software, this software was chosen for its ability of implementing the magnetic circuits. As the permeance-capacitance analogy has been implemented in PLECS by means of a special domain. The PLECS library contain all the magnetic components include windings, constant and variable permeances as well as dissipators. Now using this component, the physical structure of the transformer could be implemented.

For instance, the transformer previously modeled in Figure 4-2 could be modeled in the magnetic domain as shown in Figure 4-4. Where $\mathcal{P}_{\sigma 1}$ and $\mathcal{P}_{\sigma 2}$ they represents the primary and the secondary permeances of the leakage flux, \mathcal{P}_m represents the non-linear permeance of the core, G_{fe} represents the dissipates in the iron losses in the core, the two winding N_1 and N_1 represents the winding with their turns ratio, finally R_1 and R_2 represents the winding resistances those are the only elements represented in the electrical domain [17].

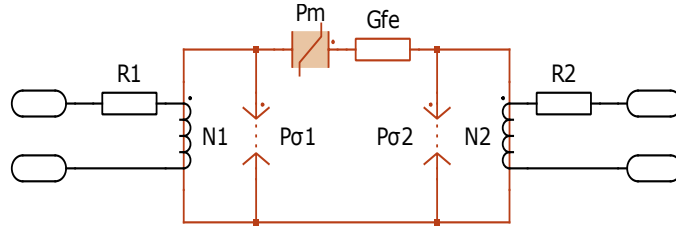


Figure 4-4: The PLECS model for the transformer shown in Figure 4-2 [17].

Now a simulation for the proposed transformer design have to be made, with the estimated parameter and also with some other parameters about the core material, and structure. Figure 4-5 shows the magnetic representation of the proposed transformer design with a two separate cores, by other words the two winding of each terminal will be magnetically decoupled.

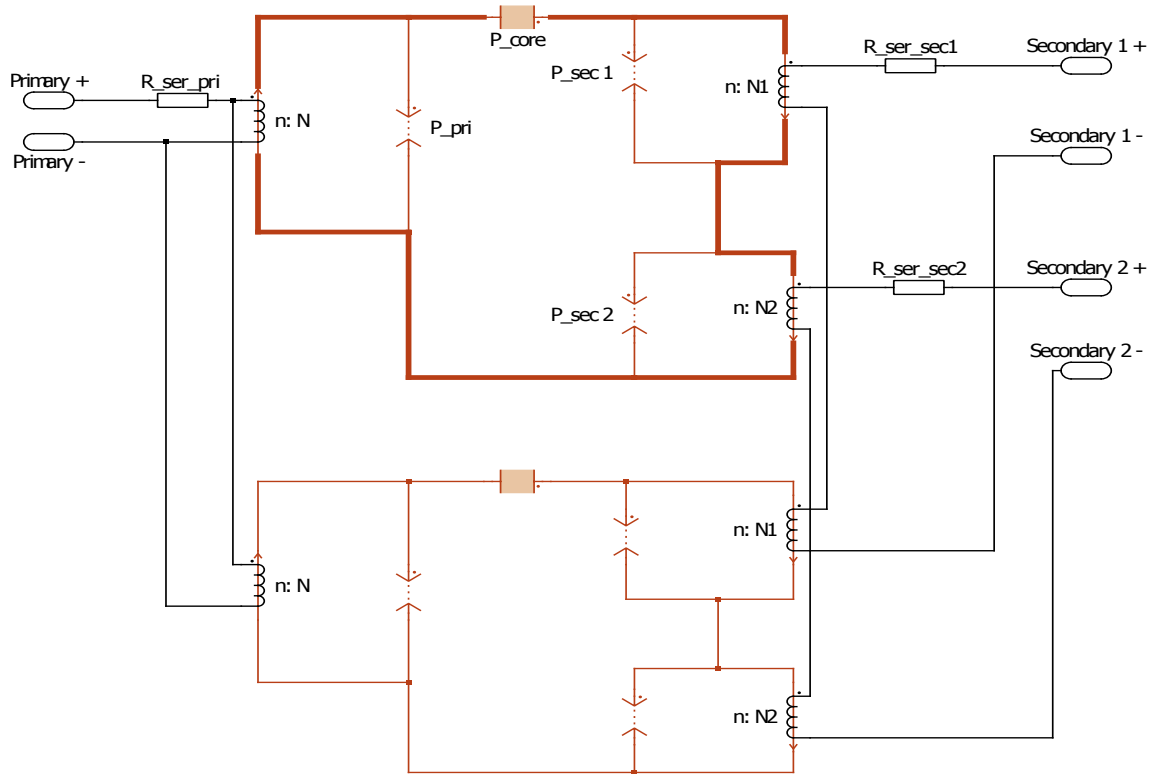


Figure 4-5: The PLECS model of the proposed three port transformer composed of two separated cores, with the two primary windings are connected in parallel, and the two winding of each secondary port are connected in series.

For completing the simulation some other parameter like the core material and

structure was required, and answered as following in table 4.3.

Table 4.2: The parameter of the Core used for the proposed transformer.

Core	Name	Ferrite N87
Material	Permeability	2444
Core	Cross-section Area (m^3)	$3694.45 * 1e^{-6}$
Structure	Effective Length (m)	0.2237

Table shows two extra pieces of information given by the company concerning the magnetic behavior of the proposed transformer.

Table 4.3: The flux density, and the leakage percentage of the proposed transformer.

The Peak flux density	210 mT
The leakage Percentage	0.1 - 1 %

Figure 4-5 shows the implementation of the transformer and here is a description for the methodology used for making this implementation. The simulation contain two identical cores, the core is represented by its main flux path (the highlighted path). The flux path contain three coupling inductors represents the ports windings, with their turns ratio specified in Figure 4-1. Also the flux path contain the Linear Core elements wish represents the magnetizing behavior of the core, by calculating its permeance for the entered parameters; the permeability of the material, the cross-section area, and the effective length, which are given in Table 4.3, putting those parameter PLECS uses the same equation (4.3) to calculate the permeance of the core. Then each coupling inductor have in parallel with it a Leakage Flux Path element, to represents the Leakage flux of each port, the element asks for the leakage flux permeance, it could be calculated by different ways one of them could be using the magnetizing inductance, the number of turns, and the leakage percentage, as

shown in equation (4.6).

$$\mathcal{P}_{Leakage} = \frac{LeakageRatio * L_m}{N^2} \quad (4.6)$$

The second core is represented exactly the same as the first one, now connecting the winding of the two cores as shown in figure 4-1. The two coupling inductors of the primary port are connected in parallel, while the two coupling inductors of each secondary port are connected in series. Finally a resistance is inserted at each port to represent the winding losses.

4.2 Transformer operation and performance

Some tests now should be done in order to first check either if the simulation is correct, and matching the specification sent by the company or no. Second to check the behavior of the proposed Transformer, if it is matching the project recommendation or no.

4.2.1 Transformer losses and non-ideality

In this test a square wave voltage source, with an amplitude equal to 750 Volts, will be placed on the primary port of the transformer. While a resistor that will represent the loads will be placed in the two secondary sides, with different values to represent different power. This test is made for testing the normal operation of the transformer by checking the voltages at each port, and the loading effect by checking the decrease of the voltage at different load values.

Figure 4-6 will be the first figure to illustrate as it will show the voltages and the current in each port, which is going to verify whether the modeling is working as a normal transformer or no. The test was made at the full load (150 KW), using a resistance at the first secondary port of value 5.625 Ω to absorb 100 KW and a resistance of 2.8125 Ω at the second secondary port in order to absorb the remaining 50 KW. fig(a) contains three plots each plot represents the voltage in blue, and the

current in red in each port, the first plot belongs to the primary port, the second plot belongs to the first secondary port (750 V) while the third plot belongs to the second secondary port (375 V). In fig(a) there is a dashed rectangle this is to indicate the part that fig (b) will show in a wide view, to will analyze it.

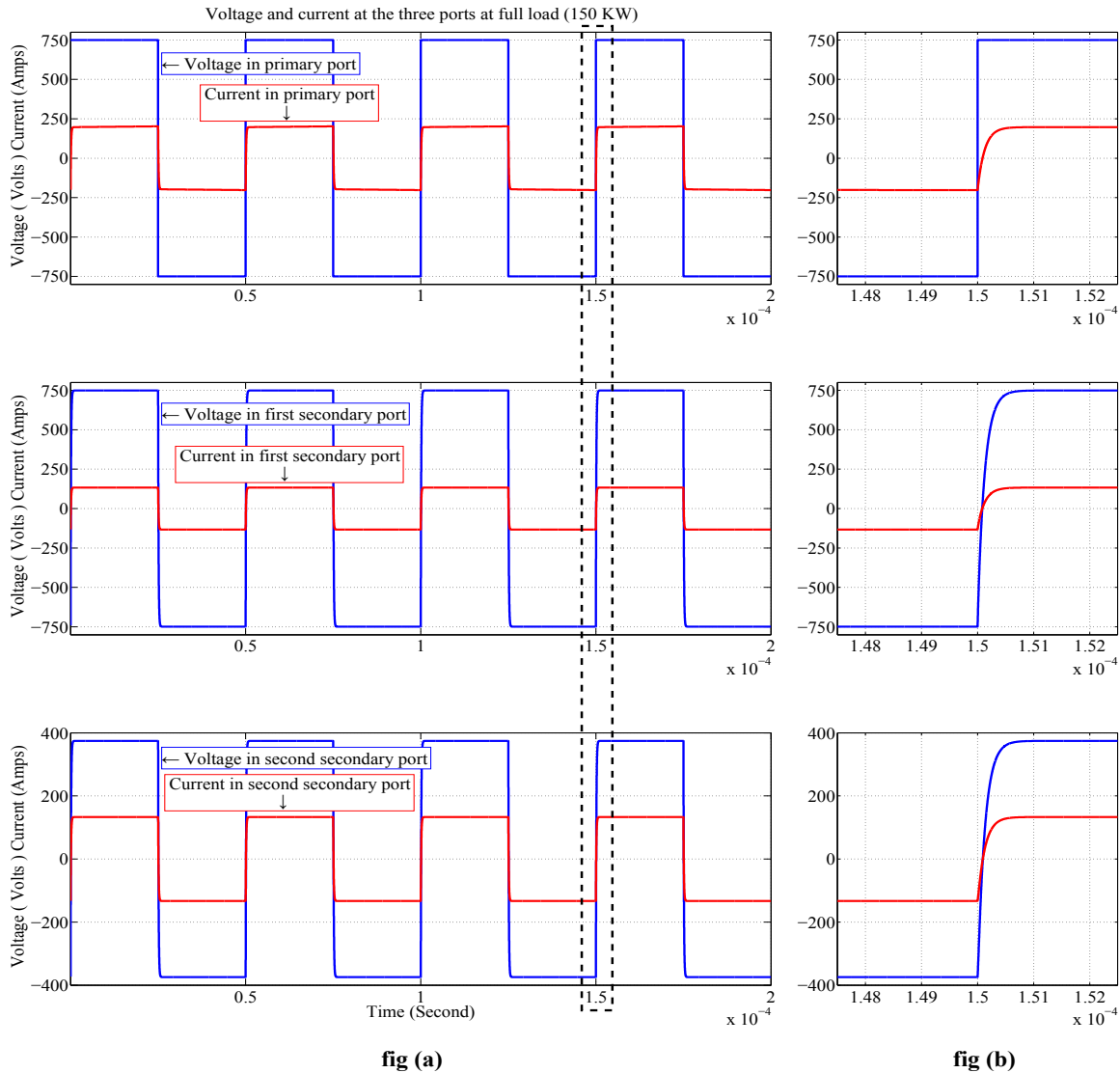


Figure 4-6: fig(a) contain three plots each plot represents the voltage in blue and the current in red in one port, the first plot belongs to the primary port, the second plot belongs to the first secondary port (750 V) while the third plot belongs to the second secondary port (375 V). In fig(a) there is a dashed rectangle this is to indicate the part that fig (b) will show in a wide view, to will analyze it.

Commenting on the previous figure, it is clear from fig(a) that the behavior of the transformer is fine as the voltages at the two secondary ports and the currents, follow the turns ratio given in the coupling inductors. Where the voltages at the three ports primary, first secondary, and second secondary are 750 V, 750 V, and 375 V respectively, and the turns ratio after taking into account the parallel and series connection will be 1:1 for the primary to the first secondary, and 2:1 for the primary to the second secondary. Where the currents peaks are equal to 200 A, 133.33 A, and 133.33 A respectively, which validate the behavior of the model. Now analyzing the effect shown in fig(b), the effect is that the current is not increased instantaneously, which make the voltage to follow it as the load is resistive load and don't follow the voltage on the primary port. This effect is due to the fact that this model is not simulating an ideal transformer, the presence of the leakage pass make the flux instantaneously goes to it then decreases to its steady state value. The opposite occurs at the core of the transformer the flux is increasing slowly till it reaches the steady state value, this flux is the one responsible of producing the current in the secondary windings, therefore the current will increase slowly till it reaches the steady state value the same occurs to the voltages as stated before the load is a resistive one.

Now looking at the real behavior of the transformer, the two important figures that could be illustrated are the losses and the voltage drop at the secondary winding at loading effect. Figure 4-7 shows in the first plot the power losses in the transformer with respect to the loading percentage, it is clear that the losses increases with the increase of the load as the power loss in the series resistance representing the winding resistance is proportional to the square of the current. One of the greatest advantages as said before of the high frequency transformer is the high efficiency, it is proved now from the simulation that the lowest efficiency which is going to be at the full load will be equal to 99.73 %. Very important this is the efficiency of the transformer only and this transformer unfortunately isn't a standalone device. The second plot shows the voltage drop at the two secondary ports it clear also that the voltage drop is increasing with the increase of the loading percentage, as the responsible of this effect is the flux leakage and it is proportional also with the current. It also clear

that the drop at the two port will be different but its percentage with the remaining voltage at each port will be the same.

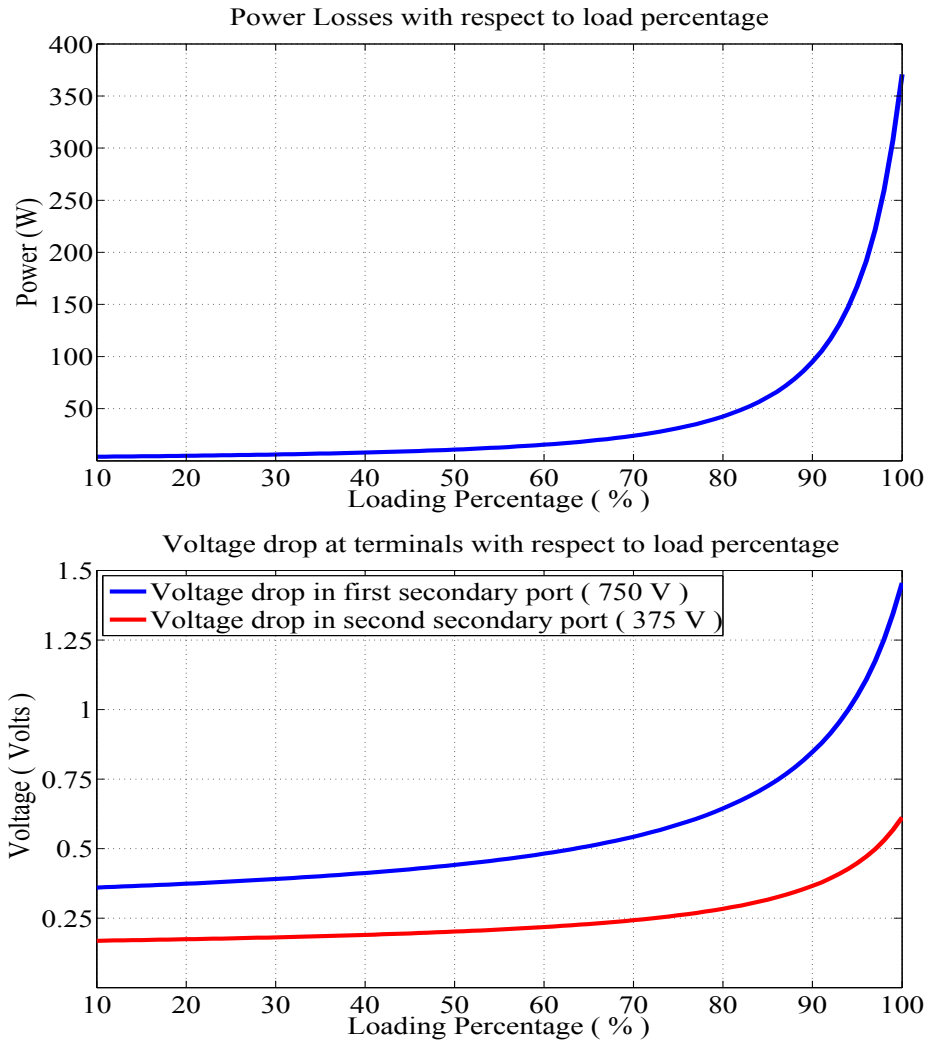


Figure 4-7: The first plot represents the Power losses, while the second one represents the voltage drop at the two secondary ports, both with respect the loading percentage.

Finally the last check for the normal operation will be, to check for either if the maximum value of the flux density inside the core of the simulated transformer is the same as the value given by the company to make sure that the modeling matches the real one. Figure 4-8 shows the flux density in the core of the proposed transformer, and it is clear from the data cursor shown in the figure that the peak of the flux density is more or less equal to the value sent by the company. (The simulation value = 206 mT while the Company one = 210 mT).

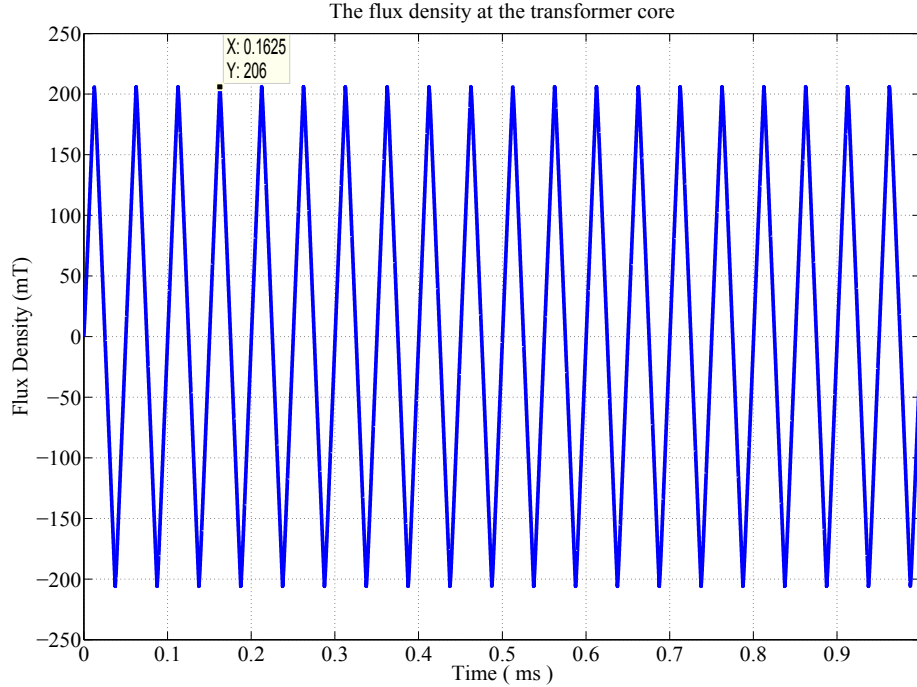


Figure 4-8: The flux density at the core of the transformer.

4.2.2 TAB operation and performance

In this test the TAB technique will be used to check the transformer behavior, as this is the topology recommended by the project. In this test the currents at each port will be illustrated at different combination of positive and negative shifts to check the shape of the current in each combination and compare it with the one shown in [12], the used inductor in this simulation is $40 \mu H$ placed at the two ports of the secondary.

Figure 4-9 is divided to six plots, each plot will show in dashed black the voltage at the primary port, in red the voltage at the first secondary port, in magenta the voltage at the second secondary port, and in blue the current, at different combination of phase shifts. Each plot of the six plots represents a combination of the two shifts of the two secondary ports which is stated on top of it. It is clear that the current in all the cases matches the behavior of the cases in [12]. Which verify the ability of the proposed transformer to work as a SST inside a triple port Active Bridge.

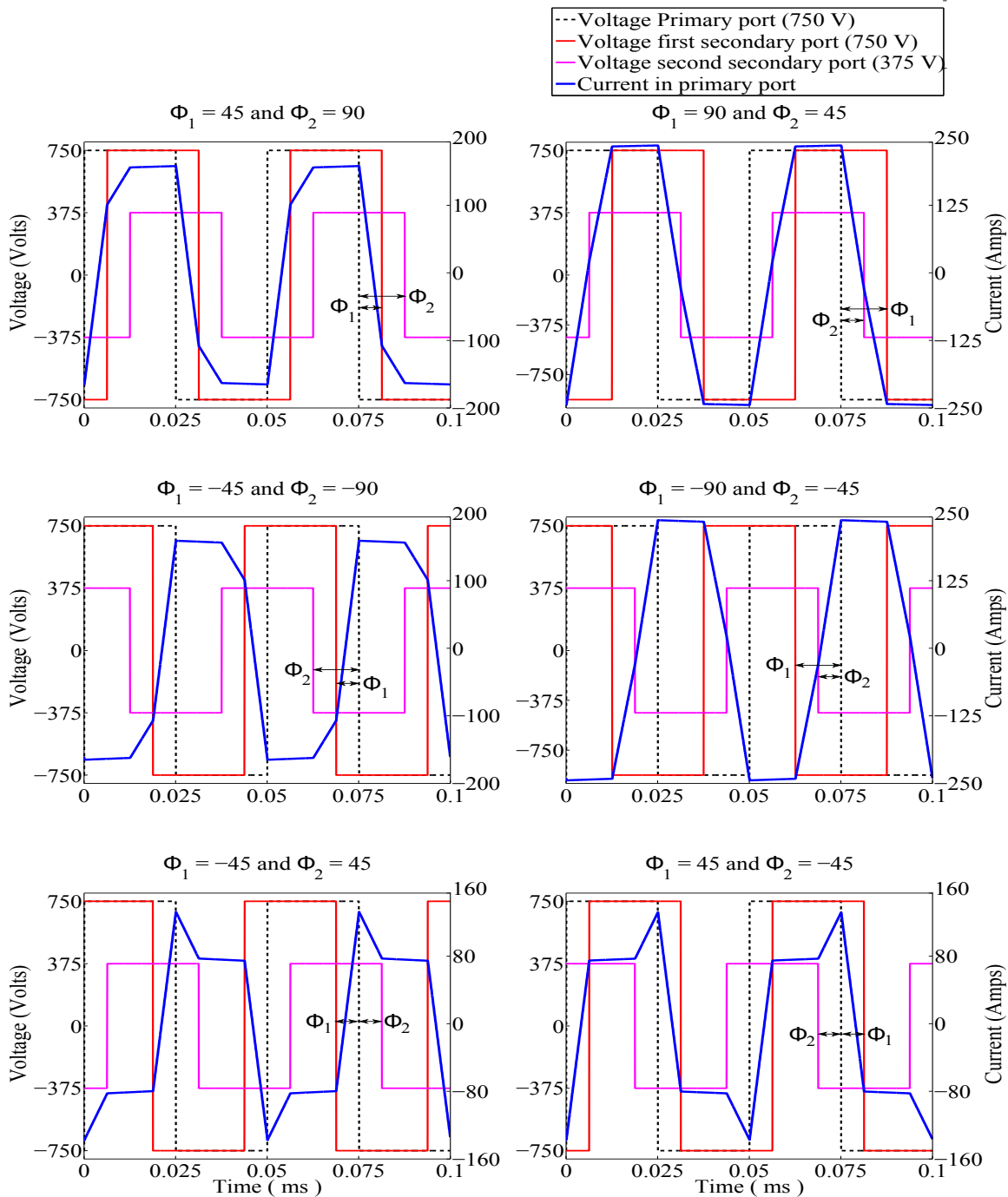


Figure 4-9: Each plot shows in dashed black the voltage at the primary port, in red the voltage at the first secondary port, in magenta the voltage at the second secondary port, and in blue the current. The combinations mainly represents two case with the two shifts are positive, the first one the shift belongs to the lower voltage port is bigger (first plot), and the second the opposite (second plot). Two others with negative shifts, the first case where the shift belongs to the low voltage port is deeper in the negative (third plot), and the second is the opposite (fourth plot), then one with negative shift at the high voltage port, and positive shift at the low voltage port (fifth plot), and the opposite (sixth plot).

4.3 Alternative design: Magnetically coupled core

One of the most important test that should be done after knowing that the transformer will be split into two cores, is a test to compare its behavior with a magnetically coupled core. To check if there will be a mismatch in the working behavior, special in the currents in the parallel winding of the primary port as it may have a rotating current.

Figure 4-10 shows the invented magnetic circuit that will represent the single core transformer. Of course now the number of turns will not be compatible with this design, so the number of turns will be changed in order to keep the voltages ratio be the same.

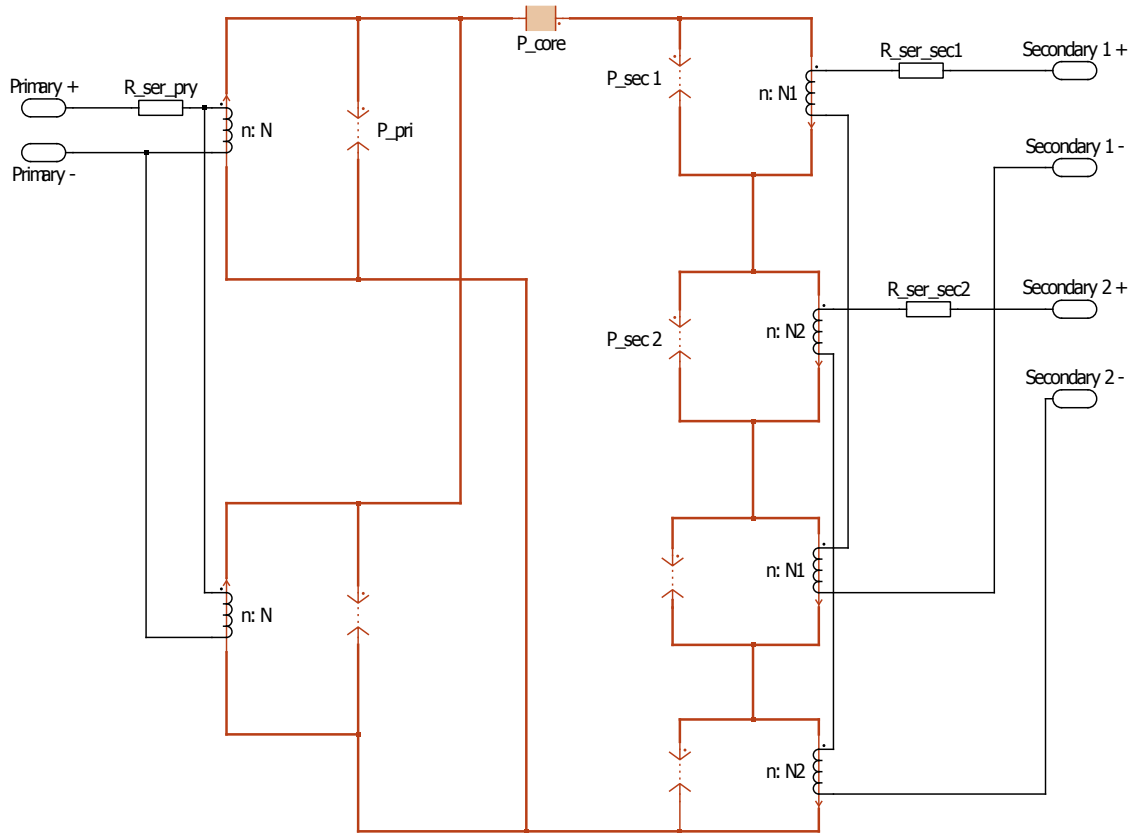


Figure 4-10: The magnetic circuit for the invented transformer that will have the same number of windings with the same connection between them, but placed on one core.

In order to determine the number of turns that will be compatible with this new

structure, Faraday's Law have to be used.

$$V = -N \frac{d\phi}{dt} \quad (4.7)$$

The ratio between the primary port voltage, and the first secondary port voltage is 1 : 1. But the flux going to each one of the secondary winding is the addition of the two flux of the two primary winding, also the voltage of the secondary is equal to the addition of the two voltages of the two windings. Therefore the number of turns at the primary windings will be equal to four times the number of turns of the windings of the first secondary port. As the ratio of the voltages of the primary to the second secondary is equal to 2 : 1, so the number of turns of the primary windings will be equal to eight times the number of turns of the second secondary windings.

The behavior of the two cases in the ideal simulation where all the parameters of the two transformers are equal. But if there is any mismatch in the parameter which could happen in the practical world, the single core transformer won't be affected but the dual core transformer will.

The following will be the effect of each parameter mismatch in the dual core transformer;

4.3.1 Effects of primary windings resistance asymmetries

This is the highest probability mismatch, as the resistance of the windings could be changing and affected also. The simulation will separate the equivalent resistance of the primary into two were each winding will have its resistance, and the current in each winding will be measured to detect the difference. As said before at two equal resistance in both the single core and the dual cores will have exactly the same current in the two windings. In this simulation the resistance of the second winding of the primary port will be equal to 150 % of the resistance of the first winding. In the single core difference in the current of the two windings will be zero. But for the dual core Figure 4-11 shows the difference in the current in the two windings of the primary ports. It is clear that even for a mismatch of 50 %, which is the double of

the error percentage proposed by the company, the error is not a problematic for the application, as it is increasing in the beginning till a maximum value equal to 0.21 Amp then goes again to zero.

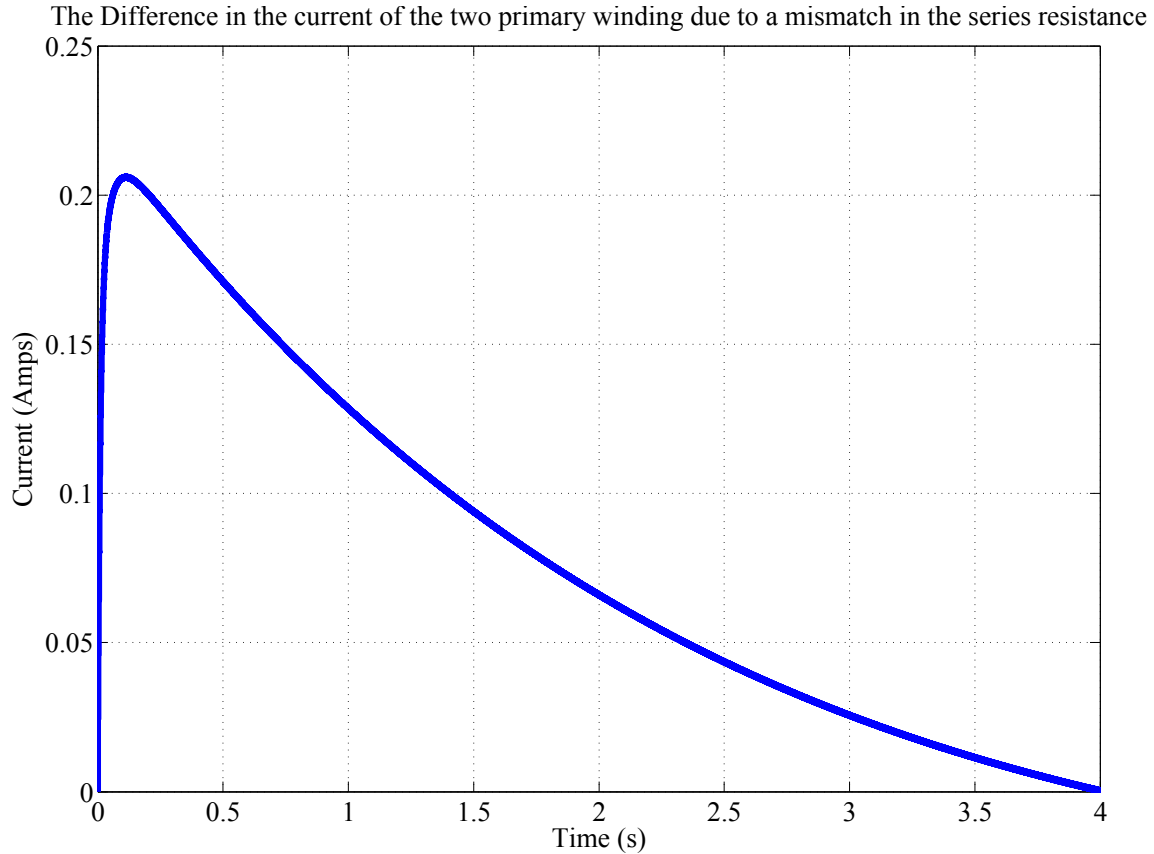


Figure 4-11: The difference in the current of the two windings of the primary port due to a change of 50 % of the series resistance of only one winding than the other winding.

4.3.2 Effects of parameters mismatch between the two cores

One other mismatch could be that one of the parameter like the effective length, or the core area of the two cores are a bit different. The following simulation will simulate a mismatch of 10 % in the effective length of one core than the other. Also the difference in the current in the single core transformer is equal zero, and Figure 4-12 shows the difference in the current in the dual core transformer. The difference make a triangular waveform with a peak value equal 0.15 Amp, and a DC value of

40 mA, which is not a problem at all.

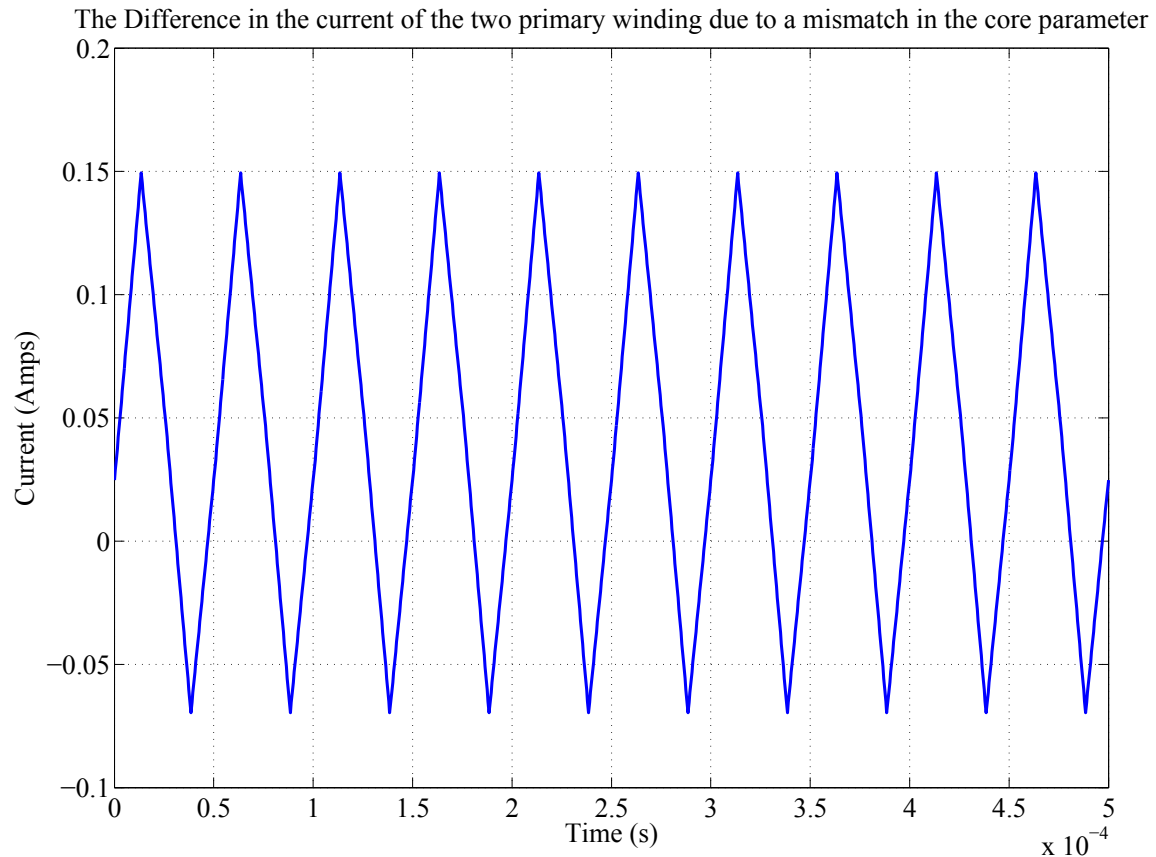


Figure 4-12: The difference in the current of the two windings of the primary port due to a change of 10 % in the effective length of the parameter of one core than the other one.

4.3.3 Effects of leakage flux asymmetries

The last mismatch that could be done is a mismatch in the leakage of the two coupling inductors, so a permeance of one of the two winding is changed to become 110 % of its value, and the second remain the same. Also for the single core the difference is zero, but Figure 4-13 shows the difference in current of the dual core transformer. The difference waveform shape is more or less like the shape of the primary current, but with a peak value equal 7.95 mA, and with a DC value equal zero.

The proposal was approved as its behavior is matching the recommended one by

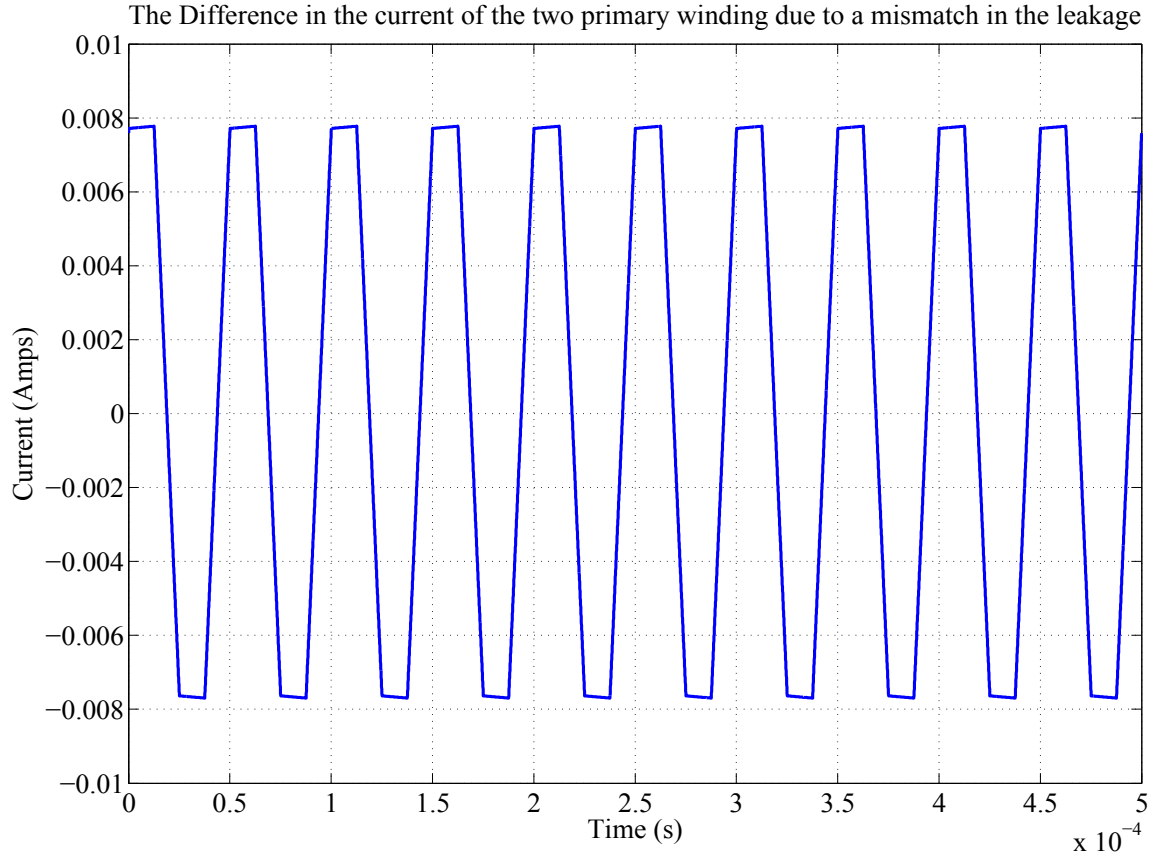


Figure 4-13: The difference in the current of the two windings of the primary port due to a change 10 % in the permeance capacitance of one coupling inductor than the other one.

the full project, and matches all the limitations specified by the project.

Table 4.4 show the dimensions of the Transformer, also Figure 4-14 shows the assembly of the mechanical design of the transformer, and finally Figure 4-15 shows a picture for the real Transformer.

Table 4.4: The Transformer Dimensions.

The Length (mm)	The Width (mm)	The Height (mm)
375	327	73

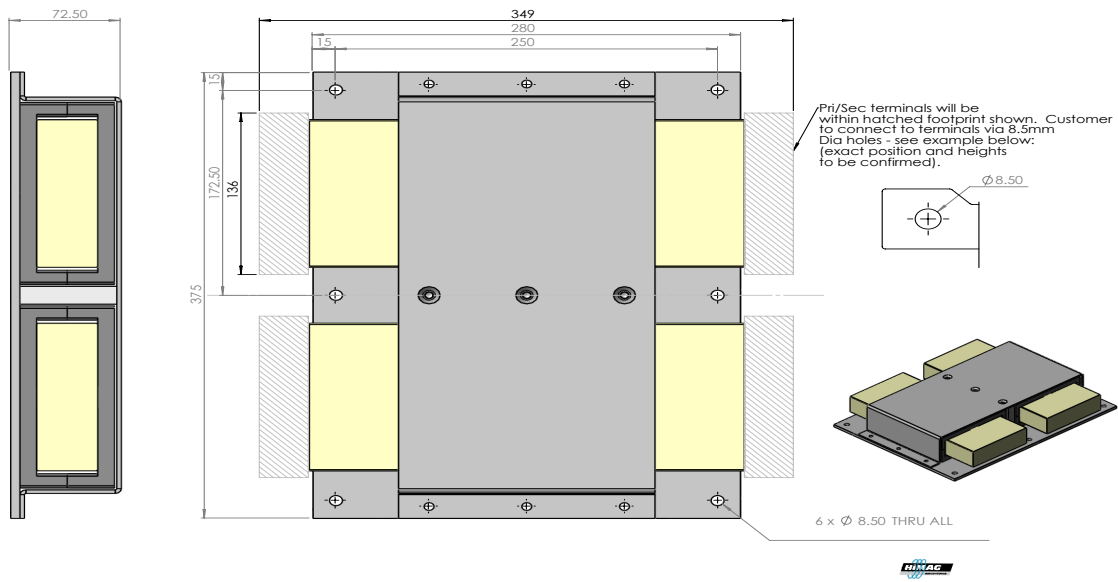


Figure 4-14: The assembly of the mechanical structure of the transformer.

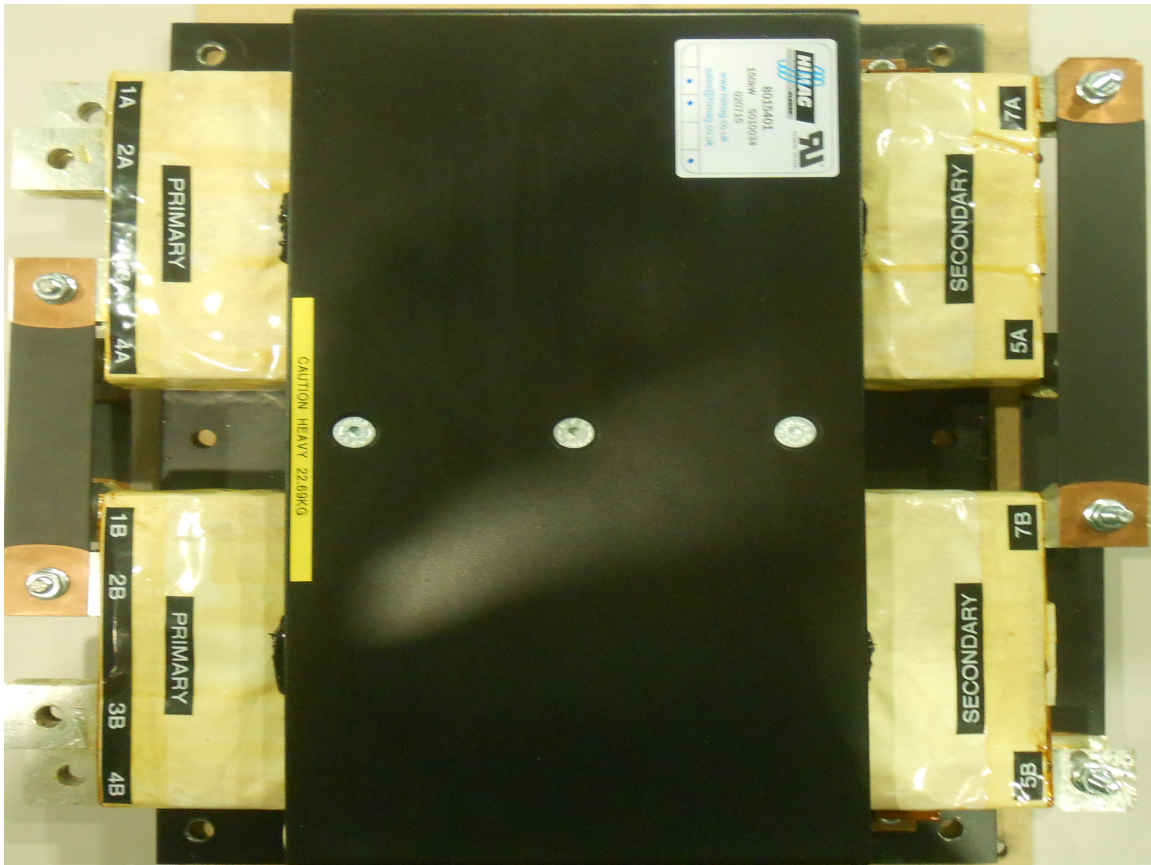


Figure 4-15: This figure show the real transformer.

Chapter 5

Reactive Elements Design

5.1 Inductor Design

The inductor in the TAB could be considered as the key element in the converter, as it is the main element that control the power flow direction and quantity, and filter the current also. For this reason this chapter will discuss how the value of the inductor will be chosen, what is the parameter that it should be taken into account in the design.

5.1.1 Role of inductor in TAB operation

The SST inside the TAB could be represented as shown in Figure 5-1. The inductors in the figure represents the Leakage inductance of the transformer, and as stated in Table 4.1 the value of the leakage inductance are very small. Which make the operation of the TAB depending only on the Leakage inductance impossible, as the ripple of the current will damage everything. Which make an additional inductor should be placed, But there will be two question coming to our mind now. How to choose the inductor values? And that's what is going to be answered in the following section. And where to place them? Which is going to be answer in the section after [12].

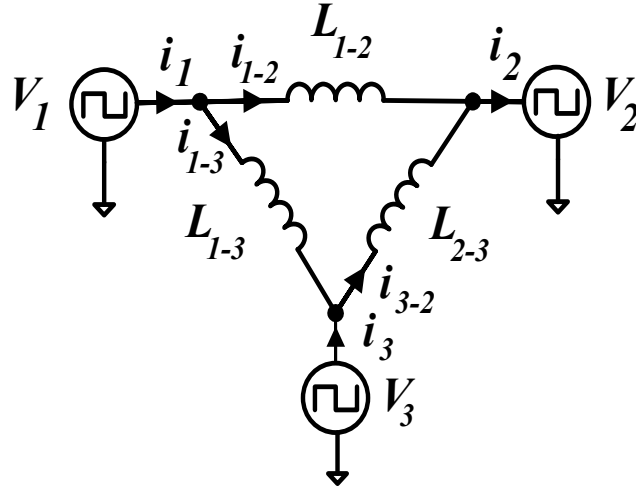


Figure 5-1: The inductor representation of the transformer [12].

5.1.2 Design of the inductor

How to select the inductor value ? to answer this question it is better to ask first what is the variables that are affected by the value of the inductor. And the answer would be two main things, the current slop, and the value of the maximum power that want to be delivered. The full project will decide the limitations that have to be fulfill be the choice of the inductor value.

Maximum Current relation and limitation

The maximum value of the current is really important in choosing the value of the inductor as the current depends only on the inductor and the voltage that is already decided by the project, and the maximum current could be a problem for the IGBT ratings. To determine the relation between the maximum current and the value of the inductance the equation of the current in the inductor previously stated Equation 2.1 will be used, with the values that already decided.

Figure 5-2 shows the waveforms of the voltage at the two inductor terminals in the first plot, in the second the voltage on it, and in the third plot the current in the inductor. Using this figure for getting a general Equation that gives the maximum value of the current in terms of the inductor value.

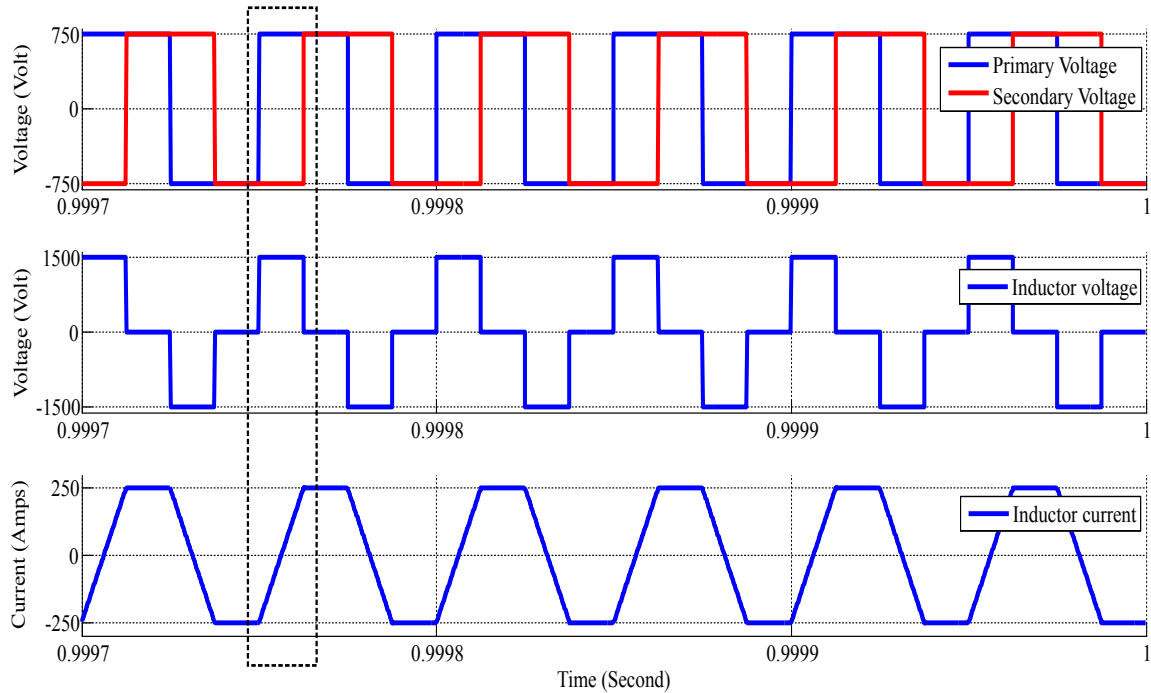


Figure 5-2: The first plot shows in blue the primary voltage and in red the secondary voltage, the second plot shows the voltage at the inductor terminal, and in the third plot shows the current in the inductor.

The current slop could be determined from following equation;

$$\frac{\Delta i}{\Delta t} = \frac{V_L}{\omega L} \quad (5.1)$$

Rearranging equation 5.1 it could be;

$$\Delta i = \frac{V_L \Delta t}{(2\pi f_{sw}) L} \quad (5.2)$$

Now using the information known about the behavior of the TAB, and as shown in the figure 5-2, the voltage on the inductor is equal to double of the voltage value of the secondary port during the phase shift, and equal zero in the rest of the half period. At the second half the voltage will be negative the double of the voltage at the phase shift and zero at the rest of the half period. This is for ideal case but for real it will be different as there is a field weakening will make the voltage will be a bit lower, but this consideration is accepted here as the design should be for the worst case.

For knowing the maximum value of the current we should focus on the dashed rectangle in Figure 5-2, and from it the following equation could be got;

$$\Delta i = \frac{2V_{sec}\phi}{(2\pi f_{sw})L} \quad (5.3)$$

For steady state the current vary from the negative maximum value to the positive maximum one. So the variation of the current could be double of the maximum value of the current. Concerning the phase shift it should be the maximum value that it will be in this case π , but normal the control limit the phase angle to be from $-\pi/2$ to $\pi/2$, so the maximum current will occur at $\pi/2$. Therefore the final equation for the maximum current could be;

$$I_{max} = \frac{V_{sec}}{4f_{sw}L} \quad (5.4)$$

The previous equation calculate the value of the maximum current at any one of the secondary ports, but for the design point of view the maximum current value will be at the primary side while the addition of both currents happen. Therefore the equation for the maximum value of the primary side current will be as following;

$$I_{primary_{max}} = \frac{N_2}{N_1} * \frac{V_{sec1}}{4f_{sw}L_1} + \frac{N_3}{N_1} * \frac{V_{sec2}}{4f_{sw}L_2} \quad (5.5)$$

Using equation (5.5), Figure 5-3 was plotted, as the colored plane represents the maximum value of the primary current with respect to the value of the two secondary inductors, the black surface indicate the 300 Amps. The intersection of those two surfaces create the blue contour (line) in the x-y plane that represent the different values of inductor that gives a 300 Amps as a maximum value for the current at the primary side. The red line in the x-y plane also represents the line for equal inductances at the two secondary sides, for symmetrical design.

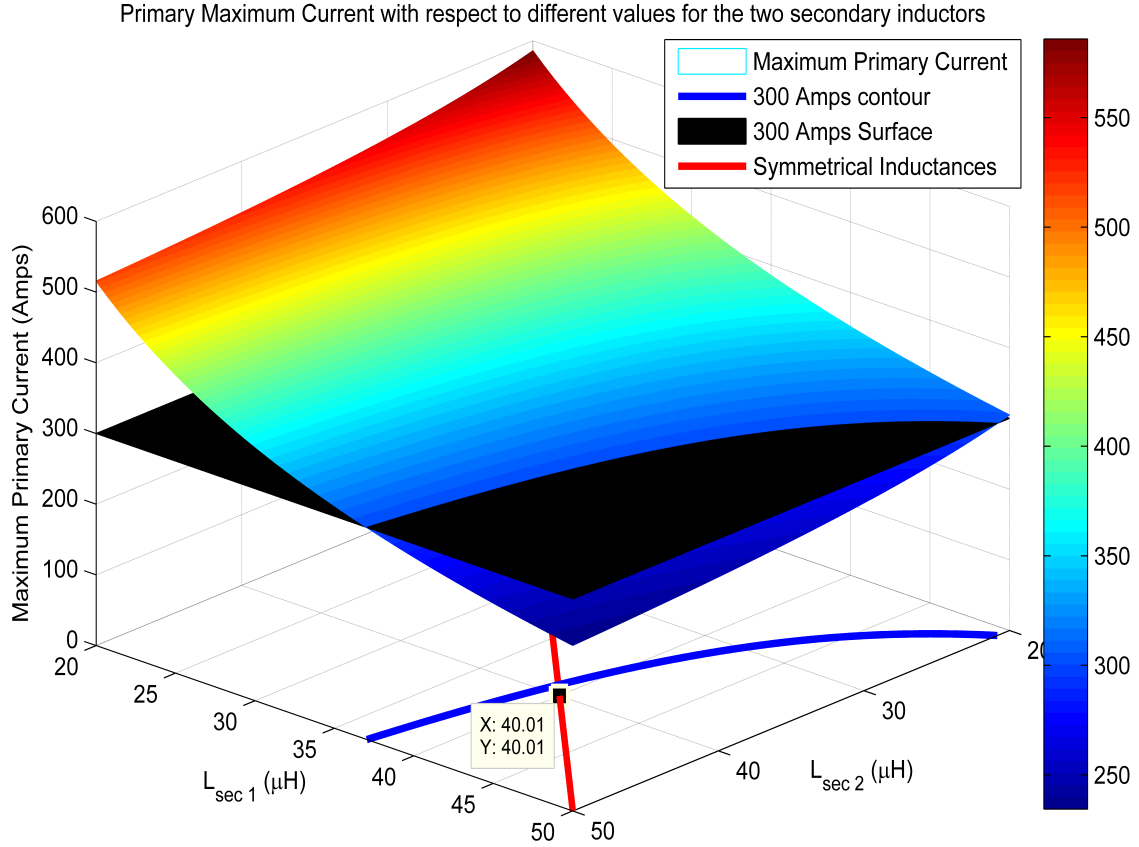


Figure 5-3: The colored plane represents the maximum value of the primary current with respect to the value of the two secondary inductors, the surface indicate the 300 Amps. The intersection of those two surfaces create the blue contour (line) in the x-y plane, The red line in the x-y plane also represents the line for equal inductances at the two secondary sides.

Maximum Power relation and limitation

As the current is only affected by the value of the inductor, this is after fixing the voltage value and the switching frequency, so the inductor will play a main role also in the values of the power. The equation of the power transfer in the TAB or even in the DAB is well known, as stated in [32, 33, 34, 35] the equation of the power could be as following;

$$P = \frac{V_{sec}^2 \phi (\pi - \phi)}{(2\pi f_{sw}) L \pi} \quad (5.6)$$

From equation (5.6), it is clear that as the value of the inductor decreases the

power transfer is maximized. A good approximated value for the two inductances in $40\mu H$.

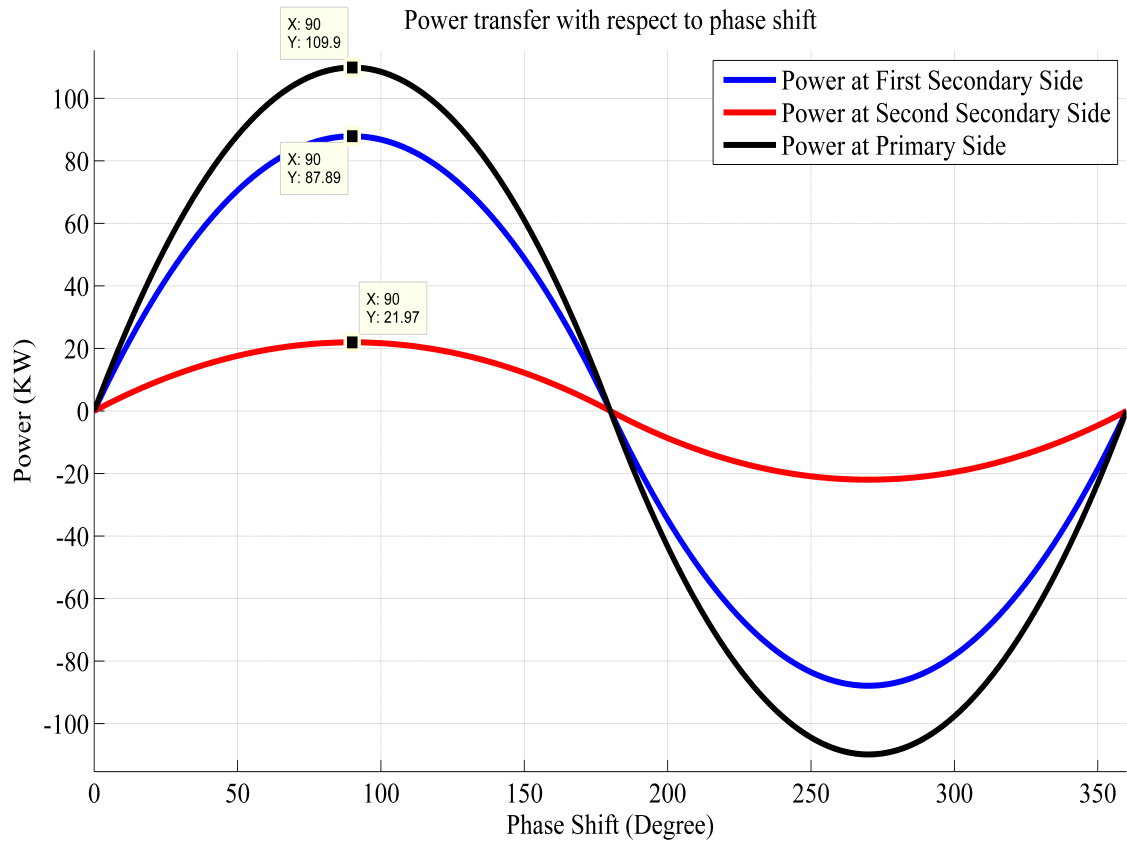


Figure 5-4: The Power Output at different phase shift value, for two secondary inductances of $40\mu H$. In red the power at the second secondary port, in blue the power at the first secondary port, and in black the primary port power.

From Figure 5-4, it is clear that the maximum power value at phase shift equal to $\pi/2$, putting this shift value in the equation 5.6, it will produce the following equation;

$$P = \frac{V_{sec}^2}{8f_{sw}L} \quad (5.7)$$

The value chosen for the inductors is $40\mu H$, now substituting it in equation (5.4) and (5.7) to generate the following table, which has the the values of the maximum powers and maximum peak current at all the three ports;

Table 5.1: The theoretical values for the maximum power and maximum peak current at all the ports of the transformer for the $40\mu H$ inductors

	Primary (750 V)	First Secondary (750 V)	Second Secondary (375 V)
Maximum Power (KW)	109.86	87.89	21.97
Maximum Peak Current (Amps)	292.97	234.375	117.1875

Finally, it is clear that the chosen inductor value gives a maximum peak current is a bit bigger than which the IGBT could support, and also the maximum value of the power is a bit bigger than the one required in the application, this due to three main reasons;

- The leakage inductance will increase the value of the series inductance which will decrease this values again.
- This equation did not take into account the value of the voltage drop due to; the series resistances, the switches forward voltages, and the loading effect.
- This maximum value are the ultimate values which will not be reached in the practical application.

5.1.3 Comparing the Symmetrical Design inductors at all the ports with the Single side inductors at the Secondary

Now answering where to put the inductors, there is mainly two options; whether the inductor that previously calculated its value is putted in a the secondary port, or to slit this inductance value to put it in the three ports, which is called the Symmetrical method. Figure 5-5 shows the inductive module after adding the inductance, fig (a) shows the TAB with only two inductors placed at the two secondary port, while fig (b) shows it but for a symmetry design where three inductors placed in all the ports.

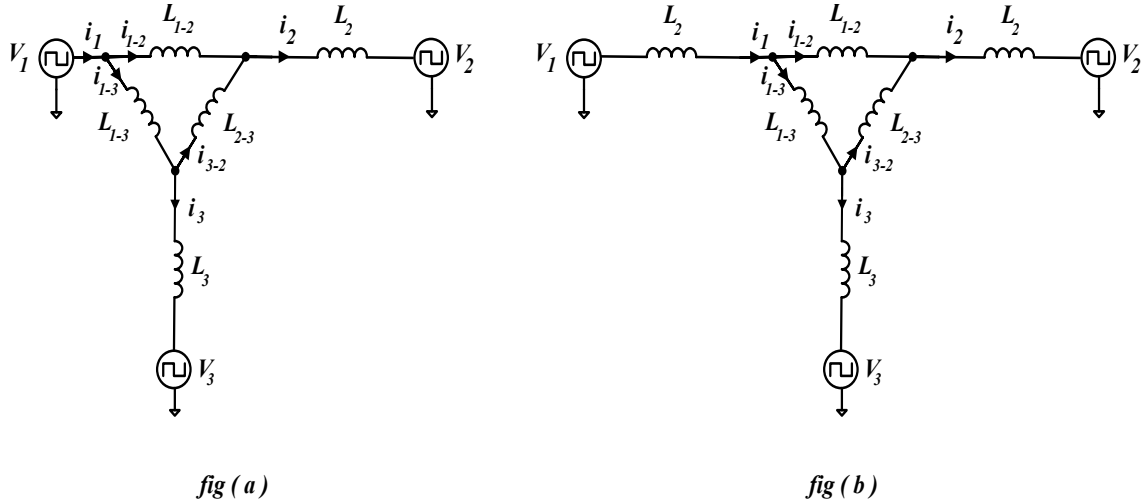


Figure 5-5: fig (a) shows the inductive model for the TAB with two inductors placed at the two secondary port, while fig (b) shows the model but for a symmetry design with inductors in all the ports.

The choice was made by analyzing the operation behavior of both options, the first option has I great advantage is that, the leakage inductance could be considered negligible with respect the Series inductance. Is this a benefit, of course it is as this is going to make the voltage at the two other terminals of the inductor fixed by the primary voltage. Now if it is needed to send power from primary to first secondary, so if a proper phase shift is made the voltage waveform of the first secondary port, the power will only flows from primary to first secondary. The same case occurs if the port waited to be send to the second secondary, and if from the first or the second secondary to the primary. Only one drawback is that if it is required to send from the first secondary port to the second secondary port or vice versa, that will make one of them will have a positive angle and the other will have a negative one that gives the same amount of power, and the drawback here is that the power will flow through the primary even if it is not used. What about the second case, it is very complicated, as for example if it is recommended to send power from the primary to the first secondary port, it is not possible to just shift the first secondary port, as if this occurs it will absorb power not only from the primary, but also from the second secondary port. Therefore the control here should shift the second secondary

port with a way that makes the average current going to this port equal zero, but the current will flow there even if it is not used. Therefore due to the complexity and the lower efficiency of the second case, the first one was chosen.

5.1.4 Manufacturing and Analysis

Finally this value was sent to the manufacturer, with some waveforms for the current passing through the inductor, at the worse case which is by sending the max. power at each port alone. The manufacturer reply by the proposal illustrated in Table 5.2 it was also a big issue to construct this value of inductance, that could support the all this current. So the proposal of the manufacturer was to split it into two series inductors each $19 \mu H$. And Table 5.3 shows the dimensions of one piece of the proposed inductor.

Table 5.2: The proposed Inductor Specification.

The Ripple current frequency	20 (KHz)	Inductance	19 (μH)
The max. RMS current	167 (A)	The max. Peak current	205 (A)
The Estimated Power Losses	106 (W)	The Estimated Hot spot Temperature	125 ($^{\circ}C$)

Table 5.3: The Inductor Dimensions.

The Length (mm)	The Width (mm)	The Height (mm)
215	136	60

Finally a simulation is made taking into account the estimated losses in the inductor. Figure 5-6 shows the efficiency of the converter taking into account the losses in the transformer and the inductors. Previously the losses of the transformer only makes the efficiency become 99.7 % , now after adding the losses of the inductor the efficiency drops to 99.24 % as shown in the figure. However this losses percentage in

the inductors are too small as they are ferrite inductor, which is characterized by its small parasitic series resistance.

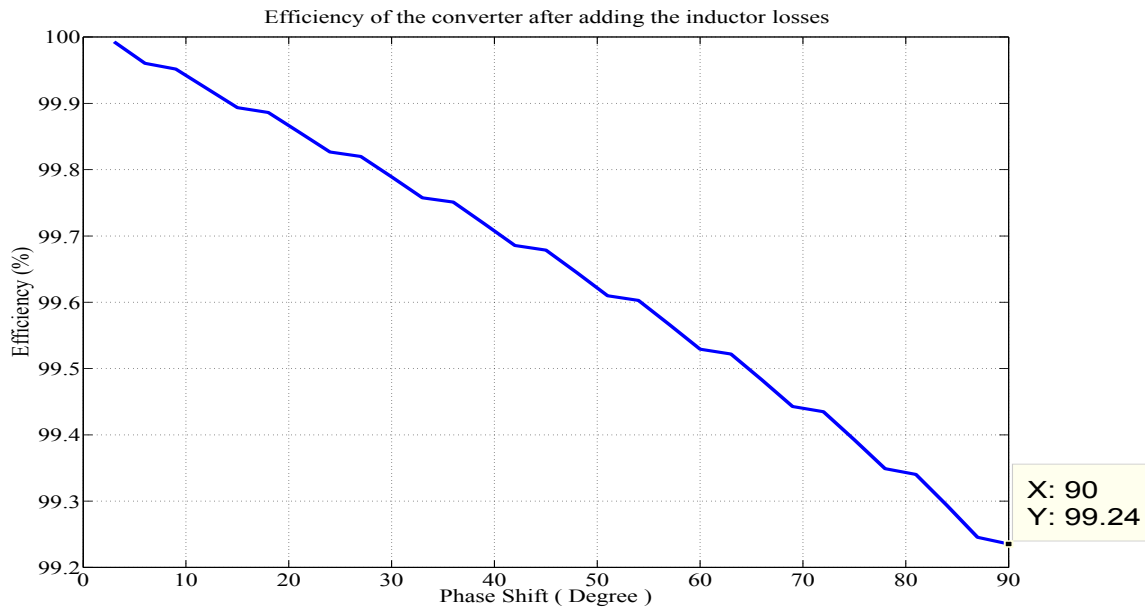


Figure 5-6: The efficiency of the converter taking into account the estimated losses in the inductor and the losses of the transformer.

5.2 DC-Link Capacitors Design

As previously said the TAB topology have one drawback which is its huge current ripple, that's what indicate the importance of the presence of the DC-Link. The DC-Link advantage is to create a new path of the high frequency ripple in the current, and paths the DC-component and a part of this ripple depending on the capacitance value used in the DC-Link [36].

Following the procedures explained in [36], but with applying it the the TAB topology. The first Step is to find the Maximum Peak to Peak ripple, as Equation (5.4) gives the maximum peak current therefore the maximum peak to peak current will be the double of this equation;

$$I_{p-p} = \frac{V_{sec}}{2f_{sw}L} \quad (5.8)$$

Now the calculation the ripple in the voltage, given the equation of the capacitor in [36];

$$dV = \frac{i_c}{c} dt \quad (5.9)$$

and the current in the capacitor is the ripple of the inductor, therefore the equation will be;

$$dV = \frac{V_{sec}}{2f_{sw}LC} \quad (5.10)$$

Applying the same integration role to this equation it will be;

$$\Delta V = \frac{V_{sec}\Delta t^2}{4LC} \quad (5.11)$$

Then as said before the maximum current appears at the maximum shift $\pi/2$ which represents 0.25 the period. Which make the final equation of the ripple in the voltage be;

$$V_{p-p} = \frac{V_{sec}}{64f_{sw}LC} \quad (5.12)$$

Figure 5-7 shows the a graph of the ripple voltage value with respect to the DC-Link capacitance value. In blue the ripple in the first secondary port where the voltage equal 750 V, and in red the ripple in the second secondary port where the voltage equal 375 V. It is clear that at the beginning the value of the ripple voltage decrease a lot with the small increase of the capacitance value, but after a while the increase of the capacitance is just increases the cost much but don't affect the ripple value much.

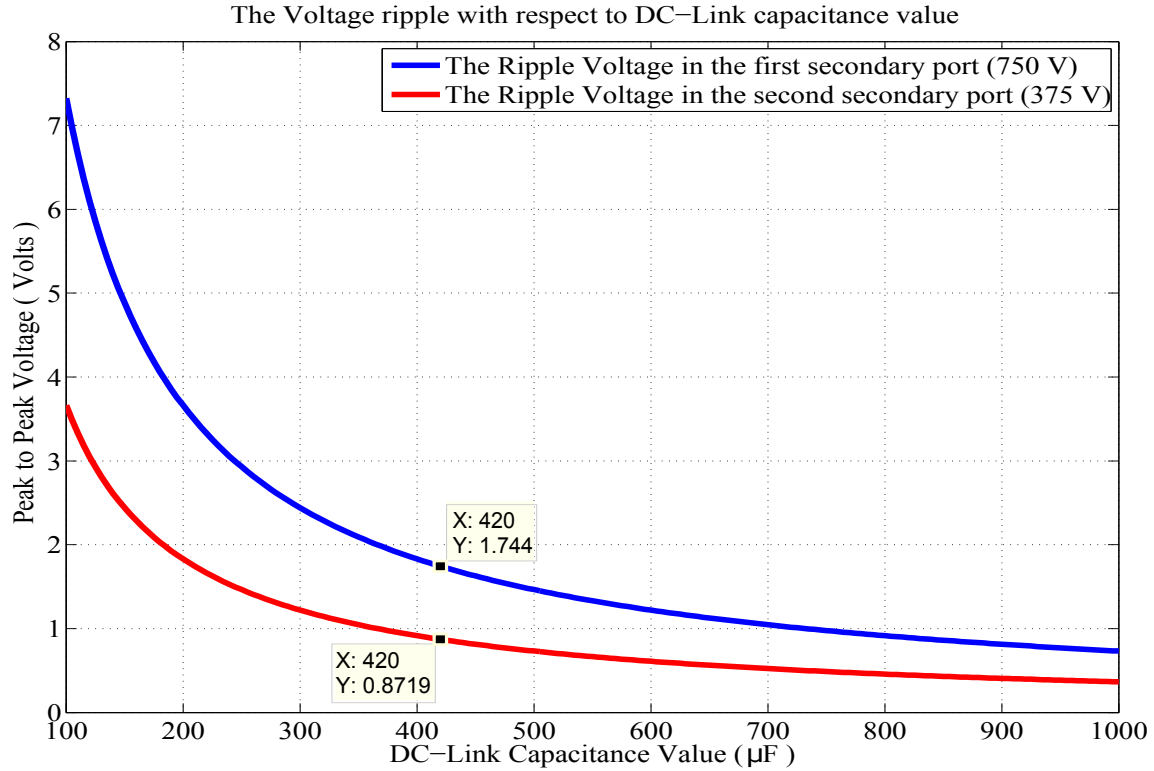


Figure 5-7: The Ripple voltage with respect to the DC-Link capacitance value, in blue the ripple at the first secondary port, and in red the ripple in the second secondary port.

Now before choosing the value of the capacitors, it is obvious to choose first its type, as for power DC-Link there is two main types; there is the normal electrolytic capacitors, which are characterized by there low cost per farad [36], or the new technology which is the film capacitors. In order to answer this question the limitation of the RMS current that can be handled by each type should be studied. Putting the project parameter values in equation (5.8) and divide it by two in order to calculate the maximum peak value of the current in each port. Then a good approximation is to consider the waveform as a sinusoidal waveform and divide by square root of two in order to calculate the RMS value. Table 5.4 shows the calculated values of the maximum peak current, the maximum calculated value of the RMS current, also shows the RMS value of the current got from the simulation, and shows also the RMS value of the current going to only the capacitors of the DC after removing the DC value of the current going to the output, for each port. The critical port is going to

by the primary port as the value of the ripple current are huge.

Table 5.4: The values of the peak, calculated RMS and simulated RMS of the currents at all the ports.

	The primary port (750 V)	The First Secondary Port (750 V)	The Second Secondary Port (375 V)
The Max. Peak Current (Amps)	292.9688	234.375	117.1875
The Max. calculated RMS Current (Amps)	207.16	165.728	82.864
The Max. simulated RMS Current (Amps)	220.981	175.266	89.63
The Max. simulated RMS Current in the DC-Link (Amps)	173.226	138.581	71.29

The first choice as it was the cheapest is the electrolytic capacitors, the model chosen was ALCON ELECTRONICS: PG-6DI, The Voltage that can withstand 500 V, the capacitance 4700 μ F Maximum Ripple current is 13.92 Amps RMS, and have a 1.35 factor for frequencies higher than 10kHz [37], which is our case. So the Maximum Ripple current will be 18.792 Amps RMS, which makes the first primary port need 12 parallel connected capacitor from this type to withstand the 220.981 Amps RMS. However the single unit is cheaper the twelve will be very expensive, and also there placement inside the cabinet will be impossible.

What about the film capacitors, the choice now goes to the capacitor with the model EGB-DCL-420-1100-1754 (HYDRA), the capacitance value is 420 μ F, and the maximum RMS current is 50 Amps, so by multiplying this value by the high frequency factor the Maximum current will be 67.5 Amps. Now using only four of this one would be enough, the connection was chosen to be by connecting each two in series and then connect them in parallel. Table 5.5 shows the parameters and the specification of the

capacitor.

Table 5.5: The chosen capacitor EGB-DCL-420-1100-1754 (HYDRA) Specification [20].

The Capacitance value	420 (μF)	Max. RMS Current	50 (A)
The max. DC Voltage	1100 (V)	The max. Peak current	2090 (A)
The series resistance value	2.4 ($\text{m}\Omega$)		

Table 5.6 shows the dimensions of the capacitor.

Table 5.6: The chosen capacitor EGB-DCL-420-1100-1754 (HYDRA) Dimensions [20].

The Diameter (mm)	The Height (mm)	The Distance between the center of the two connectors (mm)
85	135	32

Figure 5-8 shows the efficiency of the converter after adding the DC-Link losses with respect to the loading percentage. It is clear from the data cursor that at full load (100 %), the efficiency became 99.2, and it was 99.24 before adding the DC-Link losses. The losses in the DC-Link is about 0.04 % which is considered as a very small amount, and that's due to the very small series parasitic impedance of the Film capacitors.

The design was finalized by putting four capacitors of the EGB-DCL-420-1100-1754 (HYDRA) model, and they are going to be connected, two in series and the other two also in series, then the both couples will be connected in parallel. Which makes the total capacitance will be the same as for one (420 μF).

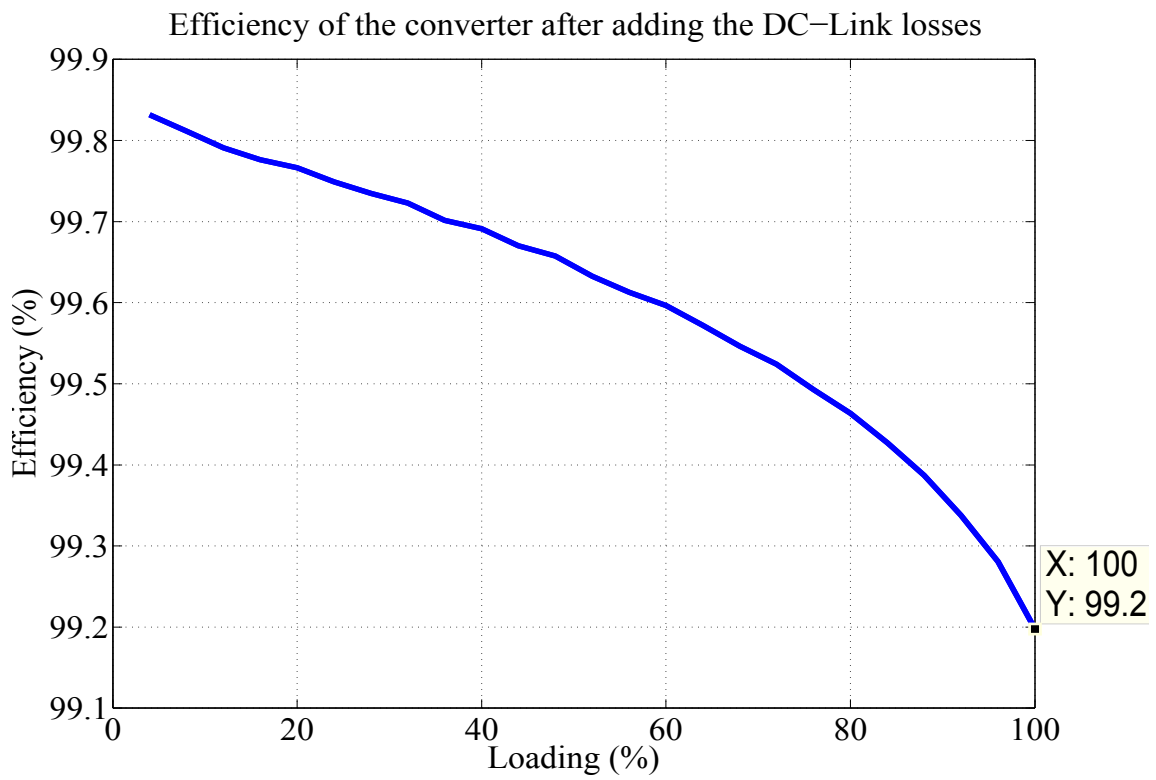


Figure 5-8: The efficiency of the converter after adding the DC-Link losses with respect to the loading percentage.

Chapter 6

IGBT, Heat sink, and stack and Cabinet design

6.1 IGBT choice and specification

6.1.1 Why Insulated-Gate Bipolar Transistor

The power semiconductor technology is a hot topic of research, as there is always a room for improvement in the power devices. The main of the manufacturer companies always is to find the ideal switch, achieve as much high frequency as possible, with the lowest possible losses, very rugged, and low cost.

The Insulated-Gate Bipolar Transistor (IGBT) has proved their success in the high-power application as a solid-state switching device, due to its great advantages [38, 39, 40, 41, 42];

- Compatible for high power applications

The IGBT are nowadays widely used in the industrial and traction application meanwhile the medium voltage medium current applications range (300–3300 V/50–1200 A).

- Easy Controllability and wide safe operating area

One of the great advantages of the IGBT is there easy controllability, and there wide safe operating area, specially compared with the GTO's.

- Fast switching and low conduction losses

Also another advantage is the tradeoff between its switching frequency, voltage drop, as it has a low conduction losses.

- high-impedance gate control

Finally it has a great advantage which is its high-impedance gate control.

Usually the IGBT is packaged in a plastic module that consists of non air proof package, injected silicone gel, and many Al wire-bonding between the main emitter electrode and the IGBT chips. In this case the IGBT chips are cooled only from the collector electrode side. Since the IGBT module structure has some week point for the reliability and compactness for the high power application area, then there are many efforts to increase the reliability of the high power IGBT module. On the other hand, a different approach for the high reliability and compactness of the high power IGBT were carried on by developing the flat-packaged structure.

6.1.2 2MBI200HH-120-50 HIGH SPEED IGBT MODULE 1200V / 200A / 2 in one package

Finally the choice for the switches is the 2MBI200HH-120-50 HIGH SPEED IGBT MODULE manufactured by FUJI electric company. One package of this Module contain two IGBTs, so one module will be configure a leg in the converter. All the parameters and the specifications of the IGBT are presented in the Appendix where there is the data sheet, from this data sheet the data of the losses graphs are extracted to be used in the simulation, in order to simulate the real behavior of the switch.

The most important specifications extracted from the data sheet is; the withstand voltage which is 1200 Volts, and it is higher than what is in the project. Also the maximum continuous current which is 300 A, and that's as previously said one of the key elements of the design of the inductor. The other data are very important also

that's why it is included in the appendix, like the gate voltage, and series resistance, preferred for the operation of the IGBT. Finally a very important piece of information if the equivalent thermal resistance of the junction is equal to $0.025 \text{ (} ^\circ\text{C/W)}$.

6.2 Heat sink choice

One of the most important things in the high power project, is to dissipate the power losses produced by the operation of the power electronics devices, and keep them generally cooled to keep the component temperature within its limits, otherwise the system would be killed. This is due to the fact that it is well known that the main cause of the malfunction of electronic devices is due to overheating [43].

That what gives the importance to the heat sinks, as it play a key role to remove the heat from the devices, and to keep them in healthy conditions [43]. The huge increase of the temperature of the device could cause its malfunction, but also the small increase is not preferred, as it will causes the decrease in the efficiency of the system.

Now the chosen heat sink for the project was the RG14236/400 Model manufactured by GUASCH company. The data sheet [19] contain two graphs, from it the thermal resistance is obtained. The first graphs belongs to the passive heat sink, while the second belongs to the active, or Forced convection, that due to the use of the fan. Figure 6-1 shows the graphs extracted from the data sheet for the forces convection, as the heat dissipation will increases, and the equivalent resistance will decrease. The chosen sub-model is the RG14236/400 it is not only for its low thermal resistance but also for its dimensions. From the graph the equivalent thermal resistance will be in the range of $0.025 \text{ (} ^\circ\text{C/W)}$, the design was chosen in order to have the same thermal resistance of the IGBT junction for maximum power dissipation.

Table 6.1 show the dimensions of the chosen heat sink as it is extremely huge which will makes some issues in the placement of the component in the cabinet, as the project will have a three units of this huge heat sink.

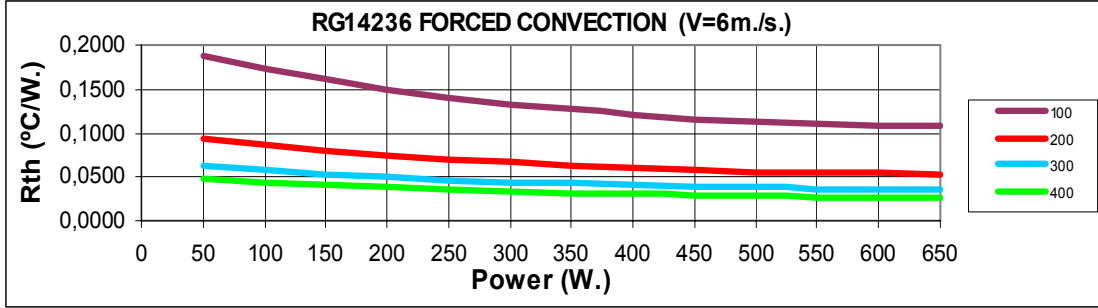


Figure 6-1: The thermal resistance of the heat sink with respect to the power dissipated for all the all the four heat sink sub-model [19].

Table 6.1: The Heat Sink Dimensions.

The Length (mm)	The Width (mm)	The Height (mm)
370	215	77

6.3 Stack design

The huge dimension of the chosen heat sink, creates an idea, to design a stack where the heat sink will not only the IGBT, but also have the other component and the Bus-Bars. The stack will contain mainly;

- The three package of the IGBT
- The snubber capacitors of the IGBT
- The DC-Link capacitors
- The Driver circuits

The driver circuit was implemented and test by one of my colleagues in the LEMUR research group, under the supervision of my supervisor. The idea is to make the driver board the same size of the IGBT unit itself, and the input gate signals coming to it using optic fibers. The board was sent to the Stack manufacturer company.

- The Voltage measurements boards

The voltage measurements boards was previously made and the design belongs to LEMUR research group. The board was sent to the stack manufacturer company.

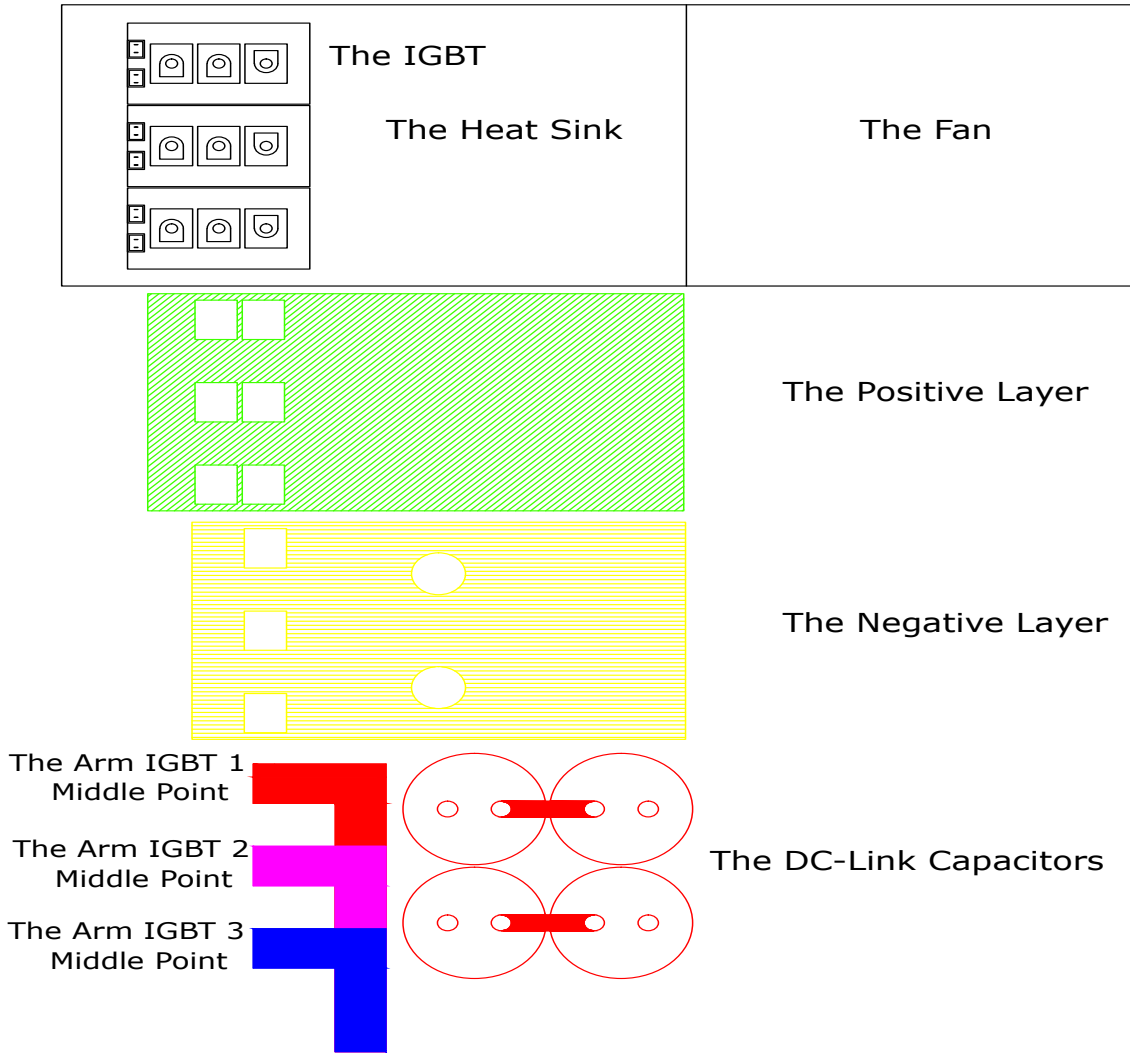


Figure 6-2: The Stack proposed design containing in the first layer the heat sink and its fan, and in the second layer the positive DC-Link layer, then the negative layer of the DC-Link, on top of it comes the DC-Link capacitors and the Bus-bar connected to the middle point of the first IGBT package, on top of it comes the Bus-bar connected to the middle point of the second IGBT package, finally comes the Bus-bar connected to the third one.

Figure 6-2 shows the proposal design, that is sent to the manufacturer company in order to have an idea of what we expect from the Stack design. The first layer contain

the heat sink and its fan, and in the second layer the positive DC-Link layer where it is connected to the each collector of the three IGBT packages, and have Holes on the middle point and the emitter of each IGBT package. Then the negative layer of the DC-Link where it is connected to the each emitter of three IGBT packages and have holes on the middle point of each IGBT package, and at the positive connector of the DC-Link capacitors. On top of it comes the DC-Link capacitors and the Bus-bar connected to the middle point of the first IGBT package, on top of it comes the Bus-bar connected to the middle point of the second IGBT package, finally comes the Bus-bar connected to the third one.

Finally the structure of the design sent to the manufacturer company, is changed by them in order to be more rigid, and stable. The design proposed by them is attached to the appendix B, and it is approved by us, and it is in its manufacture process now.

6.4 Cabinet design for fitting all the project components

The work Done in this part was made in parallel to all the design work, as before finalizing the approve of any component the check of whether the dimensions will fit in the cabinet or no is checked. One of the example of this case was the stack its width before it was 368 mm, Three of this unit with a separation between them of 30 mm the total length will be 1164 mm, which means all the cabinet. We ask them for a redesign with a smaller width, and it became 327 mm, which is acceptable.

Figure 6-3 shows a 3D view for the cabinet drawn in red, which contain in the extreme bottom the three port solid state transformer, next to it in the bottom also there is the four inductors. On top of them there is the three stacks containing the rest of the project parts, the IGBT's, the drivers, the DC-Link capacitors ... Figure 6-4 shows a front view for the cabinet, where all the dimensions are placed, in blue the three stacks, in red the transformer, and in violet tow of the four inductors.

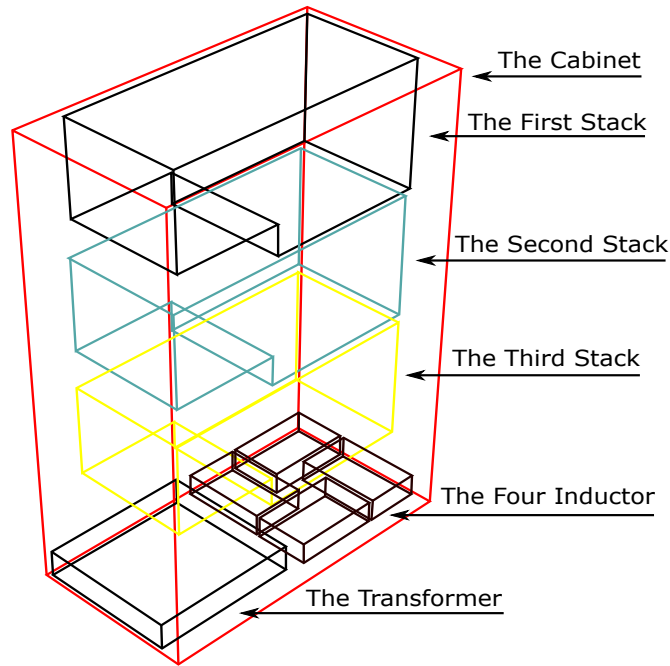


Figure 6-3: A 3D view for the cabinet drawn in red, which contain in the extreme bottom the transformer, next to it in the bottom also there is the four inductors, on top of them there is the three stacks.

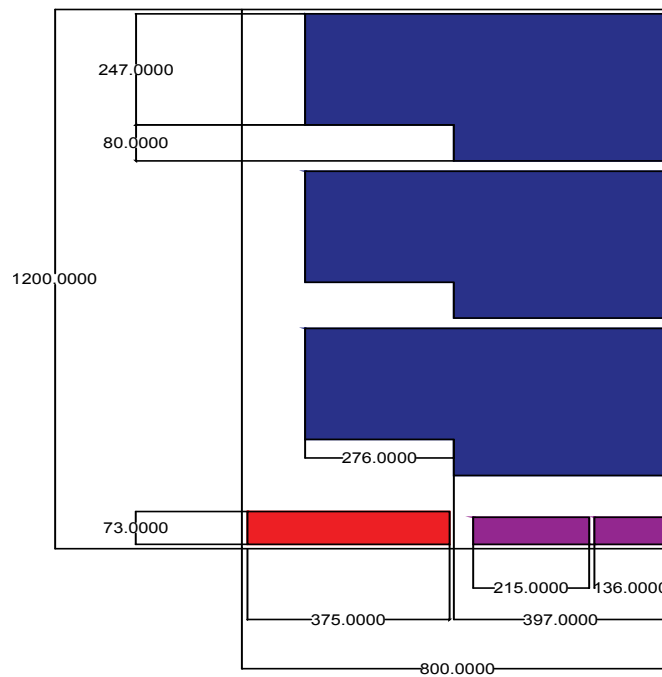


Figure 6-4: A front view for the cabinet, where all the dimensions are placed, in blue the three stacks, in red the transformer, and in violet tow of the four inductors.

Chapter 7

Simulation

7.1 Full model real simulation

The used software as previously mentioned is PLECS library added to Matlab, all the following graphs are drawn using Matlab. The idea beyond the simulation is to analyze the real behavior of all the component taking into account there parasitic elements.

Figure 7-1 shows the full schematic of the simulation, all the measurements probes were removed from the schematic for a better observation. The schematic in the top represents the full schematic of the full project, it starts with the DC voltage source which will represents in our application the primary DC bus. Then next to it the is the primary inverter, with the DC side is connected directly to the primary winding of the transformer. The two output of the secondary side of the transformer goes to two identical circuits, starts with the inductor and its series resistance, then going to the AC side of the secondary inverters. The DC side of the inverters are connected to the DC Link, to a load. In the bottom there is two circuits, the one in the left shows what is inside the inverter block, of course there is the four IGBTs with their Heat Sink. Also each heat sink is connected through its thermal resistance to a temperature voltage source representing the ambient temperature. Finally each switch will have a variable resistor with a very small capacitor in parallel to it, they are representing the losses inside the switch. Finally in the right side there is another circuit which

represents, what the DC-Link block include, simply it have the four capacitors with their series resistance, connected each two in series then the two couple connected in parallel.

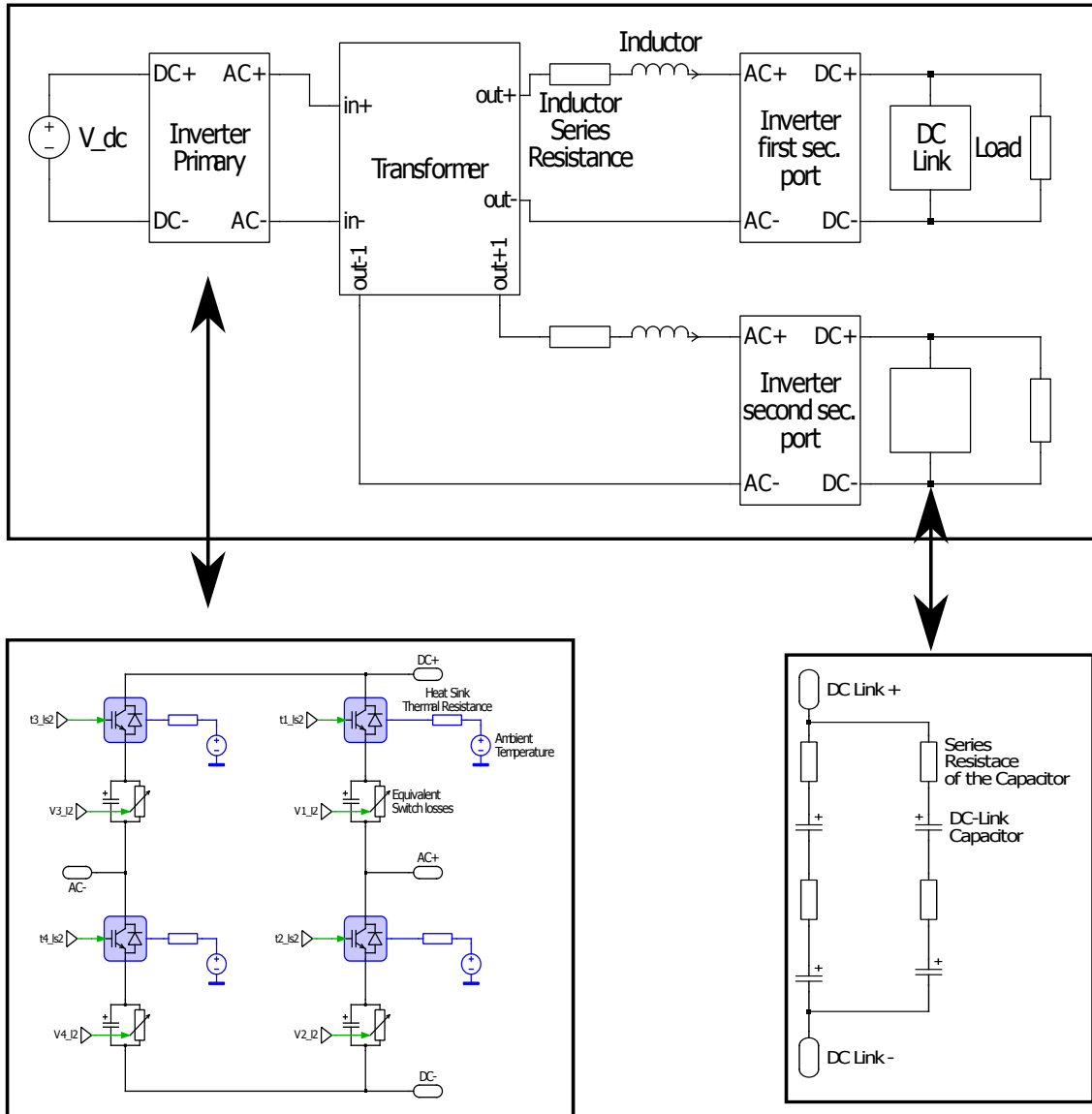


Figure 7-1: The schematic of the Full project, the top schematic shows the project overview, in the bottom there is two other schematic, the one on the left shows the schematic of the inverter, and on the right the schematic of the DC-Link.

The idea of how to implement the losses of the IGBTs is coming from the advantage, given by PLECS software which is its ability of putting inside the IGBT a created model. This model will contain some graphs for the switching turn on and

turn off losses, as shown in Figure 7-2. Also will contain the graphs of the conduction losses, as shown in Figure 7-3. Those data was got from the data sheet of the IGBT attached in the appendix A.

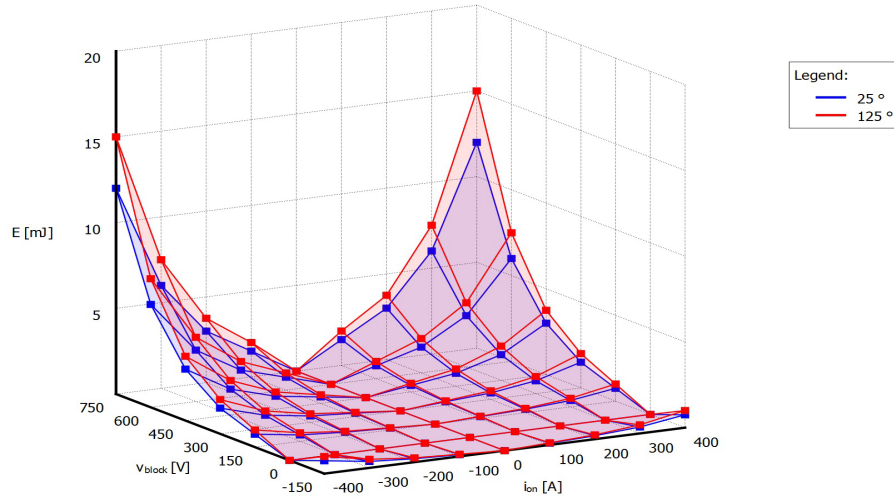


Figure 7-2: The turn on losses got it from the generated report by PLECS software for the created model for the IGBT.

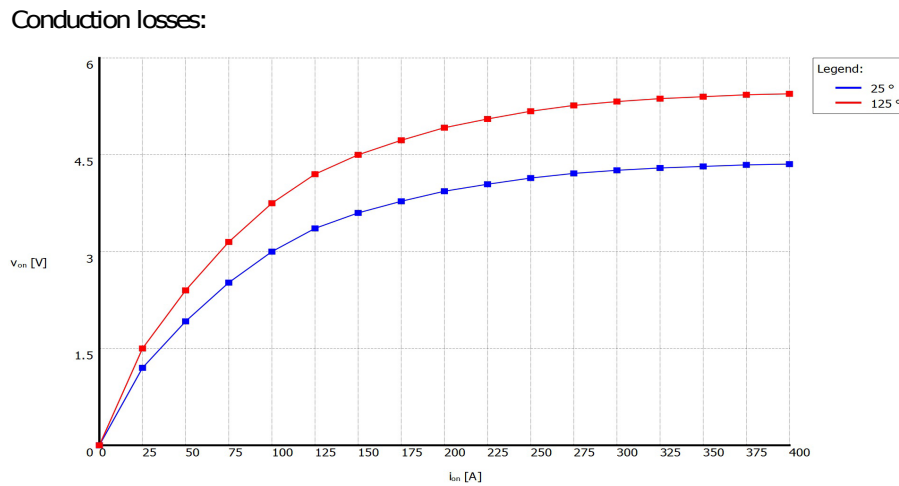


Figure 7-3: The forward voltage with respect to the current, the graph indicating the conduction losses got it from the generated report by PLECS software for the created model for the IGBT.

This was a great advantage in the PLECS software, but a drawback is that the losses power is not considered in the electrical power output. To implement this a variable resistance with a very small capacitor in parallel was putted in series with

each switch, the value of the variable resistance is coming from an instantaneous calculation using the instantaneous losses value and divide it by the square of the instantaneous current.

After having all the model ready now an interesting figure would be the efficiency of the whole project. Figure 7-4 shows the Efficiency of the whole project with respect to the Loading percentage. It is clear now the final efficiency of the project will be 97.17 % this is after adding the IGBTs losses, which indicate how much inefficient they are.

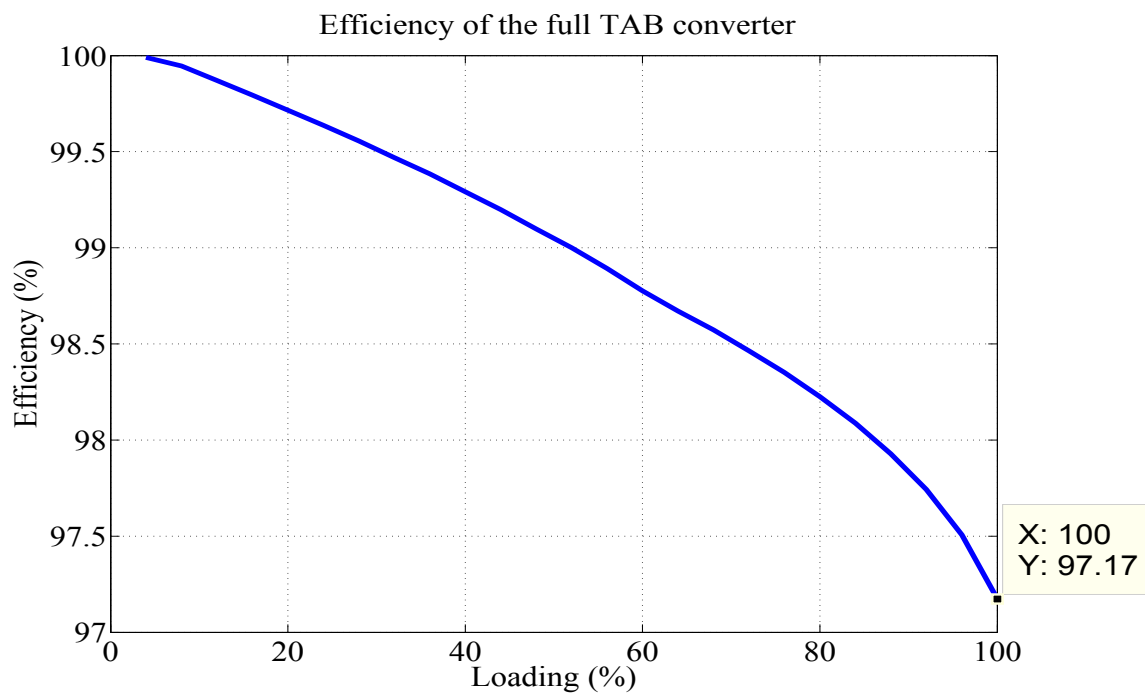


Figure 7-4: The Efficiency of the whole project with respect to the Loading percentage.

Now it would be nice to look the maximum values of the peak currents previously calculated at compare. Figure 7-5 shows the current at the primary port in blue, the first secondary port current in red, and shows also the current at the second secondary port in green. The figure also shows some numerical values, the peak current at the primary equal 270.1 Amps, at the first secondary port 220.8 Amps, and at the second secondary 99.36 Amps.

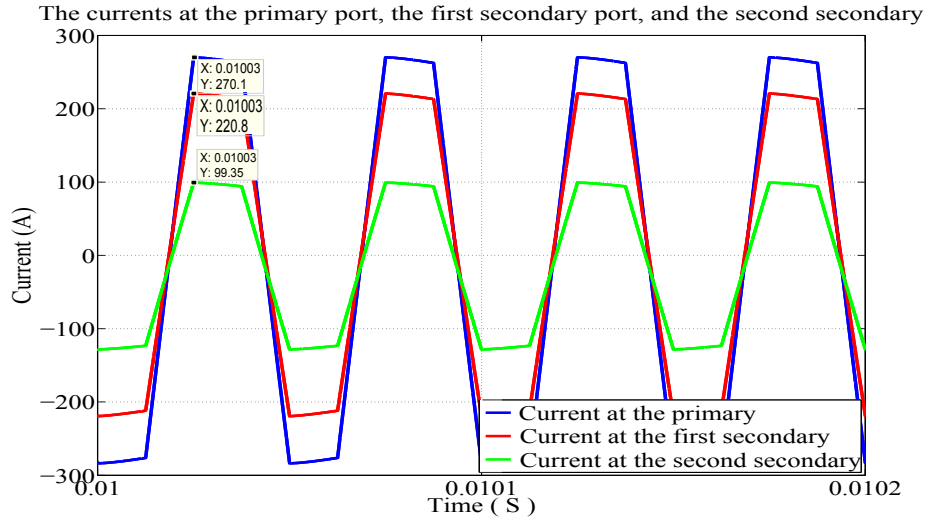


Figure 7-5: In blue the current at the primary port, in red the first secondary port current, and in green the current at the second secondary port.

One of the interesting figure to see now could be the currents before, after and inside the DC-Link. Figure 7-6 shows in blue the current before the DC-Link, in red the current inside the DC-Link, and in green the current after.

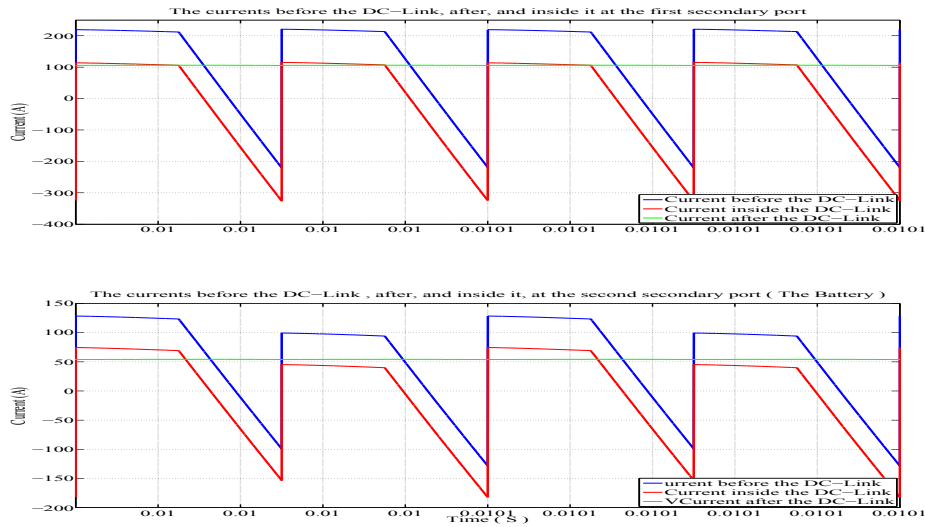


Figure 7-6: In blue the current before the DC-Link, in red the current inside the DC-Link, and in green the current after.

Finally Figure 7-7 shows the ripple after the DC-Link, in the first plot the current ripple in the first secondary port, and in the second plot the ripple in the second secondary port.

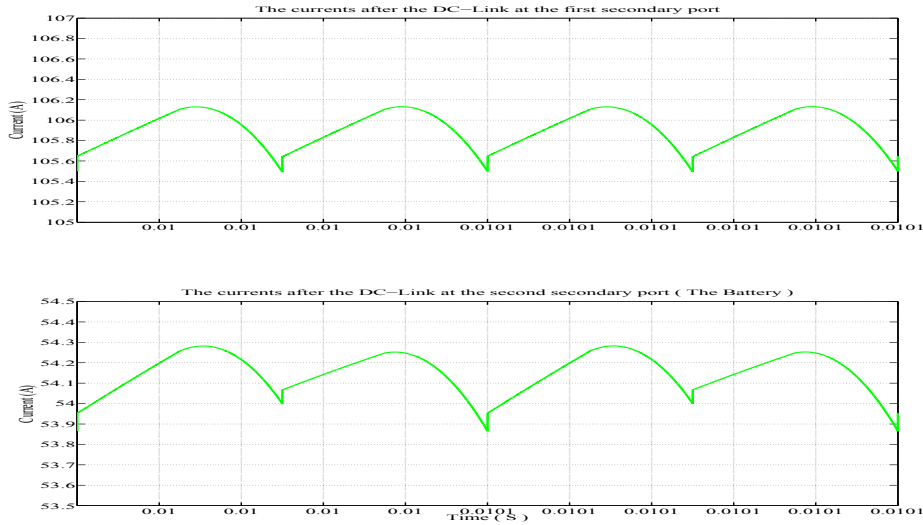


Figure 7-7: The first plot the current ripple in the first secondary port, and in the second plot the ripple in the second secondary port.

Table 7.1 is summarizing the current results.

Table 7.1: The values of currents at the two secondary ports.

	The First Secondary Port (750 V)	The Second Secondary Port (375 V)
The Max. Peak Current	220.8	99.36
The DC Current	105.9	54.1
The Ripple in the DC Current	0.7 Amps	0.4 Amps
The Max. RMS Current before the DC-Link	175.266	89.63
The Max. RMS Current in the DC-Link	138.581	71.29

As a final conclusion, it is fair enough to say that the inductor is well designed and the DC-Link capacitors are well chosen, as ripple current going to the DC-Link capacitors is less than the maximum one recommended by the manufactures. Also it is clear that the ripple current going to the battery will be much more less than the one recommended by the battery manufacturer.

7.2 Comparison with the Half-Bridge TAB

The previous illustrated issue of the huge losses due to the switches, makes the research direction goes toward the decrease of the number of switches. A brilliant idea was found which is the Half-Bridge TAB converter its operation was a bit complicated, as the two secondary ports are working as a boost converter inside the TAB converter. But the increase in the efficiency is a great aim that makes in effort done in order to increase the efficiency, is worthy.

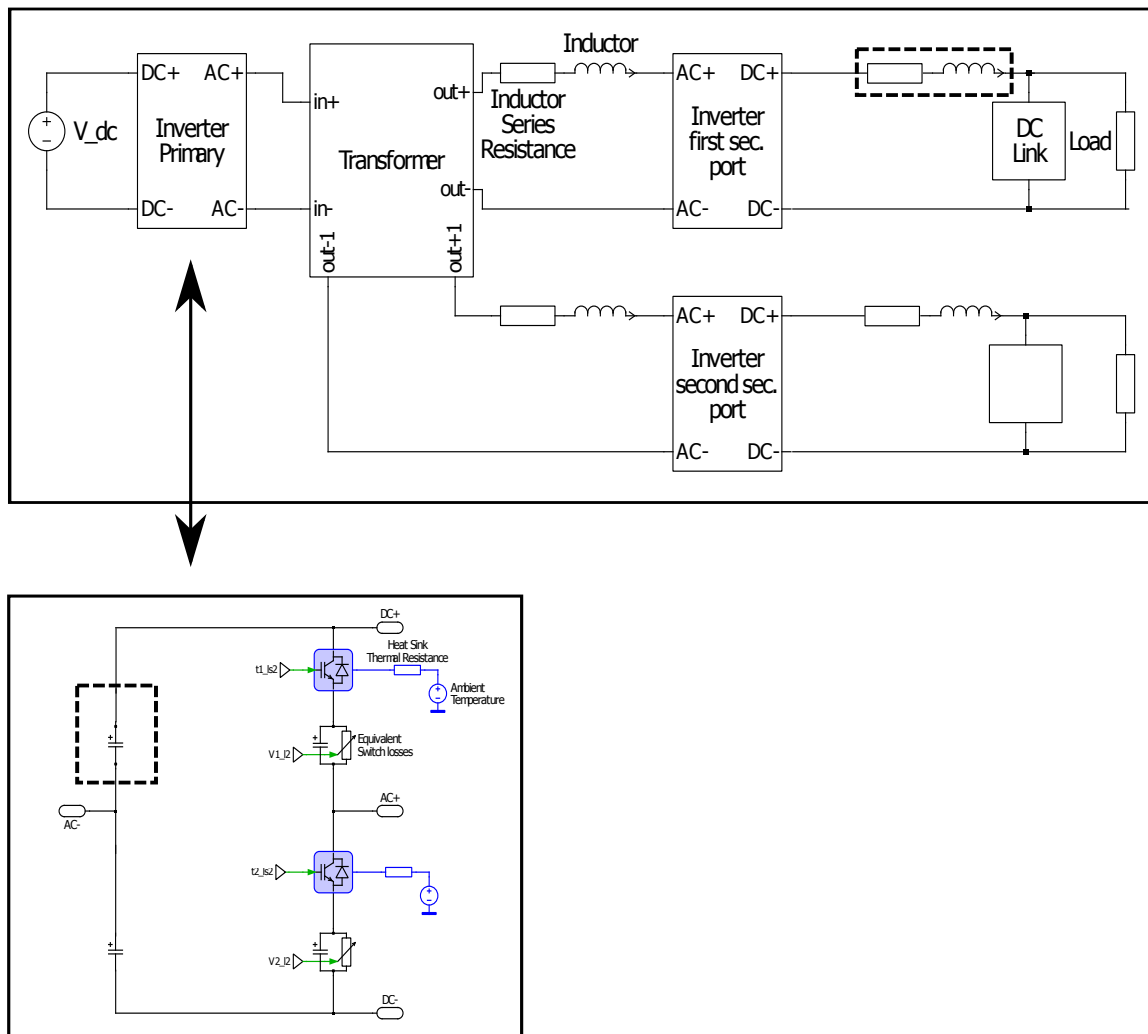


Figure 7-8: The schematic of the Full project working in Half-Bridge mode, the top schematic shows the project overview, in the bottom there is the schematic of the inverter.

Figure 7-8 shows the schematic of the Half-Bridge TAB, the figure shows two

main differences that the main one, putted inside the two dashed rectangles. The first change is an inductor is added between the DC output of the inverter, and the DC-Link. The second change is by removing two of the switches and replace them with two capacitors.

Is the efficiency increased a lot, that's what Figure 7-9 shows the efficiency of the full system using the half-Bridge technique. The figure shows that the efficiency at the full load became 97.98 %, and this means that the efficiency is increased by 0.81 % in the full load which is 150 KW, which means a savings of 1.215 KW,

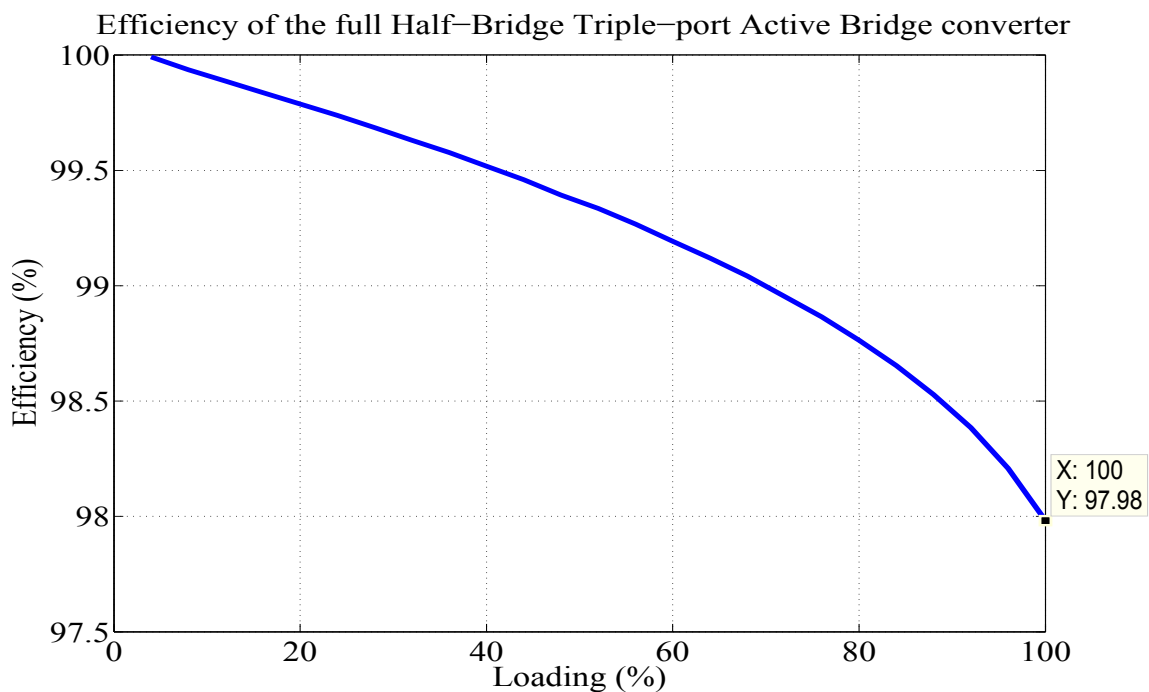


Figure 7-9: The Efficiency of the whole project using the half bridge topology with respect to the Loading percentage.

7.3 Control simulation

In this partition a control was made in order to just test the behavior of the converter in closed loop operation. The control is not made by a practical implemented using the real measurements scaling, and the filters for the noise, and so, the control is made in simulation using the simulation probes.

The full project recommend the control of the triple port to make a voltage control on the first secondary port, to fix it to a give value (750 V). While it recommend the other secondary port to work as a power port, the power commend will come to the triple port from an upper controller, then the power or the current should be sent or received as it was recommended.

The implementation control algorithm for the voltage control is the cascaded control strategy where the control algorithm is composed of two loops. the inner loop is the current control loop, where this loop control the current in the inductor. This loop bandwidth is going to be very high relative to the outer one, in this simulation 500 Hz is used for the inner current loop, while only 50 Hz is used for the outer one. As this loop is very fast it could be considered as a gain of 1 inside the outer loop which is the voltage control loop.

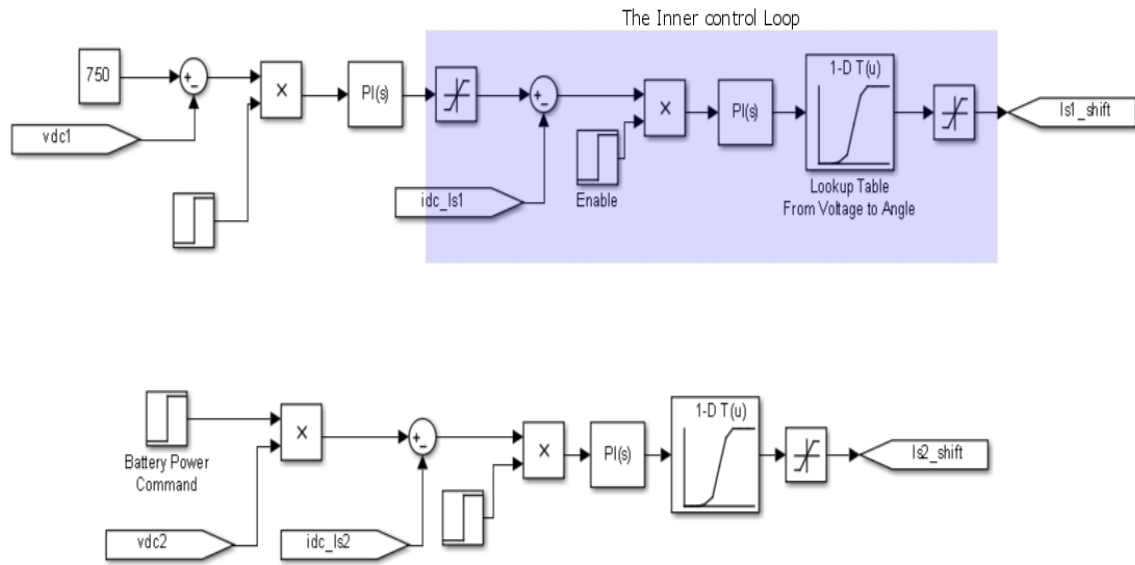


Figure 7-10: The Matlab representation of the control loops, the upper diagram represents the control of the first secondary port, while the lower one shows the control diagram for the second secondary port.

Figure 7-10 shows the control blocks used in Matlab software for implementing the control technique. Inside the blue rectangle, there is the blocks representing the inner control loop, starts with the reference coming from the outer loop, and subtract from it the actual current, the result is multiplied by an enable signal for the control.

The following step is the PI controller, which will be tuned based on the zero pole cancellation. The output of the PI is the voltage on the inductor, which should be transferred into a phase shift using the lookup table. The outer loop is the control loop, which control the voltage on the DC-Link capacitors. As shown in Figure 7-10 The voltage loop is presented by the fixed reference (750 V) subtracted from it the actual voltage of the capacitors, to a PI which will be also tuned based on the zero pole cancellation. The second diagram represents the control at the second secondary port, while there is only a current control loop, but it include only one small difference, is that the reference is a power reference, and it is divided by the voltage of the battery to get the current reference.

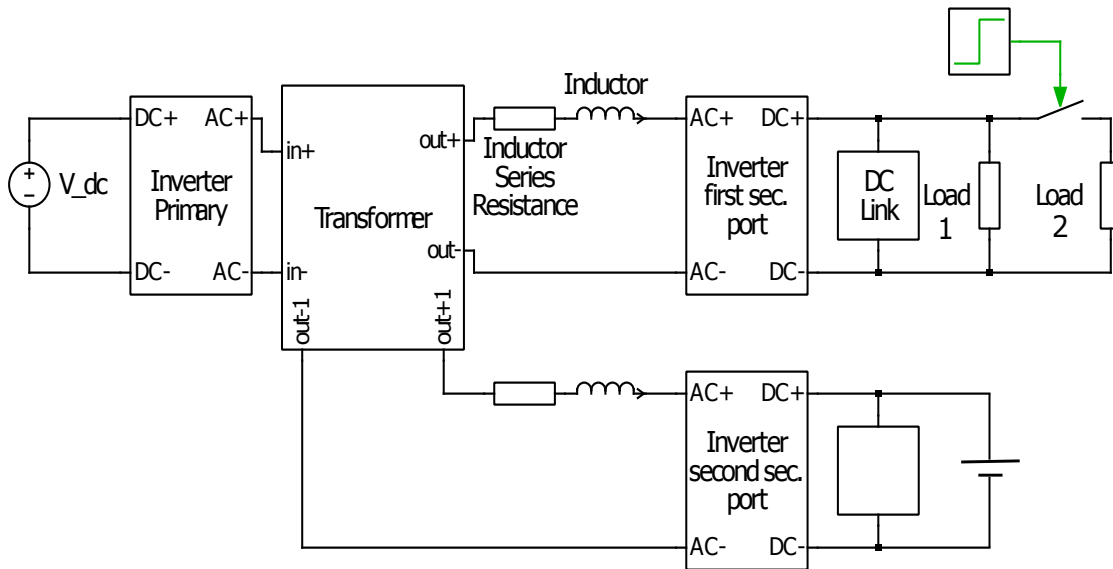


Figure 7-11: The Schematic of the main block used in the control simulation.

Figure 7-11 shows the schematic used in the control simulation, it is not fear than the normal schematic, there is only two main differences; the load placed in the second secondary port is replaced by a battery, and the first secondary port will have a second load that will be connected at the beginning and then disconnected at 0.1 second.

The simulation for all the system will be made, it lasts for 0.2 s, the simulation will include some disturbances like; a command of injecting 20 KW to the battery port

at 0.05 s, a decrease in the first secondary port load at 0.1 s, and finally a command of absorbing 20 KW from the battery at 0.15 s.

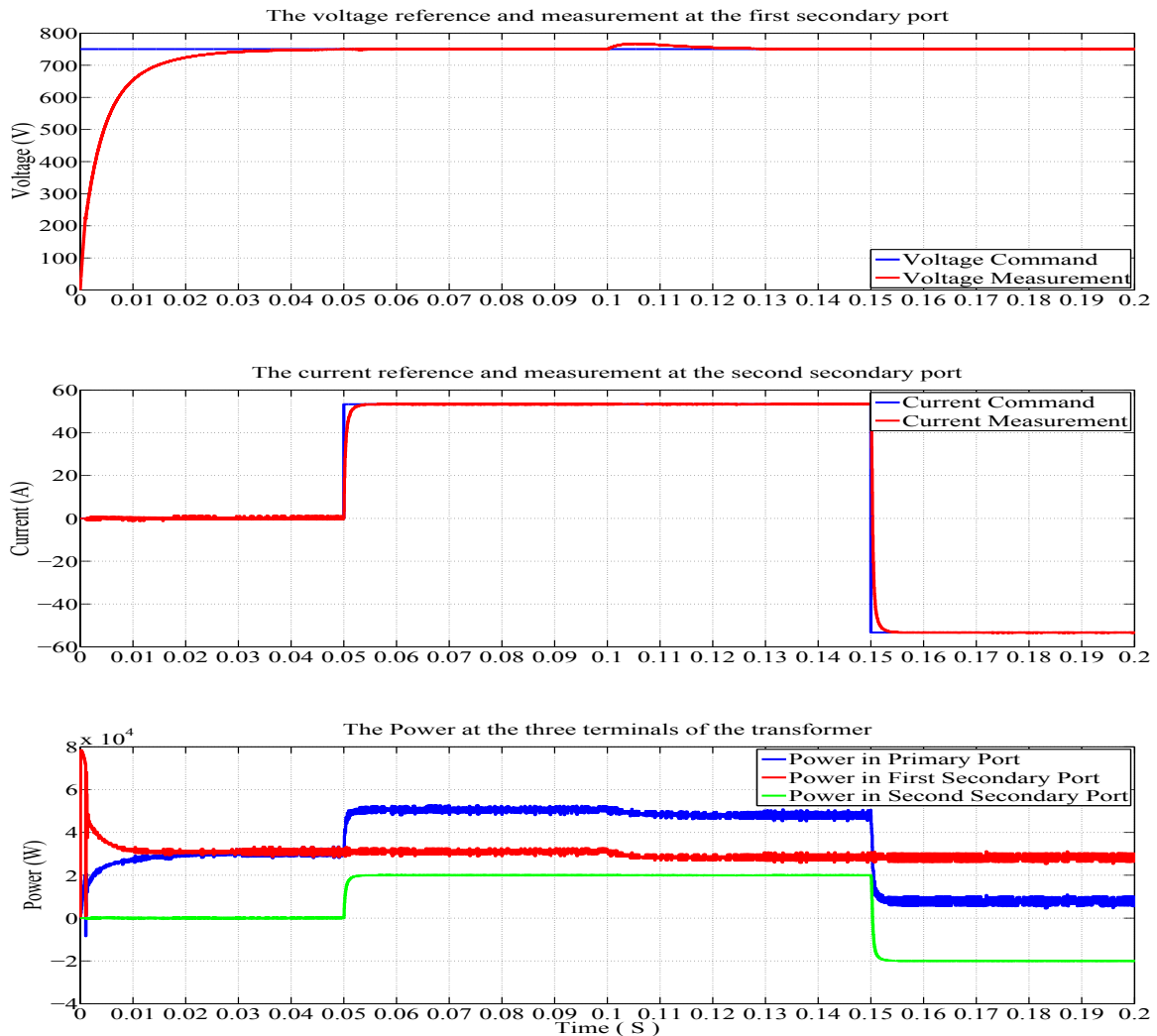


Figure 7-12: The first plot shows the voltage at the first secondary port, in blue is the reference and in red is the actual, the second plot shows the current at the battery, in blue the reference current coming from the division of the reference power to the actual battery voltage, and in red the actual current, finally the last plot shows the power at each port, in blue the power of the primary port, in red the first secondary port, and in green the power at the battery.

Figure 7-12 shows the response of the system, the first plot shows the voltage at the first secondary port, in blue is the reference and in red is the actual, the second plot shows the current at the battery, in blue the reference current coming from the division of the reference power to the actual battery voltage, and in red the actual

current, finally the last plot shows the power at each port, in blue the power of the primary port, in red the first secondary port, and in green the power at the battery. As a conclusion on the results, the voltage control seems to be working, as it tracks the reference perfectly, and after the disturbance made by the load reduction the voltage increases but goes back to its value. For the current the same exactly occurs as the actual current tracks the reference perfectly for negative and positive values. Talking about the powers shown in the last plot it seems that the power in the first part from 0.02 s after the steady state to 0.05 s is equal to the power in the first secondary port, after this time a 20 KW is absorbed by the battery which increases the power at the primary side to be the addition of both ports, at 0.1 s a decrease in the power of the first secondary, and so the primary, due to the decrease occurs in the load, at 0.15 the battery instead of absorbing 20 KW, it injects 20 KW, which decreases the power at the primary side a lot as now a big portion from the power recommended by the first secondary port, is given by the battery.

As a final comment on the control, it is fair enough to say that the system works fine, stable, and follow whatever commands given to it. But it is not the final implementation for it, as this is going to be one of the most important parts of the future work.

Chapter 8

Conclusion and Future Work

8.1 Conclusion

First of all the design was perfectly made, as all the project component are will designed in order to keep the operation of the converter under the limits and the restrictions of the full project, and of the components itself. Like the maximum power, the maximum current, the ripple, and so on.

The simulations shows that the operation of the converter is as expected, and shows how efficient is the system, except only one drawback in the switches losses. There is mainly two solution for this, the Zero Voltage Switching technique, and the Half-Bridge TAB and this one was simulated and the results was better as expected. One of those two solution could be implemented in the final project operation. The simulation also was very useful, as all the data sent to the manufacturer in order to will design the component, was extracted from it.

The mechanical structure design was implemented, with high level of excellency in order to fit all the project component inside the cabinet. The stack idea was a brilliant one, without it the project wouldn't fit at all. And also it was taken into consideration the output and the input connections of the project, coming out from the cabinet, to be as short as possible going to their connections in the other parts of the full project.

8.2 Future Work

The future work will be presented in some well organized points as following;

- Design of the Bus-bars going from the stack to the Transformer and Inductors.
- Add the protection and power supply devices.
- Mount and fix everything in the cabinet.
- The TAB Testing

A series of test should be done for the Triple Port active bridge itself alone, in order to check its functionally;

- Low power test for the normal operation in open loop.
- High power test for the normal operation in open loop.
- Control implementation.
- Low power test for the control operation in closed loop.
- High power test for the control operation in closed loop.

- The LEMUR project Testing

A series of test should be done for the Triple Port active bridge working inside the full project, in order to check its functionally also;

- Testing the TAB after connecting to the battery only.
- Testing the TAB after connecting all the ports.
- Full power, full project testing.

- Research

After powering up the project a research process will starts in order to optimize and increase its performance;

- Efficiency optimization using the half bridge, and the zero voltage switching technique.

- Adding some algorithm in the upper control, for optimization the price of the total KWh. This is done by using the price of the electricity and depending on this price, and check whether it is cheap or expensive. if it is cheap charge the battery, and if it is expensive use the battery, and decrease the amount of power coming from the grid.

Appendix A

Data sheets

The following data sheet is the data sheet of the 2MBI200HH-120-50 IGBT Model, it is included here due to its importance, as all the losses curves of the IGBT added to the simulation is got from it.

2MBI200HH-120-50

IGBT Modules

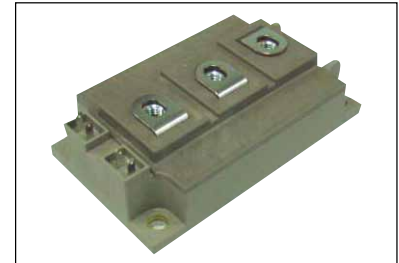
HIGH SPEED IGBT MODULE 1200V / 200A / 2 in one package

■ Features

- High speed switching
- Voltage drive
- Low Inductance module structure

■ Applications

- Soft-switching Application
- Industrial machines, such as Welding machines



■ Maximum Ratings and Characteristics

● Absolute Maximum Ratings (at Tc=25°C unless otherwise specified)

Items	Symbols	Conditions	Maximum ratings	Units	
Collector-Emitter voltage	V _{CES}		1200	V	
Gate-Emitter voltage	V _{GES}		±20	V	
Collector current	I _c	Continuous	Tc=25°C	300	A
			Tc=80°C	200	
	I _c pulse	1ms	Tc=25°C	600	
			Tc=80°C	400	
	-I _c			75	
-I _c pulse	1ms		150		
Collector Power Dissipation	P _c	1 device	1790	W	
Junction temperature	T _j		+150	°C	
Storage temperature	T _{stg}		-40 ~ +125		
Isolation voltage	Between terminal and copper base (*1) V _{iso}	AC : 1min.	2500	VAC	
Screw torque	Mounting (*2)		3.5	N m	
	Terminals (*3)		4.5		

Note *1: All terminals should be connected together when isolation test will be done.

Note *2: Recommendable Value : Mounting 2.5 to 3.5 Nm (M5 or M6)

Note *3: Recommendable Value : Terminals 3.5 to 4.5 Nm (M6)

● Electrical characteristics (at Tj= 25°C unless otherwise specified)

Items	Symbols	Conditions	Characteristics			Units	
			min.	typ.	max.		
Zero gate voltage collector current	I _{CES}	V _{GE} = 0V, V _{CE} = 1200V	-	-	2.0	mA	
Gate-Emitter leakage current	I _{GES}	V _{CE} = 0V, V _{GE} = ±20V	-	-	400	nA	
Gate-Emitter threshold voltage	V _{GE(th)}	V _{CE} = 20V, I _c = 200mA	5.7	6.2	6.7	V	
Collector-Emitter saturation voltage	V _{CE(sat)} (terminal)	V _{GE} = 15V I _c = 200A	Tj=25°C	-	3.35	3.65	V
			Tj=125°C	-	4.25	-	
	V _{CE(sat)} (chip)	Tj=25°C	-	3.10	3.40		
		Tj=125°C	-	4.00	-		
Input capacitance	C _{ies}	V _{CE} = 10V, V _{GE} = 0V, f = 1MHz	-	18	-	nF	
Turn-off time	t _{off}	V _{CC} = 600V, I _c = 200A	-	0.30	0.60	μs	
	t _f	V _{GE} = ±15V, R _G = 1.6Ω L _s = 20nH	-	0.05	0.20		
Forward on voltage	V _F (terminal)	V _{GE} = 0V I _F = 75A	Tj=25°C	-	1.85	2.30	V
			Tj=125°C	-	2.00	-	
	V _F (chip)	Tj=25°C	-	1.70	2.15		
		Tj=125°C	-	1.85	-		
Lead resistance, terminal-chip (*4)	R _{lead}		-	1.20	-	mΩ	

Note *4: Biggest internal terminal resistance among arm.

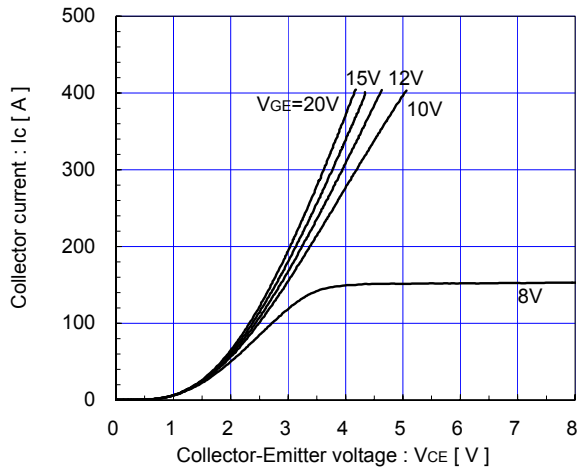
● Thermal resistance characteristics

Items	Symbols	Conditions	Characteristics			Units
			min.	typ.	max.	
Thermal resistance (1device)	R _{th(j-c)}	IGBT	-	-	0.07	°C/W
		FWD	-	-	0.46	
Contact Thermal resistance (1 device) (*5)	R _{th(c-f)}	with Thermal Compound	-	0.025	-	

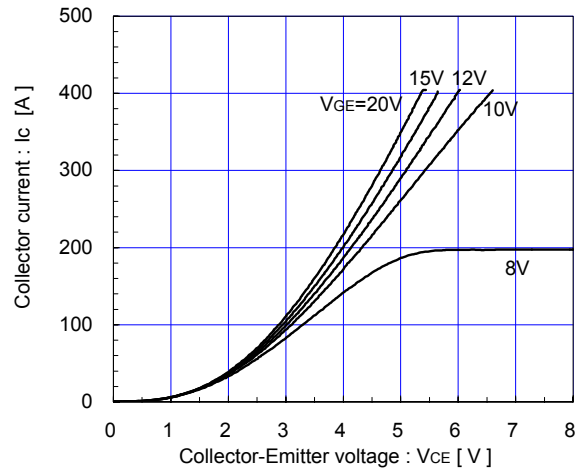
Note *5: This is the value which is defined mounting on the additional cooling fin with thermal compound.

■ Characteristics (Representative)

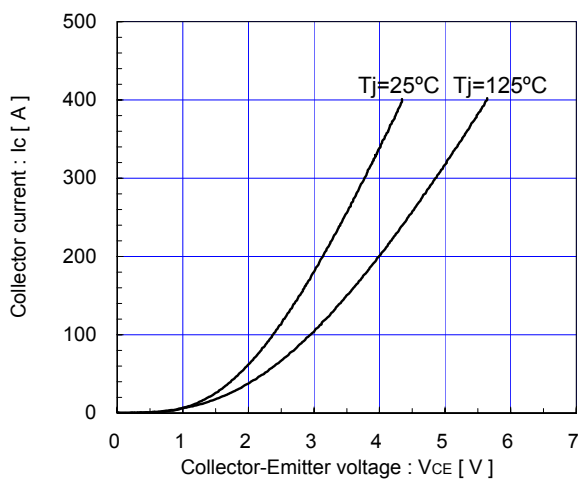
Collector current vs. Collector-Emmitter voltage (typ.)
T_j=25°C / chip



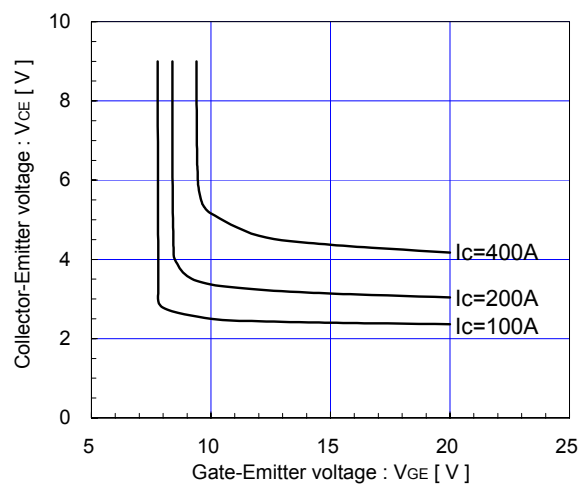
Collector current vs. Collector-Emmitter voltage (typ.)
T_j=125°C / chip



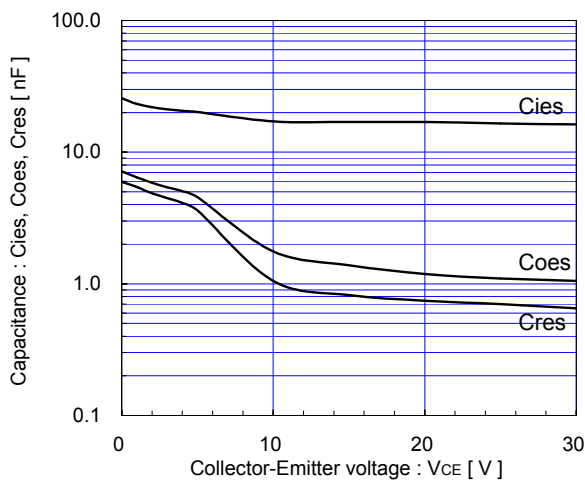
Collector current vs. Collector-Emmitter voltage (typ.)
V_{GE}=15V / chip



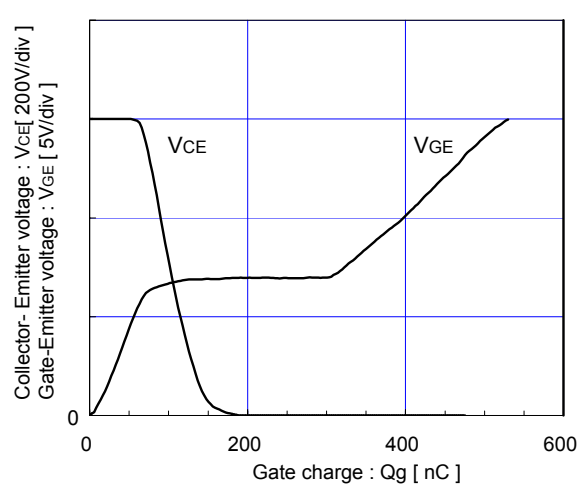
Collector-Emmitter voltage vs. Gate-Emmitter voltage (typ.)
T_j=25°C / chip

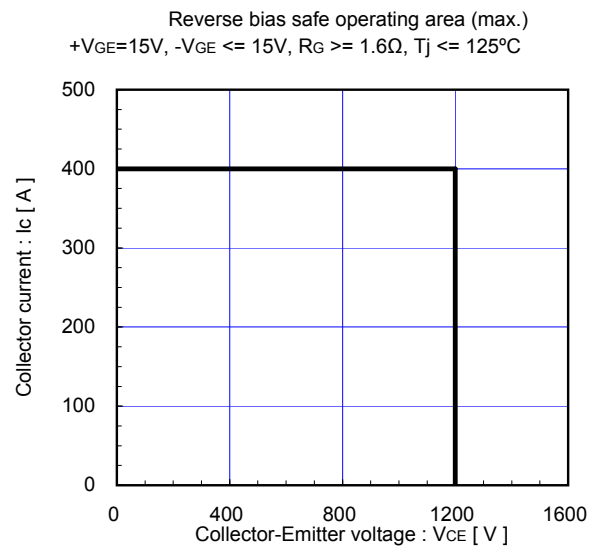
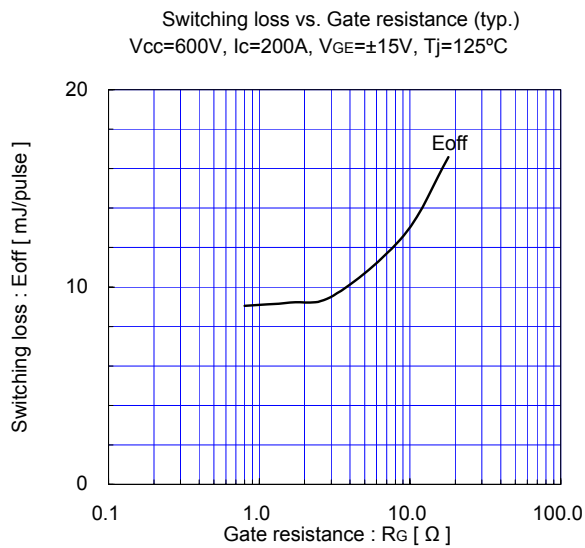
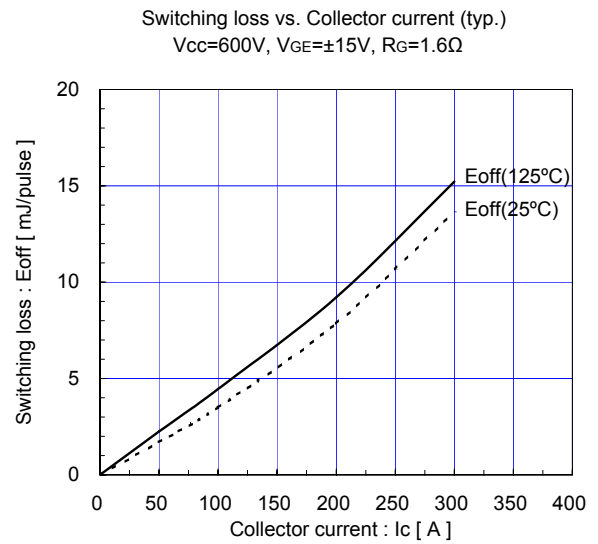
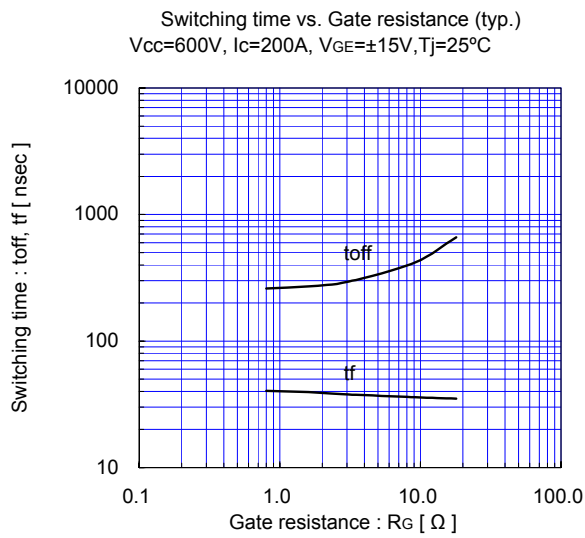
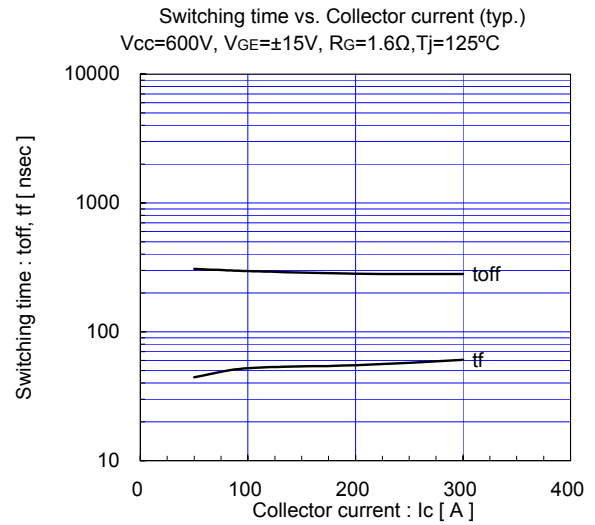
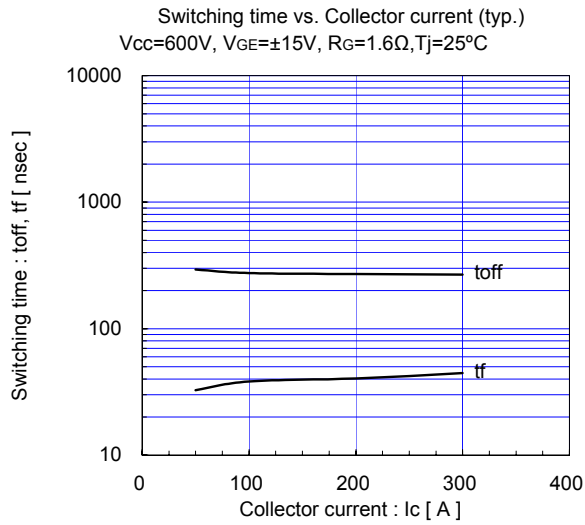


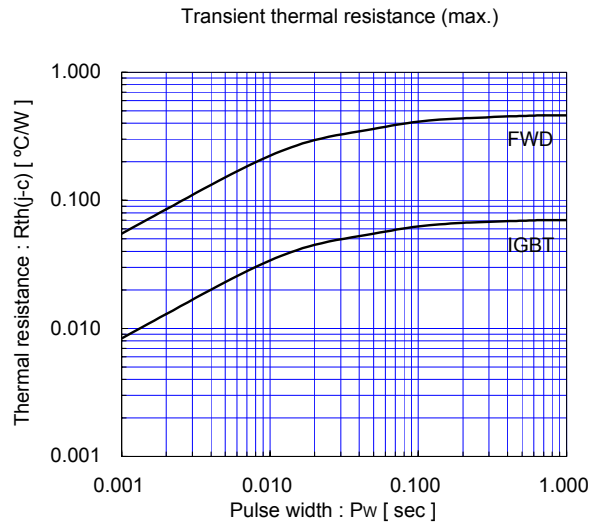
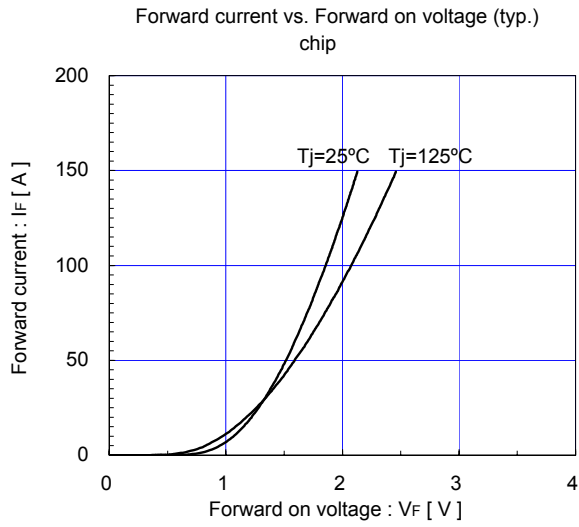
Capacitance vs. Collector-Emmitter voltage (typ.)
V_{GE}=0V, f=1MHz, T_j=25°C



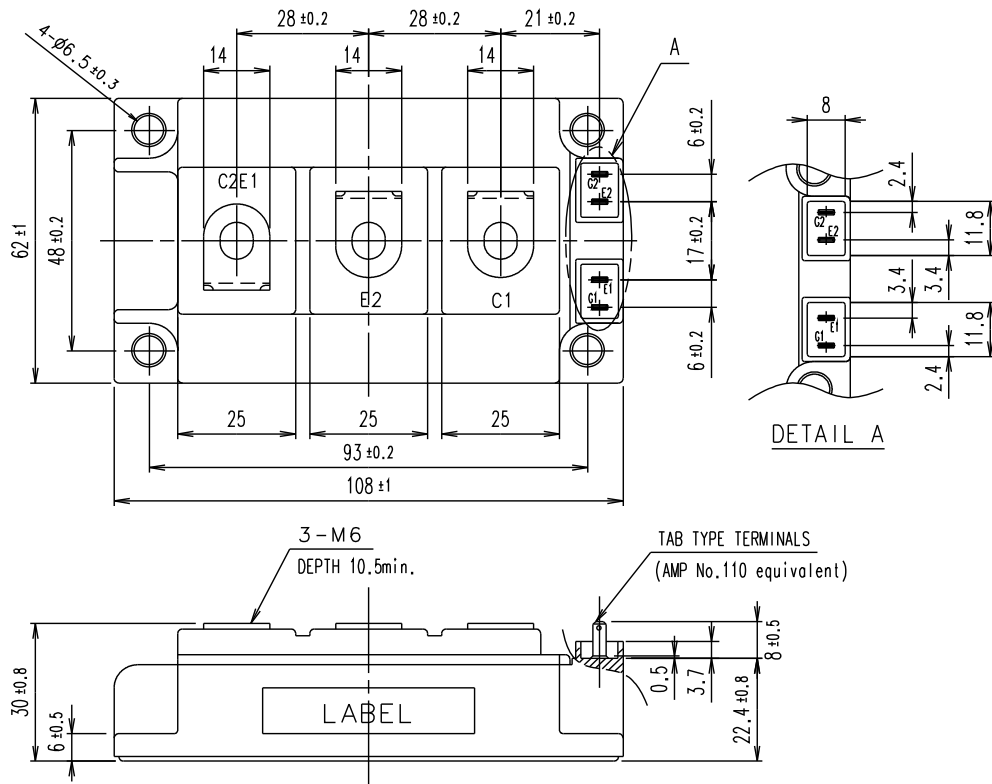
Dynamic Gate charge (typ.)
V_{cc}=600V, I_c=200A, T_j=25°C



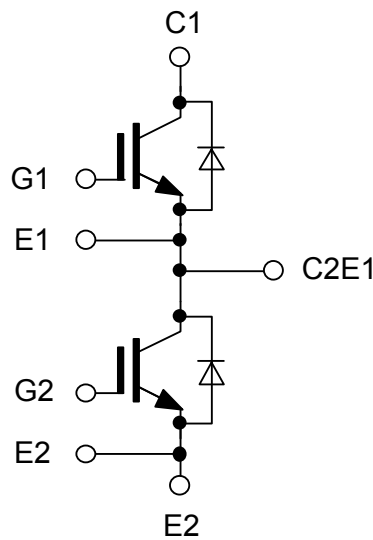




■ Outline Drawings, mm



■ Equivalent Circuit Schematic



WARNING

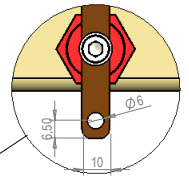
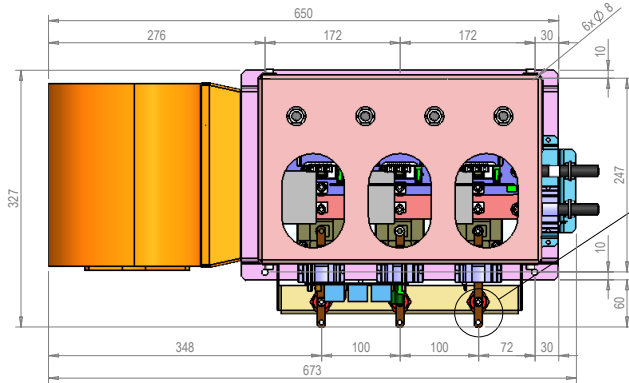
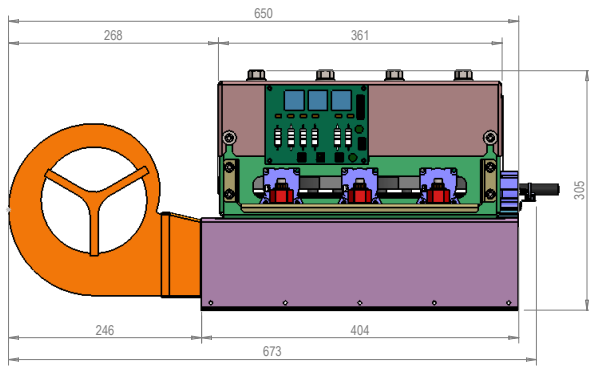
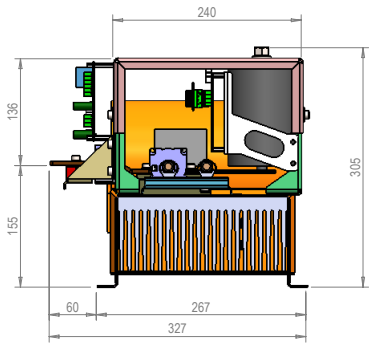
1. This Catalog contains the product specifications, characteristics, data, materials, and structures as of May 2011.
The contents are subject to change without notice for specification changes or other reasons. When using a product listed in this Catalog, be sure to obtain the latest specifications.
2. All applications described in this Catalog exemplify the use of Fuji's products for your reference only. No right or license, either express or implied, under any patent, copyright, trade secret or other intellectual property right owned by Fuji Electric Co., Ltd. is (or shall be deemed) granted. Fuji Electric Co., Ltd. makes no representation or warranty, whether express or implied, relating to the infringement or alleged infringement of other's intellectual property rights which may arise from the use of the applications described herein.
3. Although Fuji Electric Co., Ltd. is enhancing product quality and reliability, a small percentage of semiconductor products may become faulty. When using Fuji Electric semiconductor products in your equipment, you are requested to take adequate safety measures to prevent the equipment from causing a physical injury, fire, or other problem if any of the products become faulty. It is recommended to make your design failsafe, flame retardant, and free of malfunction.
4. The products introduced in this Catalog are intended for use in the following electronic and electrical equipment which has normal reliability requirements.
 - Computers
 - OA equipment
 - Communications equipment (terminal devices)
 - Measurement equipment
 - Machine tools
 - Audiovisual equipment
 - Electrical home appliances
 - Personal equipment
 - Industrial robots etc.
5. If you need to use a product in this Catalog for equipment requiring higher reliability than normal, such as for the equipment listed below, it is imperative to contact Fuji Electric Co., Ltd. to obtain prior approval. When using these products for such equipment, take adequate measures such as a backup system to prevent the equipment from malfunctioning even if a Fuji's product incorporated in the equipment becomes faulty.
 - Transportation equipment (mounted on cars and ships)
 - Trunk communications equipment
 - Traffic-signal control equipment
 - Gas leakage detectors with an auto-shut-off feature
 - Emergency equipment for responding to disasters and anti-burglary devices
 - Safety devices
 - Medical equipment
6. Do not use products in this Catalog for the equipment requiring strict reliability such as the following and equivalents to strategic equipment (without limitation).
 - Space equipment
 - Aeronautic equipment
 - Nuclear control equipment
 - Submarine repeater equipment
7. Copyright ©1996-2011 by Fuji Electric Co., Ltd. All rights reserved.
No part of this Catalog may be reproduced in any form or by any means without the express permission of Fuji Electric Co., Ltd.
8. If you have any question about any portion in this Catalog, ask Fuji Electric Co., Ltd. or its sales agents before using the product.
Neither Fuji Electric Co., Ltd. nor its agents shall be liable for any injury caused by any use of the products not in accordance with instructions set forth herein.

Appendix B

Stack Design

In this appendix the Stack design proposed by the manufacturer company, and approved by us, is illustrated.

0 1 2 3 4 5 6 7 8 9



DETALLE Q
ESCALA 1 : 2

TOLERANCIAS MÁXIMAS ADMISIBLES (mm)	
0.5 hasta 3	± 0.2
más de 3 hasta 6	± 0.3
más de 6 hasta 30	± 0.5
más de 30 hasta 120	± 0.8
más de 120 hasta 400	± 1.2
más de 400 hasta 1000	± 2.0
más de 1000 hasta 1200	± 3.0
más de 1200 hasta 4000	± 4.0



Diseñ.por:
 Dibuj.por: Luis P.
 Valid.por:

Fecha: 08-05-15
 Rev: 00
 Obra:

Stack



Dimensiones generales

Material: Peso: -

Espesor: Superf: -

Escala: 1:7

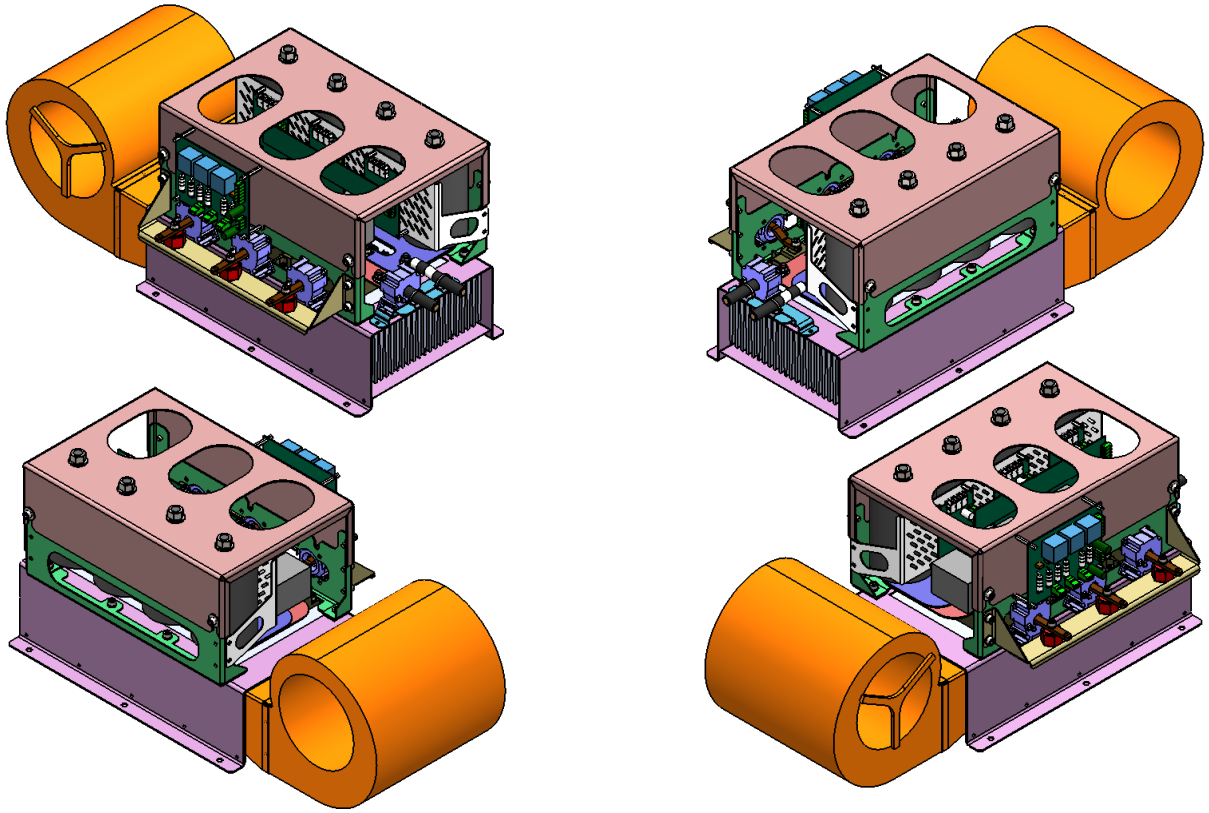
Proy.Nº.U. Oviedo

Pag.: 1 de 2

Tratamiento: -

A4

0 1 2 3 4 5 6 7 8 9



TOLERANCIAS MÁXIMAS ADMISIBLES (mm)	
0.5 hasta 3	± 0.2
más de 3 hasta 6	± 0.3
más de 6 hasta 30	± 0.5
más de 30 hasta 120	± 0.8
más de 120 hasta 400	± 1.2
más de 400 hasta 1000	± 2.0
más de 1000 hasta 1200	± 3.0
más de 1200 hasta 4000	± 4.0



Diseñ.por:	Fecha: 08-05-15
Dibuj.por: Luis P.	Rev: 00
Valid.por:	Obra:

Stack



Dimensiones generales

Material:	Peso: -
Espesor:	Superf: -

Escala: 1:7	Proy.Nº.U. Oviedo	Pag.: 2 de 2	Tratamiento: -	A4
-------------	-------------------	--------------	----------------	----

Bibliography

- [1] https://www.e-education.psu.edu/egee401/content/p5_p4.html.
- [2] V.C. Gungor, D. Sahin, T. Kocak, S. Ergut, C. Buccella, C. Cecati, and G.P. Hancke. Smart grid technologies: Communication technologies and standards. *IEEE Transactions on Industrial Informatics*, 7(4):529–539, Nov 2011.
- [3] L. Solero, F. Caricchi, F. Crescimbeni, O. Honorati, and F. Mezzetti. Performance of a 10 kw power electronic interface for combined wind/pv isolated generating systems. In *Power Electronics Specialists Conference, 1996. PESC '96 Record., 27th Annual IEEE*, volume 2, pages 1027–1032 vol.2, Jun 1996.
- [4] Zhijun Qian, O. Abdel-Rahman, Haibing Hu, and I. Batarseh. An integrated three-port inverter for stand-alone pv applications. In *Energy Conversion Congress and Exposition (ECCE), 2010 IEEE*, pages 1471–1478, Sept 2010.
- [5] J.W. van der Merwe and H. du T.Mouton. The solid-state transformer concept: A new era in power distribution. In *AFRICON, 2009. AFRICON '09.*, pages 1–6, Sept 2009.
- [6] S. Falcones, Xiaolin Mao, and R. Ayyanar. Topology comparison for solid state transformer implementation. In *Power and Energy Society General Meeting, 2010 IEEE*, pages 1–8, July 2010.
- [7] V. Jeyakarthikha and K.R. Vairamani. Multiport bidirectional dc-dc converter for energy storage applications. In *Circuit, Power and Computing Technologies (ICCPCT), 2014 International Conference on*, pages 411–417, March 2014.
- [8] Biao Zhao, Qiang Song, Wenhua Liu, and Yandong Sun. Overview of dual-active-bridge isolated bidirectional dc-dc converter for high-frequency-link power-conversion system. *Power Electronics, IEEE Transactions on*, 29(8):4091–4106, Aug 2014.
- [9] Myunghyo Ryu, Donggeun Jung, Juwon Baek, and Heunggeun Kim. An optimized design of bi-directional dual active bridge converter for low voltage battery charger. In *Power Electronics and Motion Control Conference and Exposition (PEMC), 2014 16th International*, pages 177–183, Sept 2014.

- [10] Hui Li and F.Z. Peng. Modeling of a new zvs bi-directional dc-dc converter. *Aerospace and Electronic Systems, IEEE Transactions on*, 40(1):272–283, Jan 2004.
- [11] T. Todorovic, P. Bauer, J.A. Ferreira, and R. van Kessel. A modulation strategy for wide voltage output in dab based dc-dc modular multilevel converter. In *Industrial Electronics Society, IECON 2014 - 40th Annual Conference of the IEEE*, pages 4514–4520, Oct 2014.
- [12] R. Yapa and A. Forsyth. Extended soft switching operation of the triple active bridge converter. In *Power Electronics, Machines and Drives (PEMD 2012), 6th IET International Conference on*, pages 1–6, March 2012.
- [13] J.L. Duarte, M. Hendrix, and M.G. Simoes. Three-port bidirectional converter for hybrid fuel cell systems. *Power Electronics, IEEE Transactions on*, 22(2):480–487, March 2007.
- [14] Seunghun Baek, S. Roy, S. Bhattacharya, and Sungmin Kim. Power flow analysis for 3-port 3-phase dual active bridge dc/dc converter and design validation using high frequency planar transformer. In *Energy Conversion Congress and Exposition (ECCE), 2013 IEEE*, pages 388–395, Sept 2013.
- [15] Haimin Tao, J.L. Duarte, and M.A.M. Hendrix. High-power three-port three-phase bidirectional dc-dc converter. In *Industry Applications Conference, 2007. 42nd IAS Annual Meeting. Conference Record of the 2007 IEEE*, pages 2022–2029, Sept 2007.
- [16] Danwei Liu, Hui Li, and Laura D. Marilino. Design of a 6 kw multiple-input bi-directional dc-dc converter with decoupled current sharing control for hybrid energy storage elements. In *Applied Power Electronics Conference, APEC 2007 - Twenty Second Annual IEEE*, pages 509–513, Feb 2007.
- [17] J. Allmeling, W. Hammer, and J. Schonberger. Transient simulation of magnetic circuits using the permeance-capacitance analogy. In *Control and Modeling for Power Electronics (COMPEL), 2012 IEEE 13th Workshop on*, pages 1–6, June 2012.
- [18] S.-A. El-Hamamsy and E.I. Chang. Magnetics modeling for computer-aided design of power electronics circuits. In *Power Electronics Specialists Conference, 1989. PESC '89 Record., 20th Annual IEEE*, pages 635–645 vol.2, Jun 1989.
- [19] GAUSCH. *RG14236 EXTRUDED HEATSINK FOR POWER ELECTRONICS*.
- [20] HYDRA. *EGB DCL/EBB DCL*.
- [21] Yaow-Ming Chen, Yuan-Chuan Liu, Shih-Chieh Hung, and Chung-Sheng Cheng. Multi-input inverter for grid-connected hybrid pv/wind power system. *IEEE Transactions on Power Electronics*, 22(3):1070–1077, May 2007.

- [22] Edward R. Ronan, S.D. Sudhoff, S.F. Glover, and D.L. Galloway. Application of power electronics to the distribution transformer. In *Applied Power Electronics Conference and Exposition, 2000. APEC 2000. Fifteenth Annual IEEE*, volume 2, pages 861–867 vol.2, 2000.
- [23] L. Heinemann and G. Mauthe. The universal power electronics based distribution transformer, an unified approach. In *Power Electronics Specialists Conference, 2001. PESC. 2001 IEEE 32nd Annual*, volume 2, pages 504–509 vol.2, 2001.
- [24] M. Kabalo, B. Blunier, D. Bouquain, and A. Miraoui. State-of-the-art of dc-dc converters for fuel cell vehicles. In *Vehicle Power and Propulsion Conference (VPPC), 2010 IEEE*, pages 1–6, Sept 2010.
- [25] R.W.A.A. De Doncker, D.M. Divan, and M.H. Kheraluwala. A three-phase soft-switched high-power-density dc/dc converter for high-power applications. *Industry Applications, IEEE Transactions on*, 27(1):63–73, Jan 1991.
- [26] M.N. Kheraluwala, R.W. Gascoigne, D.M. Divan, and E.D. Baumann. Performance characterization of a high-power dual active bridge dc-to-dc converter. *Industry Applications, IEEE Transactions on*, 28(6):1294–1301, Nov 1992.
- [27] Lei Wang and Hui Li. Maximum fuel economy-oriented power management design for a fuel cell vehicle using battery and ultracapacitor. *Industry Applications, IEEE Transactions on*, 46(3):1011–1020, May 2010.
- [28] Haimin Tao, J.L. Duarte, and M.A.M. Hendrix. Three-port triple-half-bridge bidirectional converter with zero-voltage switching. *Power Electronics, IEEE Transactions on*, 23(2):782–792, March 2008.
- [29] Haimin Tao, A. Kotsopoulos, J.L. Duarte, and M.A.M. Hendrix. Triple-half-bridge bidirectional converter controlled by phase shift and pwm. In *Applied Power Electronics Conference and Exposition, 2006. APEC '06. Twenty-First Annual IEEE*, pages 7 pp.–, March 2006.
- [30] Danwei Liu. *Topology , Development, and Control of a Three-Port Triple-Half-Bridge DC-DC Converter for Hybrid Energy Storage Application*. PhD thesis, Florida State University, 2006.
- [31] D.C. Hamill. Lumped equivalent circuits of magnetic components: the gyrator-capacitor approach. *Power Electronics, IEEE Transactions on*, 8(2):97–103, Apr 1993.
- [32] F.Z. Peng, Hui Li, Gui-Jia Su, and J.S. Lawler. A new zvs bidirectional dc-dc converter for fuel cell and battery application. *Power Electronics, IEEE Transactions on*, 19(1):54–65, Jan 2004.
- [33] Chuanhong Zhao and J.W. Kolar. A novel three-phase three-port ups employing a single high-frequency isolation transformer. In *Power Electronics Specialists*

Conference, 2004. PESC 04. 2004 IEEE 35th Annual, volume 6, pages 4135–4141 Vol.6, June 2004.

- [34] Chuanhong Zhao, S.D. Round, and J.W. Kolar. An isolated three-port bidirectional dc-dc converter with decoupled power flow management. *Power Electronics, IEEE Transactions on*, 23(5):2443–2453, Sept 2008.
- [35] Chun kit Leung, S. Dutta, Seunghun Baek, and S. Bhattacharya. Design considerations of high voltage and high frequency three phase transformer for solid state transformer application. In *Energy Conversion Congress and Exposition (ECCE), 2010 IEEE*, pages 1551–1558, Sept 2010.
- [36] M. Salcone and J. Bond. Selecting film bus link capacitors for high performance inverter applications. In *Electric Machines and Drives Conference, 2009. IEMDC '09. IEEE International*, pages 1692–1699, May 2009.
- [37] Alcon Electronics. *ALUMINIUM ELECTROLYTIC CAPACITORS PG - 6DI*, jan 2011.
- [38] S. Castagno, R.D. Curry, and E. Loree. Analysis and comparison of a fast turn-on series igbt stack and high-voltage-rated commercial igbts. *Plasma Science, IEEE Transactions on*, 34(5):1692–1696, Oct 2006.
- [39] S. Azzopardi, J.-M. Vinassa, E. Woirgard, C. Zardini, and O. Briat. A systematic hard- and soft-switching performances evaluation of 1200 v punchthrough igbt structures. *Power Electronics, IEEE Transactions on*, 19(1):231–241, Jan 2004.
- [40] Y. Takahashi, K. Yoshikawa, M. Soutome, T. Fujii, H. Kirihata, and Y. Seki. 2.5 kv-1000 a power pack igbt (high power flat-packaged npt type rc-igbt). *Electron Devices, IEEE Transactions on*, 46(1):245–250, Jan 1999.
- [41] J. Yedinak, J. Merges, J. Wojslawowicz, A. Bhalla, D. Burke, and G. Dolny. Operation of an igbt in a self-clamped inductive switching circuit (scis) for automotive ignition. In *Power Semiconductor Devices and ICs, 1998. ISPSD 98. Proceedings of the 10th International Symposium on*, pages 399–402, Jun 1998.
- [42] He Niu and R.D. Lorenz. Sensing igbt junction temperature using gate drive output transient properties. In *Applied Power Electronics Conference and Exposition (APEC), 2015 IEEE*, pages 2492–2499, March 2015.
- [43] Xueguan Song, Jie Zhang, Sanghoon Kang, Mingyao Ma, Bing Ji, Wenping Cao, and V. Pickert. Surrogate-based analysis and optimization for the design of heat sinks with jet impingement. *Components, Packaging and Manufacturing Technology, IEEE Transactions on*, 4(3):429–437, March 2014.